The Optical Design of an Adaptive Optics System Imaging Two Selectable Atmospheric Layers

by

John Stanley Pazder
B.Sc., University of Victoria, 1991

A Thesis Submitted in Partial Fulfillment of the
Requirements for the Degree of

MASTER OF APPLIED SCIENCE

in the
Department of Mechanical Engineering

We accept this thesis as conforming
to the required standard

[redacted]
Dr. E.H. Richardson, Supervisor (Dept. of Mechanical Engineering)

[redacted]
Dr. G.W. Vickers, Supervisor (Dept. of Mechanical Engineering)

[redacted]
Dr. C. Bradley, Member (Dept. of Mechanical Engineering)

[redacted]
Dr. S. Dost, Member (Dept. of Mechanical Engineering)

[redacted]
Dr. R.D. McClure, External Examiner (Dominion Astrophysical Observatory, NRC)

Supervisor: Dr. E.H. Richardson / Dr. G.W. Vickers

Abstract

An optical design for an astronomical adaptive optics system using two deformable mirrors is presented. The design is intended to test the principles of multiconjugate adaptive optics. Multiconjugate adaptive optics is a technique which uses multiple deformable mirrors placed in the system so that they are optically conjugate to different altitudes in the atmosphere. The purpose of the multiple deformable mirrors is to enlarge the isoplanatic angle for the adaptive optics system. The principle of adaptive optics and the current work in multiconjugate optics are reviewed in this thesis. The optical design was made to be used at the $F/8$ Cassegrain focus of the $3.58m$ Canada-France-Hawaii telescope. The design has two deformable mirrors, a SCIDAR camera, a natural guide star wavefront sensor, four laser guide star wavefront sensors, and an atmospheric dispersion corrector. The system field of view is 22 *arcseconds* with the four laser guide stars placed at 37 *arcseconds* from the center of the field. The ranges of altitude which the deformable mirrors can be placed optically conjugate to are : $0\,km$ to $7.2\,km$ for the lower deformable mirror, and $1.8\,km$ to $9\,km$ for the upper deformable mirror, with a minimum conjugate distance of $1.8\,km$ between the mirrors. The image quality at the science camera is better than a Strehl ratio of 0.93 over the whole field of view with the effects of atmospheric dispersion being corrected by an atmospheric dispersion corrector.

Examiners:

[redacted]

Dr. E.H. Richardson, Supervisor (Dept. of Mechanical Engineering)

[redacted]

Dr. G.W. Vickers, Supervisor (Dept. of Mechanical Engineering)

[redacted]

Dr. C. Bradley, Member (Dept. of Mechanical Engineering)

[redacted]

Dr. S. Dost, Member (Dept. of Mechanical Engineering)

[redacted]

Dr. R.D. McClure, External Examiner (Dominion Astrophysical Observatory, NRC)

Table of Contents

List of Tables

List of Figures

Acknowledgements

I would like to thank my advisor, Professor Harvey Richardson, for his constant assistance and guidance throughout my program, and for his financial support. His motivating influence is greatly appreciated. Special thanks to my family for their support helping me to complete this program. I must also thank my friends for their help and support: Allen, Andrew, Ashraf, Barb, Dan, Frank, Gin, Glen, Greg, Hal, Hank, Judith, Kath, Karen, Leila, Malcolm, Mike, Sandra, Seaman Hewett, Shannon, Steve, Ted, Tom and William.

Chapter 1

Introduction

Adaptive optics is the opto-mechanical techniques whose aim is to compensate the wavefront distortions caused by turbulence in atmospheric propagation. Adaptive optics has applications in laser propagation, communications, and optical imaging. Astronomical imaging will be the only application considered in this thesis. In astronomy these techniques hold the promise of increasing the scientific productivity of observatories around the world by improving the ability of the telescope to resolve spatial details on the objects being observed, and increasing the signal to noise of the images obtained. These techniques can provide near perfect images from ground based observatories previously only obtainable from spacecraft above the earths atmosphere.

One of the major limits of adaptive optics in astronomy is the limited field of view of the corrected area, termed the isoplanatic angle, θ_0. With conventional single conjugate adaptive optics systems all the wavefront correction occurs at a single deformable mirror located at the pupil (image of the primary mirror) of the telescope. The deformable mirror corrects for the wavefront incident from the reference object. Wavefronts from other objects of interest that are not coincident with the reference

object pass through a different path in the atmosphere and are not optimally corrected by the deformable mirror. This is the isoplanatic effect.

The isoplanatic angle, θ_0, is defined as the angular field of view of the sky, which the root mean square wavefront distortions, due to the isoplanatic effect, are less then $\lambda/6$ where λ is the mean observing wavelength [42]. Typical values for good observing sites are; $\theta_0 = 1.8$ arc-seconds at $\lambda = 0.5\mu m$, $\theta_0 = 10$ arc-seconds at $\lambda = 2.2\mu m$, and $\theta_0 = 30$ arc-seconds at $\lambda = 5\mu m$.

Recent research has shown that the turbulence in the atmosphere is often concentrated in several layers rather than being continuously distributed. Researchers have proposed to use the layering of the turbulence in the atmosphere to increase the isoplanatic angle. The idea is to place deformable mirrors optically conjugate to each of these layers to eliminate the path difference between the turbulent layer and the deformable mirror. Each deformable mirror corrects for the wavefront distortions from the layer it is conjugate to. This technique has been termed multiconjugate adaptive optics.

The ideas of multiconjugate adaptive optics can also be applied to the atmosphere when it is not strongly layered. The atmosphere is sectioned into a series of sections with a deformable mirror correcting for the wavefront distortions in each section. This sectioning of the atmosphere into serially corrected layers reduces the path differences for the off axis rays increasing the isoplanatic angle.

This thesis presents the optical design of an adaptive optics system imaging two selectable atmospheric layers. The system is designed to be used on the Canada-France-Hawaii telescope in a configuration similar to the adaptive optics bonnette[24, 34] to test the principles of multiconjugate adaptive optics. The principles of adaptive optics are presented and the extension of these ideas to multiconjugate adaptive optics are given. Several adaptive optics systems are presented and the components

of an adaptive optics system are explained. The design of a multiconjugate adaptive optics system imaging two selectable layers is presented along with the procedure used to generate the design. A glossary of technical terms and acronyms is provided in appendix E as a convenience to the reader.

Chapter 2

The Principles of Adaptive Optics

The romantic notion of twinkling stars is the nightmare of every astronomer who tries to unlock the secrets of the universe with observations through optical telescopes. It is in the last microseconds of travel that the light from stars becomes corrupted by the atmosphere which limits the resolution of the largest telescopes at the best mountain-top sites to 0.3 *arcseconds* in the visible. Based on the Rayleigh criteria, a telescope should have a spacial resolution of $\alpha = 1.22\lambda/D$. A resolution of 0.3 *arcseconds* is theoretically obtainable with a 0.5 *meters* aperture telescope. The theoretical resolution of 0.02 *arcseconds* for new 8 m telescopes now being built is not achieved because of the atmospheric turbulence.

The first proposal to compensate the atmospheric turbulence with adaptive optics was by Horace W. Babcock in 1953 [2]. The original proposal is very similar to modern adaptive optics systems, with the major difference being the hardware employed. The deformable mirror was an eidophor mirror that worked with a surface deforming oil film. The wavefront sensor was composed of a rotating knife edge with an image orthicon tube. The Babcock proposal was never built.

The first adaptive optics system implemented was by Leighton, an amateur astronomer in the early 1950's [29, 55]. The device was designed specifically for planetary photography and was used on the 60-inch telescope at Mt. Wilson Observatory. The system corrected only for the image motion of the planet as a whole by the translation of a small lens. This system would be termed a partial adaptive optics system because it only corrected for the tip tilt of the image. The device produced the best planetary images of the era, but, further research developments were not made on the camera system.

The development of adaptive optics in the astronomical community was very slow until the early 1980's when the quantum limit of the image detector was reached [7]. Adaptive optics is now touted as the next frontier for the improvement of ground based optical astronomy capabilities. Currently there are eleven demonstrated or functioning astronomical adaptive optics systems, with fourteen more in the planning stage [61]. In September, 1989, the first diffraction limited images using adaptive optics were obtained with 1.52m telescope at Haute Provence Observatory in France [31].

The term adaptive optics is often confused with active optics. Active optics are the techniques that correct for the image distortion due to environmental changes in the instrument. The temporal frequency of corrections in active optics is of the order of one Hertz or less, yet the temporal frequency in adaptive optics is ten Hertz or greater.

2.1 Adaptive Optics System Components

A schematic of a single deformable mirror pupil conjugate adaptive optics system is shown in figure 2.1. The light from the object under investigation is perturbed by the

atmosphere resulting in a degraded wavefront. This perturbed light is gathered by the telescope. A collimating mirror images the entrance pupil of the telescope onto the deformable mirror. An image of the atmosphere is also formed by the telescope at a location before the deformable mirror as shown in the figure.

The image of the pupil is the wavefront after the passage of the light from the star through the atmosphere. The wavefront perturbation due to the atmosphere can be expressed as the complex function 2.1.

$$\Psi = \phi(\mathbf{r}, t) - \imath A(\mathbf{r}, t) \tag{2.1}$$

The phase distortion of the wavefront, usually termed seeing, is expressed by the term, $\phi(\mathbf{r}, t)$. The imaginary part of the function, $A(\mathbf{r}, t)$, represents the intensity fluctuations of the wavefront due to the atmosphere. The intensity fluctuations are usually termed scintillation.

For an astronomical adaptive optics system the aperture and integration time is large relative to the scale of the intensity fluctuations over the entrance pupil. The scintillation term, $A(\mathbf{r}, t)$, of the atmospheric perturbations can be neglected. Only the phase distortions need to be corrected.

The light is then re-imaged with the camera mirror to form a real image of the object at the science instrument. Part of the light is directed into the wavefront sensor with a beam splitter. The wavefront sensor measures the net wavefront after perturbation by the atmosphere and correction by the deformable mirror.

Sometimes the astronomical object under investigation (the science object) is not intense enough to provide the necessary wavefront information for the control system to correct the perturbed wavefront. In this case a second brighter object (the reference object) is used to provide the light for the wavefront sensor to correct the perturbed wavefront. The adaptive optics system will not perfectly correct for the

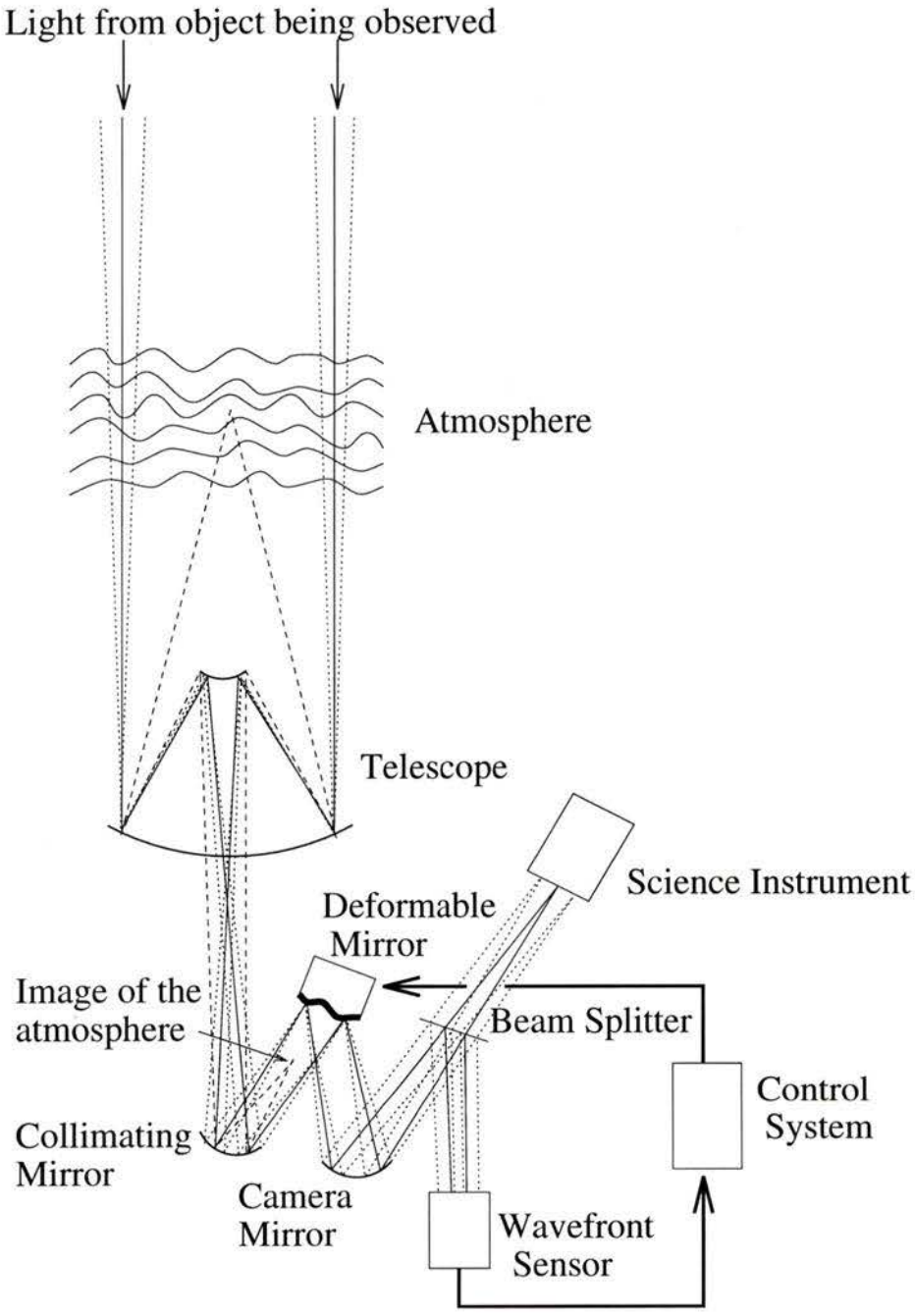

Figure 2.1: Single deformable mirror pupil conjugate adaptive optics system

perturbed wavefront of the science object because the wavefronts pass through slightly different paths in the atmosphere. This degradation of wavefront correction due to the science object not being coincident with the reference object is the isoplanatic effect. The angular area of the sky in which the degradation in the ability to correct the wavefront due to the isoplanatic effect is less than $\lambda/6$ RMS on the wavefront in the mean observing wavelength is termed the isoplanatic angle [42]. The adaptive optics system corrects, with a high degree of accuracy, objects within the isoplanatic angle.

The adaptive optics control system is operated in a closed loop system. The control system applies a phase correction $\phi_c(\mathbf{r}, t)$ to the deformable mirror such that the measured phase distortion by mirror $\phi_m(\mathbf{r}, t)$ is a minimum.

2.2 Characteristics of the Atmosphere

The random fluctuation in the physical properties of the atmosphere that cause the wavefront perturbations have been characterized in terms of statistical structure functions. The most successful statistical model was by Kolmogorov [7, 60]. In general, the statistical structure function for mean-square velocity difference between two points in the atmosphere, separated by a displacement vector $\mathbf{r}$, can be expressed as the tensor D_{ij}, defined in equation 2.2.

$$D_{ij} = \langle [v_i(\mathbf{r}_1 + \mathbf{r}) - v_i(\mathbf{r}_1)] [v_j(\mathbf{r}_1 + \mathbf{r}) - v_j(\mathbf{r}_1)] \rangle \tag{2.2}$$

Kolmogorov assumed that the velocity in the atmospheric medium is locally homogeneous, isotropic, and the turbulence is incompressible. With these assumptions, the tenser 2.2 is reduced to a single structure function 2.3.

$$D_v = \langle [v_i(\mathbf{r}_1 + \mathbf{r}) - v_i(\mathbf{r}_1)]^2 \rangle \tag{2.3}$$

When the separation $\mathbf{r}$ is within the inertial subrange of turbulence, the Kolmogorov spectrum is said to be valid. For this range of $\mathbf{r}$ the structure function obeys a 2/3 power law shown in equation 2.4.

$$D_v = C_v^2 \mathbf{r}^{2/3} \; ; \; l_0 < \mathbf{r} < L_0 \tag{2.4}$$

Where C_v^2 is referred to as the velocity structure constant, and is related to the energy in the turbulence. The inertial subrange of turbulence is valid for $\mathbf{r}$ greater then l_0, the small eddy size, where viscous effects due to molecular friction become dominant. The large eddy size, L_0, is the upper limit where the turbulence is isotropic. The inertial subrange l_0 to L_0 can be approximated to the order of a few millimeters to a few meters.

The velocity structure has been related to the index of refraction structure for Kolmogorov turbulence. This resulted in expression 2.5 which describes the structure of the mean-square difference of refractive index D_n for two points separated by a displacement vector $\mathbf{r}$.

$$D_n = C_n^2 \mathbf{r}^{2/3} \; ; \; l_0 < \mathbf{r} < L_0 \tag{2.5}$$

The refractive index structure constant C_n^2 is similar to the structure constant for the velocity and is also a measure of the strength of turbulence. C_n^2 is not constant throughout the atmosphere as it varies with altitude, location, and current weather conditions. The measurement of C_n^2 is needed for the derivation of the system parameters for adaptive optics systems and the optimization of multiconjugate systems.

2.3 System Parameters

The atmospheric seeing at the ground for a given C_n^2 distribution in the atmosphere is characterized by Fried's parameter, r_0. Fried's parameter is the correlation length of the atmosphere and it is defined as the maximum lateral size of a wavefront observed at the ground where the wavefront deformations are less than $\lambda/6$. The theoretical value of r_0 is calculated using the equation 2.6.

$$r_0(\lambda, \zeta) = 0.185\, \lambda^{6/5} cos^{3/5}(\zeta) \left(\int_0^H C_n^2(h) dh \right)^{-3/5} \tag{2.6}$$

The mean observing wavelength is λ, and ζ is the zenith distance (the angle the object is from the zenith). It is important to note that r_0 scales with wavelength to the power of six fifths. The implication is a larger r_0, and thus, less wavefront distortion at longer wavelengths. Many of the current efforts in adaptive optics are targeted to operate in the infrared to take advantage of the larger correlation length.

The isoplanatic angle, θ_0, is the field of view over which the wavefront distortions, due to the isoplanatic effect, are less than $\lambda/6$ RMS in the mean observing wavelength. The isoplanatic effect is the difference in wavefront distortions between the reference object and the target object due to the differing path followed by the light through the atmosphere because of the angular separation of the objects. The isoplanatic angle is given to a good approximation by equation 2.7.

$$\theta_0 = 0.314 r_0 / H_{av} \tag{2.7}$$

H_{av} is the average distance to the seeing layer and is calculated using equation 2.8.

$$H_{av} = sec(\zeta) \left(\frac{\int_0^H C_n^2(h) h^{5/3} dh}{\int_0^H C_n^2(h) dh} \right)^{3/5} \tag{2.8}$$

The time scale at which the wavefront changes is characterized by coherence time, τ_0. This is the time scale at which the wavefront can be considered to be the same. The reciprocal of this is the frequency at which corrections to the wavefront must be made. The coherence time for a wind velocity profile $V(h)$ is given by equation 2.9.

$$\tau_0 = \frac{0.314\, r_0}{\left(\int_0^H C_n^2(h)\, V^{\frac{5}{3}}(h)\, dh \,/\, \int_0^H C_n^2(h) dh \right)^{-3/5}} \tag{2.9}$$

The atmospheric parameters, r_0, τ_0 and θ_0, completely characterize the atmospheric turbulence for single conjugate adaptive optics systems. Typical values of these parameters for a good site taken from Merkle [31] are given in table 2.3.

λ	$0.5\,\mu m$	$2.2\,\mu m$	$5.0\,\mu m$	$10\,\mu m$
r_0	$10\,cm$	$60\,cm$	$160\,cm$	$360cm$
τ_0	$6\,ms$	$35\,ms$	$95\,ms$	$220\,ms$
θ_0	$1.8\,arcseconds$	$10\,arcseconds$	$30\,arcseconds$	$70\,arcseconds$

Table 2.1: Typical atmospheric parameters

2.4 Deformable Mirrors

The deformable mirror applies the phase correction to the wavefront as determined by the control system and the wavefront sensor. An excellent review of deformable

mirror technology is given by Ealey[10] and also by Ribak [36]. A brief overview of deformable mirrors is given here.

The deformable mirror consists of a reflective substrate and a number of actuators which are able to deform the shape of the mirror to correct the wavefront. There are three common substrates used in deformable mirrors: segmented, continuous faceplate, and membrane.

The segmented mirror consists of a mirror substrate which is cut into a number of separate segments. The segments are bonded to either one or three actuators. With one actuator per element only a piston movement is avaliable over each element. With three actuators per element the tip/tilt and piston of each element can be controlled. The most common actuators used for segmented mirrors in adaptive optics are stacked piezoelectric actuators. In this actuator many thin layers of piezoelectric material are stacked on top of each other to provide the necessary stroke length to operate the deformable mirror.

The advantage of the segmented deformable mirror is the independent control of each segment or zone of the mirror. The main problem with the segmented deformable mirror is light diffraction from the spaces between the mirror segments. This causes spurious features in the image formed by the adaptive optics system.

The continuous faceplate mirror is made by bonding actuators to a single thin flexible mirror. Two configurations for mounting the actuators to the mirror surface are commonly used, a piston configuration and a bending moment configuration. In the piston configuration one side of the actuator is bonded to a rigid surface and the other is bonded to the mirror substrate. The actuators work to deform the mirror by pushing or pulling the surface with respect to the rigid surface. In the bending moment configuration both ends of the actuator are bonded to the mirror surface in a configuration to cause the surface of the mirror to flex when the length of the actuator

is changed. The stacked piezoelectric actuator is the actuator which is normally used for continuous faceplate deformable mirrors. The continuous nature of the mirror substrate must be considered when controlling these mirrors. Each actuator deforms the surface of the mirror in a characteristic way dependent on the faceplate material and the influence of the neighboring actuators. The shape of deformation by the actuator is described by the influence function. To obtain a specific surface shape a calculation has to be made by inverting the influence function to obtain the necessary control voltages for the actuators.

The membrane deformable mirror uses a thin membrane surface as the mirror substrate. The thinner substrate surface permits a larger deformation of the mirror surface than the continuous faceplate deformable mirror. The disadvantage of the thin substrate is spurious vibration of the mirror surface due to mechanical and acoustic noise. The membrane mirror must be carefully isolated from the environment.

There are two kinds of membrane mirrors, the electrostatic and bimorph. The electrostatic membrane mirror uses electrostatic actuators in a piston configuration. The deformable mirror is constructed with membrane made of a conductive material. Electrodes are placed behind the membrane to form a capacitor between the mirror surface and the electrode, forming the electrostatic actuator. Because the electrostatic force between the surface is only attractive the actuators must be biased to allow a bidirectional control of the mirror surface. This bias creates a parabolic deformation of the mirror surface that must be included in the design of the adaptive optics system. An alternative to biasing the actuators is to place a second set of transparent electrodes on a window paced in front of the deformable mirror. This requires a second set of control electronics for the electrodes on the window.

Vdovin and Sarro[62] have recently fabricated an electrostatic deformable mirror using bulk micromachining. The electrodes are micromachined onto a silicon wafer

using process developed for integrated circuit manufacture. The prototype mirror was a $10.5mm$ square mirror with nine electrodes. The result has the potential of a low cost deformable mirror which can be mass produced.

The bimorph mirror is constructed by bonding a sheet of thin piezoelectric material to a thin mirror with a conductive backing. Electrodes are bonded to the back of the piezoelectric material forming a circuit between the electrode and the conductive backing on the mirror. When a voltage is applied to the circuit the piezoelectric material bends, flexing the mirror surface. The stroke of the bimorph mirror is limited by the fragility of the ceramic piezoelectric material which limits the thickness of piezoelectric material that can be bonded to the mirror.

The optical engineer must ensure that there is enough clearance around the deformable mirror for the mirror support and actuator control cables. On average, a volume in the shape of a cylinder with a diameter equal to twice the clear aperture, and a depth equal to it's clear aperture provides the necessary clearance for the deformable mirror.

2.5 Wavefront Sensors

The wavefront sensor measures the wavefront of the reference object and determines the distortions due to the atmospheric turbulence. There are three types of wavefront sensors which are commonly used in adaptive optics systems. These are the Shack--Hartman, shearing interferometer, and curvature wavefront sensors. All of these wavefront sensors have similar characteristics in terms of single photon noise [47].

2.5.1 Shack-Hartman Wavefront Sensors

The Shack-Hartman wavefront sensor is a modification of the classical Hartman test used in optical shop testing [30]. In the Hartman test a diaphragm with small apertures is placed in front of the element under test. The apertures are positioned on the diaphragm to test a specific zone on the element under test. By analyzing the resulting image formed by the apertures the aberrations of the lens can be determined.

In the Shack-Hartman wavefront sensor, the diaphragm is placed at a pupil of the system and lenses are placed in the apertures of the diaphragm to form a lenslet array. A diagram of the Shack-Hartmann is shown in figure 2.2. The position of the image formed by each lenslet determines the local wavefront tilt for the respective aperture covered by the lenslet. The sensor was first produced by Shack and Platt in 1971 [51].

The advantages of the Shack-Hartmann wavefront sensor are the high optical efficiency, white light capability, wide dynamic range, and no phase ambiguity. The disadvantages are, high sensitivity to alignment and flexure errors, and difficulties in manufacturing the lenslet array. Various techniques have been proposed to reduce alignment and flexure errors.

The most common methods to reduce alignment errors are the introduction of a reference beam to calibrate the wavefront sensor and the introduction of a modulated reference beam as well as a nutating mirror as in the integrated imaging irradiance (I^3, "I-cubed") sensor [60]. In the I-cubed sensor the modulated reference beam and the wavefront being measured are nutated using a mirror so they describe a small circular path on a quad-cell detector at the focus of the lenslet. The time that each spot spends in each quadrant of the quad cell is used to determine the center of the circular path described by the two moving spots. The modulation of the reference

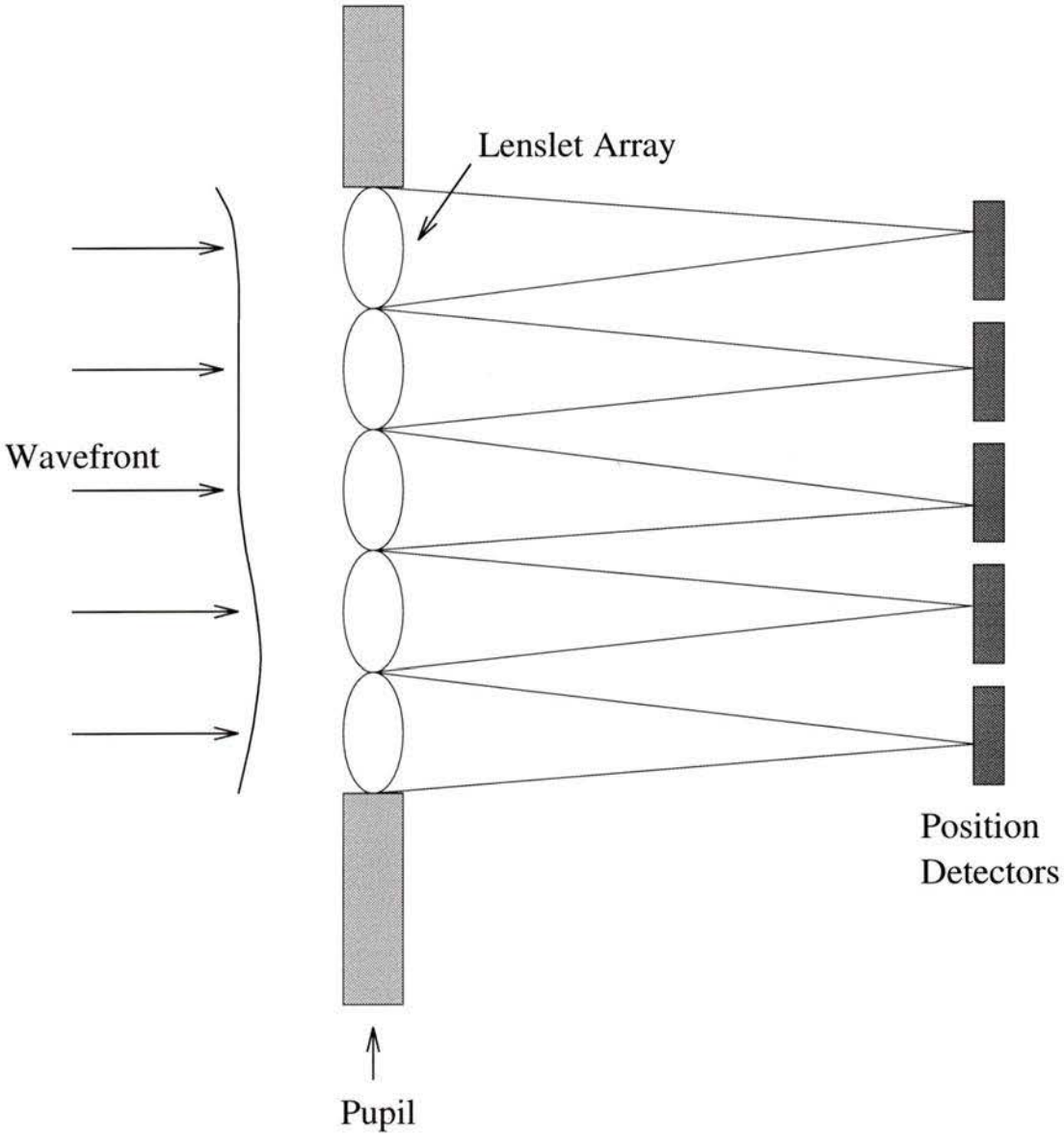

Figure 2.2: Schematic of the Shack-Hartmann wavefront sensor

beam is used to distinguish the spot generated by reference beam and spot generated by the wavefront being measured.

Another method to reduce cost and alignment errors has been used by LASERDOT[16]. They have developed an integrated CCD and lenslet array system termed the 'micro Shack-Hartmann' wavefront sensor. A micro lens array of $69\mu m$ diameter, $500\mu m$ focal length lenses is etched directly onto the CCD window. The CCD used for the system has $23\mu m$ pixels so there are 3 pixels for each sub-aperture. The 'micro Shack-Hartmann' wavefront sensor made by LASERDOT has $5X5$ sub-apertures. This method of making the lenslet array by etching the CCD window provides a rugged assembly with minimal alignment and flexure errors.

2.5.2 Shearing Interferometer Wavefront Sensors

Shearing interferometers use the principle of self referencing to produce an interferogram of a wavefront without the use of a plane reference wavefront. With self referencing the resulting interferogram is a map of regions of constant slope rather than a contour map that is produced when a plane reference wavefront is used. The advantage of a map of constant slope is the ability to determine the sign of the slope on the wavefront. Because the sign of the slope is known the valleys and peaks on the wavefront can be distinguished.

The most common method of producing the shear is with the use of diffraction gratings. The dual-frequency grating shearing interferometer [60] uses a special grating with two different line spacings, d_1 and d_2. This dual-frequency grating is a specially manufactured grating with the two different sets of lines on the single grating. The dual-frequency grating is equivalent to two gratings, one of line spacing d_1, and the second of line spacing d_2, being superimposed on top of each other. Two

resulting first order beams are produced with a shear of $\Delta\Theta = \lambda(1/d_1 - 1/d_2)$. Since the diffraction by the grating is wavelength dependent, a second grating must be placed after the dual-frequency grating to allow the system to be used with white light. The line spacing of the second grating is $(d_1 + d_2)/2$ to make the absolute fringe position independent of wavelength.

To detect the fringe pattern an imaging lens is placed after the second grating to produce an image on a detector array. The phase is determined by modulating the interference pattern by translating the dual frequency grating perpendicular to its rulings. This translation is usually accomplished by making the dual-frequency grating an annulus on a disk with ruling lines orientated radially from the center of the disk and rotating the disk about it's axis. The translation of the grating introduces a Doppler shift in the phase. The Doppler shift will cause the intensity at the array detector to temporally vary at each point in a sinusoidal pattern, phase shifted by the fringe pattern due to the slope of the wave front being detected. The time of the zero crossing point of the signal is used to determine the slope of the wavefront being detected. A schematic diagram of a dual-frequency lateral shearing interferometer is shown in figure 2.3. An interferometer as shown in figure 2.3 would measure the slope in one axis only. A second set of gratings are required to produce an orthogonal set of measurement and a complete wavefront map. The primary advantage of the shearing interferometer is its ability to be used with extended objects. For this reason is it the choice wavefront detector for use in adaptive optics systems with military and planetary targets.

2.5.3 Curvature Wavefront Sensors

The curvature wavefront sensor measures the local curvature of the wavefront[46]. There are two different methods which have be used to measure the local curvature

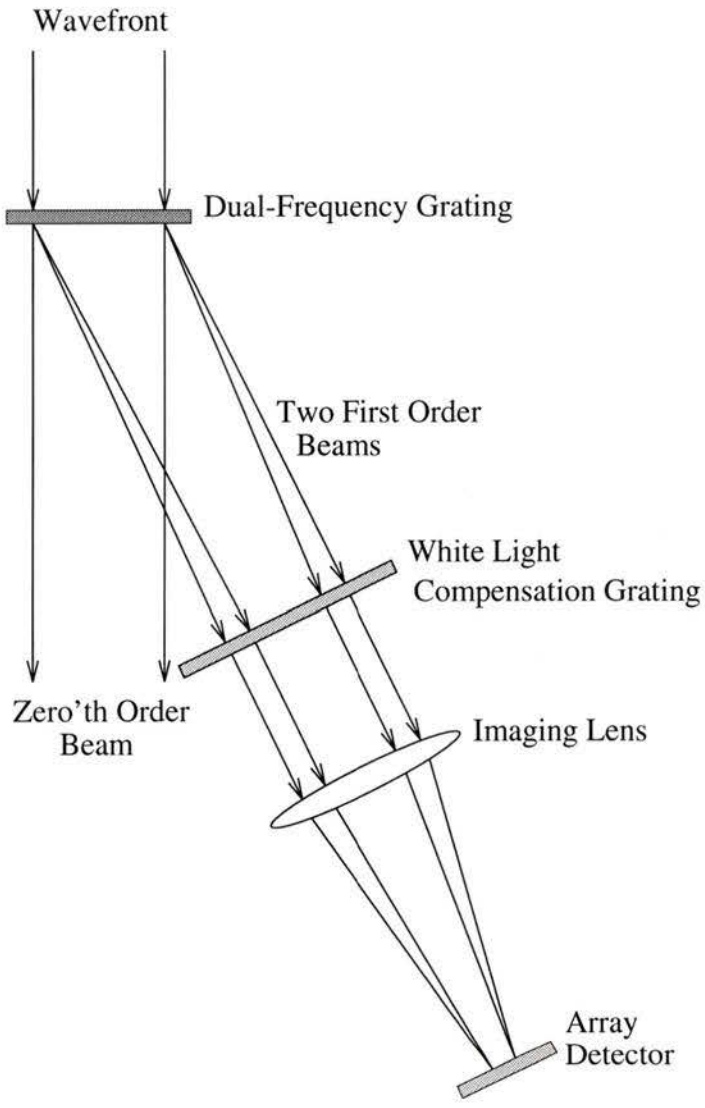

Figure 2.3: Schematic of a dual-frequency lateral shearing interferometer

of the wavefront. The first method measures the local curvature by measuring the irradiance distribution before and after the focal plane of the system, and taking the difference of these two measurements. For this method to work the blur of the object at the positions before and after the focal plane must be much smaller than the scale of the wavefront distortion being measured. This limits the curvature wavefront sensor to use with guide objects which are point sources. The sensitivity of the wavefront sensor can be adjusted by changing the distance before and after the focal plane that the irradiance is measured.

The second method measures the local curvature by measuring the irradiance distribution before and after an image of the pupil, and taking the difference of these two measurements. This method has the advantage that the size of the image on the detector changes very little when the sensitivity is adjusted by changing the distance before and after the pupil that the irradiance is measured.

The output of the wavefront sensor, the local curvature, must be integrated twice to obtain the wavefront map. When the curvature wavefront sensor is used with a membrane mirror it is not necessary to convert the local curvature to the wavefront map. This is because the curvature of the membrane mirror is proportional to the signal applied to the actuator. The output from the curvature sensor, the local curvature, can be used to control the shape of a membrane mirror, to compensate the wavefront, with minimal signal processing.

2.6 System Performance Estimation

The expected performance for an adaptive optics system can be estimated from the system parameters [59, 60]. The performance of the adaptive optics system is normally expressed in terms of the Strehl ratio of the corrected image. The Strehl ratio is

defined as the ratio of the peak intensity to theoretical peak intensity for the image profile of an un-aberrated diffraction image of a point light source. The Strehl ratio is directly related to the RMS wavefront variance σ^2 by equation 2.10.

$$Sr = exp(-\sigma^2) \tag{2.10}$$

The RMS wavefront variance is defined by equation 2.11.

$$\sigma^2 = \int \Psi^2 dA \tag{2.11}$$

By using Kolmogorov statistics the RMS wavefront variance for a system with no adaptive optics correction can be calculated. For a system with an aperture D the variance is given by equation 2.12.

$$\sigma^2 = 1.03 \left(\frac{D}{r_0}\right)^{5/3} \tag{2.12}$$

A number of systems have been developed that only correct for the tip and tilt of the image [20, 33, 40]. For these systems the RMS wavefront variance is given by equation 2.13. The variance is reduced by a factor of 7.6 for systems with only tip tilt correction over the uncorrected image.

$$\sigma^2 = 0.135 \left(\frac{D}{r_0}\right)^{5/3} \tag{2.13}$$

The wavefront variance can be broken down into a sum of contributing factors in relation to the system. Equation 2.14 represents a decomposition of the variance into four independent factors.

$$\sigma^2 = \sigma^2_{fit} + \sigma^2_{temp} + \sigma^2_{WFS} + \sigma^2_{iso} \tag{2.14}$$

The deformable mirror fitting variance, σ^2_{fit}, is expressed by equation 2.15.

$$\sigma^2_{fit} = \kappa \left(\frac{r_s}{r_0}\right)^{5/3} \tag{2.15}$$

Where κ is the fitting constant and r_s is the actuator spacing. Estimates of the fitting constant range from 0.2 to 1.302 depending on the deformable mirror.

The variance due to the limited response time in the feedback loop is expressed in σ^2_{temp}. This factor is dependent on the control bandwidth of the servo loop, f_c and the effective transverse wind velocity V, as expressed in equation 2.16.

$$\sigma^2_{temp} = \left(\frac{0.4V}{r_0 f_c}\right) \tag{2.16}$$

The wavefront sensors contribution to the variance is expressed in σ^2_{WFS}. Expression for the variance have been derived for the shearing interferometer and the Shack-Hartman sensor. The variance for the shearing interferometer is expressed in equation 2.17.

$$\sigma^2_{WFS(S)} = \frac{2d_s^2}{\pi\gamma^2 n s^2} \tag{2.17}$$

The fringe visibility is γ, n is the number of photons per sub-aperture per integration time, s is the shear distance, and d_s is the sub-aperture spacing.

The variance for the Shack-Hartmann sensor is given by equation 2.18. It is dependent on the *SNR* (Signal to Noise Ratio) of the sensor.

$$\sigma^2_{WFS(SH)} = \frac{0.35\pi^2}{4(SNR)^2} \tag{2.18}$$

The variance due to the anisoplanatism between the reference object and science object is expressed in σ^2_{iso}. For an angular deviation of θ between the reference object and the science object the variance is given by equation 2.19.

$$\sigma^2_{iso} = \left(\frac{\theta}{\theta_0}\right)^{5/3} \tag{2.19}$$

From these expression the expected system performance can be derived for a given system configuration. The inversion of these expression can be used to optimize an adaptive optics system based on a target performance. The expected performance for adaptive optics systems currently under construction or in use is in the range of 0.1 to 0.9 Strehl Ratio [61].

Chapter 3

Atmospheric Turbulence Profiles

The vertical profile of atmospheric turbulence determines the system parameters for adaptive optics systems. The atmospheric turbulence is normally quantified with the refractive index structure constant C_n^2. There are several methods for measuring the C_n^2 distribution as well as empirical models.

The most complete model is the Hufnagel-Valley-Boundary model [60]. This model is based on experimental observations and is an extension of a Hufnagel's model by Valley and Ulrich to include the effects of anisoplanatism and the boundary layer. This model is expressed in equation 3.1.

$$C_n^2(h) = A\left[2.2\times 10^{-23}h^{10}e^{-h}\left(\frac{V}{V_0}\right)^2 + 10^{-16}e^{-h/1.5} + 1.7\times 10^{-14}e^{-h/0.1}\right] \qquad (3.1)$$

Where V is the upper atmospheric wind speed, V_0 is the mean upper atmospheric wind speed, and h is the height in kilometers.

Variation in environmental conditions from location to location cause large variation in the C_n^2 profile. Because of the large variation, general models such as the

Hufnagel-Valley-Boundary model only provide an approximation of the C_n^2 profile for a site. The C_n^2 profile is site dependent and must be measured.

The C_n^2 profile can be measured directly using optical methods or indirectly by measuring the temperature structure constant C_T^2. The modern direct method of measurement is through SCIDAR (Scintillation Detection and Ranging) [14, 63]. The SCIDAR method is based on the statistical analysis of the scintillation of a double star. A large number of high speed images with exposures the order of a millisecond are taken at the pupil to provide a statistical sample of the speckle pattern of the star pair. The speckle patterns of the two stars produced by a specific layer will be the same but shifted because of the angular separation of the stars. By statistically analysing the correlation of the speckle patterns of the two stars the vertical C_n^2 profile is determined. The SCIDAR method can determine the vertical C_n^2 profile with a resolution of about 1 km at a rate of one profile per a minute.

The most common indirect method is the measurement of the temperature gradient using temperature sensors flown from an air balloon [3, 63]. The temperature structure constant C_T^2 is determined from a pair of temperature probes mounted at a know distance using equation 3.2. The Kolmogorov turbulence spectrum is assumed to be valid.

$$C_T^2 = D_T(r) r^{-2/3} \tag{3.2}$$

The refractive index structure constant C_n^2 is then determined with equation 3.3 using the relationship between the refractive index and the temperature and pressure of air.

$$C_n^2 = \left[\frac{79.9 P(h)}{(T(h))^2} \times 10^{-6} \right]^2 C_T^2(h) \tag{3.3}$$

where $P(h)$ is the atmospheric pressure in millibars and $T(h)$ is the temperature in Kelvin. The vertical resolution using the balloon measurement is typically $6m$ for an ascent speed of $4m/s$ where the total time for a complete profile to 25km is 100 minutes.

Balloon measurements by Bufton [15] show a general agreement with the Hufnagel model but with strong random C_n^2 fluctuation over small altitude increments. These fluctuations indicate a layered turbulence with an average layer thickness of $100m$ to $200m$.

The layered structure of the C_n^2 profile has also been observed by Caccia [8], Tallon [57, 58], and Racine [35]. Caccia reported observation of three predominant layers at altitudes of 0.5 , 2, and $12.5km$ at Observatoire de Haute-Provence (OHP, South of France, 800m above sea level). A fourth layer was occasionally observed at $4km$.

Tallon studied the C_n^2 profiles at Observatorio del Roque de los Muchachos (La Palma, Canary Islands, 2200m above sea level), OHP, and La Silla (Chile, 2350m above sea level). The data consisted of four balloon soundings from La Palma and OHP, and ten nights of SCIDAR data taken at La Silla.

The balloon data was analysed to determine the relative distribution of the turbulence by integrating the C_n^2 profile over $100m$ slabs. Using this analysis the relative contribution of each layer to the overall seeing can be determined. Tallon found that the turbulence was extremely concentrated in very few intense layers. In three cases an average of 80% of the turbulence was concentrated in three layers of an average thickness of $250m$, and in the remaining data set 62% of the turbulence was concentrated in one layer $200m$ thick. The ten nights of SCIDAR data from La Silla was averaged together. The average C_n^2 profile still showed pronounced layers at $6km$, $11km$, and $17km$.

The most complete analysis of C_n^2 profiles is by Racine [35]. Racine analysed

414 SCIDAR profiles taken at Canada-France-Hawaii Telescope (CFHT, Mauna Kea, Hawaii, 4,200m) by F. Roddier. An example of one profile is given in figure 3.1. Racine found that frequently a single dominant layer was present. The altitude of the layer was stable for many days, while the strength was highly variable. The layer was typically at an altitude between 2km and 4km. Occasionally a dominant layer was observed between 6km to 8km. Layers above 8km were uncommon.

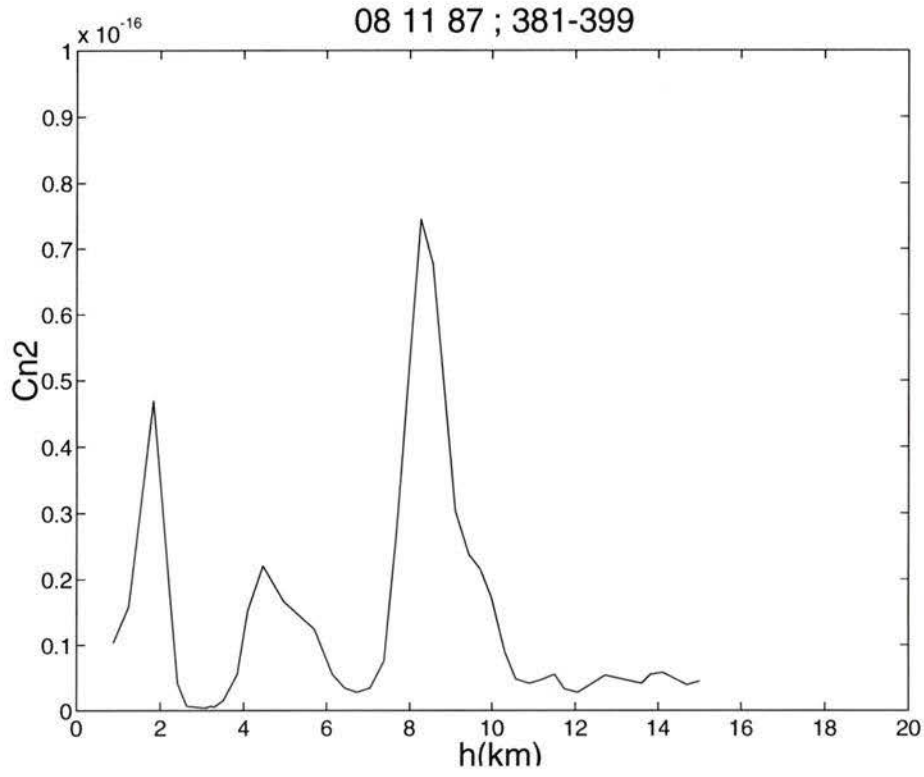

Figure 3.1: C_n^2 profile on Nov. 8, 1987. FWHM seeing was 0.47 arc-seconds

Three profile classes were defined to classify the turbulence profiles observed. Class 1 represented a profile with a single layer which had a peak $3X$ higher than any other feature in the C_n^2 profile. This profile class was the most common, occurring 60% of the time. Class 2 represented the profiles with two dominant layers. The class

2 profile occurred 15% of the time. The class 3 profile represented the profiles with more than two dominant layers or no dominant layer, and this occurred 25% of the time.

Racine proposed a configuration where a deformable mirror is placed conjugate to the dominant layer which would compensate only that layer. A second mirror would then compensate the residual profile. Modeling showed that the mirror conjugate to the dominant layer would on average reduce the image spread by a factor of two from an uncorrected image. The second mirror would only need half the actuators of a system with one deformable mirror because the residual r_0 is twice as large.

Racine determined the average background profile by clipping the dominant layers from the individual profiles and then averaging them. This profile represented the theoretical residual profile remaining if a deformable mirror were to compensate the dominant layer perfectly. The average background profile is given in figure 3.2.

In summary, current research has shown that the turbulence is often concentrated in layers rather than being continuously distributed in the atmosphere. If a single mirror was place conjugate to the dominant layer and compensated for the dominate layer the residual turbulence would be considerably reduced. This multiconjugate adaptive optics system, where the deformable mirrors are placed in a serial configuration, would have an increased isoplanatic patch due to the reduced path differences for the off axis rays from the deformable mirror sub-apertures. In an optimal configuration the number of actuators would not be increased over a single conjugate system because the r_0 of the residual profile would be less after the correction for the dominant profile [4].

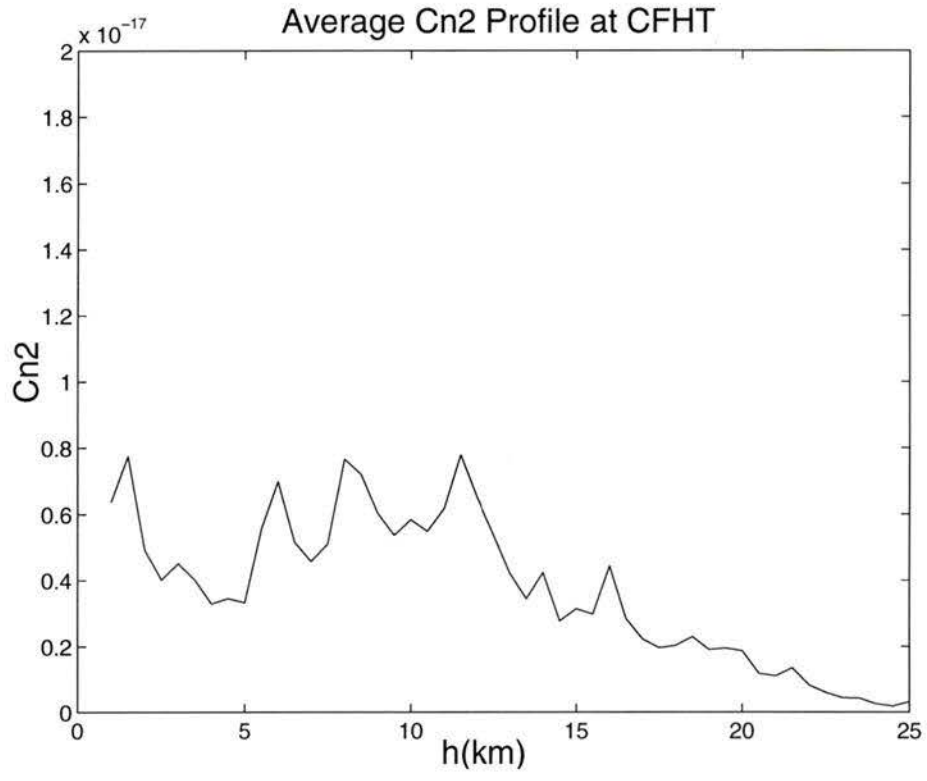

Figure 3.2: Average SCIDAR C_n^2 background profile above Mauna Kea

Chapter 4

Multiconjugate Adaptive Optics

In multiconjugate optics several deformable mirrors conjugate to different heights are used to correct the distortions of the atmosphere rather than a single mirror conjugate to the entrance pupil of the telescope. The objective is to increase the isoplanatic angle by sectioning the atmosphere into layers with each deformable mirror correcting for the wavefront distortions of its conjugate layer. This sectioning of the atmosphere into serially corrected layers will reduce the path differences for the off axis rays increasing the isoplanatic angle.

The principle of using multiconjugate optics to increase the isoplanatic angle was suggested by Dicke [9] in 1974 and Foy [21] in 1985. The advantages of multiconjugate correction was outlined in Dicke's work but there was no detailed analysis of the expected performance. The first analytical analysis of the principle was by Beckers [4, 6, 5]. Beckers' analysis showed that multiconjugate optics can substantially increase the isoplanatic angle for an atmospheric model with a constant C_n^2 distribution. Beckers also showed, for the case of a constant C_n^2 distribution, that a serial arrangement of deformable mirrors in a multiconjugate adaptive optics system is superior to a parallel arrangement of a single conjugate adaptive optics systems (A

parallel arrangement of single conjugate adaptive optics systems is a number of complete independent adaptive optics systems working beside each other to increase the field of view). Beckers determined that for a serial arrangement the size of the sub-aperture on the deformable mirror which corrected for it's segment of the atmosphere would be larger than the size of the sub-aperture on the single deformable mirror used in the single conjugate adaptive optics system. The total number of actuators in the multiconjugate system was calculated to be less than for a single conjugate system. Beckers conceptualised a method for determining the three dimensional map of wavefront distortions for the control of the deformable mirror in the multiconjugate adaptive optics system but no detailed analysis was done.

Beckers' research was followed by work by Tallon [56, 57, 58] who analyzed the problem of determining the three dimensional map of the wavefront distortions using sodium laser guide stars. Laser guide stars were considered because of the low probability of finding the satisfactory natural guide stars in a random field in the sky. The sodium laser guide star is formed by exciting the $95km$ high, $10km$ thick layer of sodium atoms in the mesosphere using a laser tuned to the sodium D_2 line ($598nm$) [12]. Tallon determined that for the simplest multiconjugate system, where there are two deformable mirrors, one conjugate to the low level turbulence and a second conjugate to the high level turbulence, wavefront distortions for these regions could be determined using as few as three sodium laser guide stars and one natural guide star. The natural guide star is needed because of the inability of the laser guide stars to determine the tip-tilt of the science object because the laser light returns along the same path as it originates. The wavefront distortions of the layers are found by using tomographic mapping techniques similar to what is used in ultrasonic medical imaging.

The problem of determining the three dimensional map of the wavefront distor-

tions has been explored by several other researchers [25, 26, 27, 37, 52, 65]. In these papers several algorithms have been proposed to determine the three dimensional map of wavefront distortions from the wavefront measurements. Some of these algorithms have been numerically simulated to estimate the gain in isoplanatic angle. These simulations have shown that an appreciable gain in isoplanatic angle can be made by multiconjugate adaptive optics using multiple guide stars to determine the three dimensional map of the wavefront distortions.

The optimal placement of the deformable mirrors for a particular vertical distribution of turbulence has been investigated by Yan [66] and Wallner [64]. They have determined the optimal placing of the deformable mirrors for a given distribution to obtain the largest gain in isoplanatic angle.

One of the major limitations of adaptive optics is the requirement of a natural guide star to determine the tip-tilt of the object. Work has also been done by Foy [19, 22] to solve the problem of determining the tip-tilt of the object using laser guide stars. When the sodium layer is stimulated with the same wavelength of light as the light emitted from the sodium layer the light returns along the same path as it originates and the tip-tilt of the science object can not be determined, only higher order terms can be determined. Foy researched the idea of using two different wavelengths of laser light to stimulate the sodium layer so the returned light would be at a different wavelength than the stimulating light. It was calculated that the dispersion of the atmosphere provided enough difference in path to provide an indication of the tip-tilt of the object and, with current laser technology, a bright enough guide star can be produced for the tip-tilt to be measured. This eliminates the need for the natural guide star in the adaptive optics system. This method of sensing the tip-tilt by using a polychromatic artificial star has been shown to be theoretically feasible but it has yet to be implemented in a working system so the actual performance is not known.

The limitations of using a natural guide star with a laser guide star system was studied by Olivier and Gavel [33]. The limiting error in the correction of tip-tilt is the higher-order aberrations of the star. Because these higher-order aberrations are asymmetrical the system can not differentiate between these aberrations and the centroid of the beam when measuring the tip-tilt of the object. If multiple stars are measured to improve the signal to noise ratio an asymptotic limit is reached where the error is dominated by the higher-order aberrations in the beam because the asymmetrical aberrations are not statistically independent between the multiple stars. When the higher order aberrations are corrected with the laser guide star system the error in the measurement of the tip-tilt is significantly reduced. Significant gain can be made with multiple measurements of the tip-tilts of several natural stars because the asymptotic limit due to the higher aberrations has been reduced by the laser guide star system. Also, when the tip-tilt of the natural guide star is measured in a laser guide star system, the whole aperture of the telescope is used so much more light is available as compared to a non-laser guide star system where the aperture is divided into sub-apertures equal to the seeing cell size. Olivier and Gavel concluded that if the laser guide star system corrects the high order aberrations of the natural guide star the limitation of the requirement of a natural guide star to determine the tip-tilt of the object is significantly reduced because several fainter natural guide stars can be used.

In Oliver and Gavel's example calculation of the limiting resolution of a telescope with a $10m$ aperture, he found that, without correction, the limiting resolution due to the asymmetrical aberrations is 4.4 times the diffraction limit of the telescope. When the distribution and intensity of the stars are considered the resolution of tip-tilt correction obtainable for at least 99% of all objects in the sky is 8.5 times the diffraction limit for one reference star and 7.3 times the diffraction limit when two

reference objects are used. When the higher order aberrations are corrected with a laser guide star system the resolution of tip-tilt correction obtainable for at least 99% of all objects in the sky is 4.2 times the diffraction limit for one reference star and 2.9 times the diffraction limit when two reference objects are used. For a sky coverage of at least 1% of all the objects in the sky the resolution of tip-tilt correction obtainable is 1.8 times the diffraction limit of the telescope.

4.1 Predicted Gain in Isoplanatic Angle

Beckers produced the first analytical estimate of the gain in isoplanatic angle by using multiconjugate optics. Figure 4.1 shows a schematic view of the atmosphere for the case where all the turbulence is concentrated in one thin layer at a height h above the telescope. As shown in the figure the ray paths of the reference object and the science object are coincident at the pupil of the telescope, which is at ground level. In single conjugate adaptive optics systems the deformable mirror is placed conjugate to the pupil of the telescope. At the turbulent layer, ray paths of the reference object and the science object are offset by an amount $\theta_0 * h$. This offset of the ray paths results in different wavefront distortions for the reference and the science object. This is the isoplanatic effect which limits the angular field of view which the adaptive optics system can correct. If the angle between the reference object and the science object is equal to the isoplanatic angle the linear separation between the reference object and the science object at the turbulent layer in relation to the correlation length of the atmosphere, r_0 , will be $0.314\,r_0$ from the definition of the isoplanatic angle in equation 2.7.

If the deformable mirror is placed conjugate to the turbulent layer the difference in path between the rays of the reference object and the science object is eliminated,

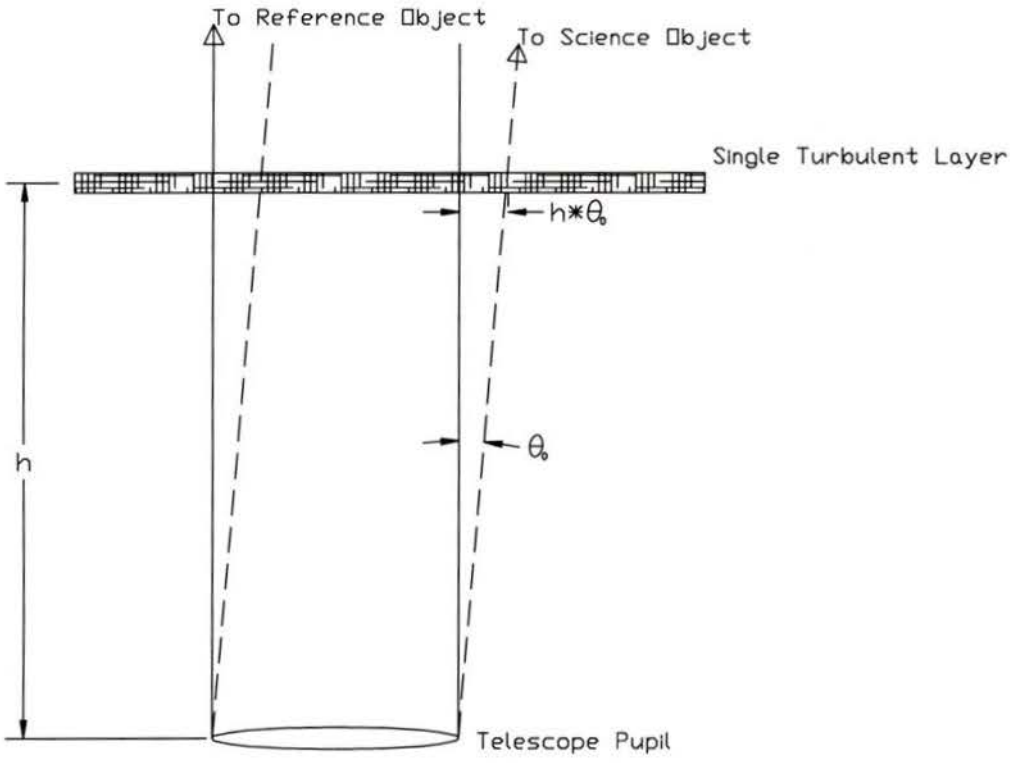

Figure 4.1: Schematic view of a single thin layer of turbulence

eliminating the isoplanatic effect. However, for a finite field of view the deformable mirror would have to be enlarged to cover the larger beam diameter at the height of the deformable mirror. Multiple reference objects would also be required to provide the wavefront information for the correction of the deformable mirror over the larger area. Another benefit of the deformable mirror being located at the turbulent layer is the elimination of scintillation effects, the intensity fluctuations over the field, which result from the turbulent layer acting as a lens. Alternatively, the pupil of the telescope could be moved from the ground level to the deformable mirror conjugate to the turbulent layer. This would reduce the effective aperture of the telescope but would allow a wide field of view with one reference object. This configuration, with the pupil of the telescope moved to the deformable mirror conjugate to the turbulent layer, would be applicable to large telescopes investigating large bright objects where the loss of light gathering capability, due to the pupil being moved, would be acceptable.

The configuration with the deformable mirror placed conjugate to the turbulent layer is termed a single-layer conjugate adaptive optics system. In reality, the atmospheric turbulence is not in one thin layer, but predominant layering is observed. From analysis of C_n^2 profiles by Racine [35] the profile class with a single peak $3X$ higher than any other feature in the C_n^2 profile occurred 60% of the time. When these seeing conditions are present the single-layer conjugate system would have a wider field of view than the single deformable mirror, pupil conjugate system. The field of view would still be limited by the residual turbulence not at the dominant layer and the size of the deformable mirror. The need for other reference objects to correct the larger deformable mirror or the loss of aperture (in the case of the pupil being moved to the deformable mirror conjugate to the turbulent layer) would also limit the field of view. The single-layer conjugate adaptive system would also require the altitude

of the turbulent layer to be determined.

This examination of a single-layer conjugate adaptive optics system illustrates the advantages of placing the deformable mirror conjugate to the turbulent layer. This type of adaptive optics system can provide a wider field of view than the single deformable mirror pupil conjugate system when the turbulence is predominantly concentrated in a single layer and the height of the layer is known. When more than one strong layer is present or no dominant layers are present, multiple deformable mirrors conjugate to different altitudes can be used to reduce the isoplanatic effect and increase the field of view of the system.

To produce an analytical estimate of the gain in isoplanatic angle, Beckers [4, 6, 5] used a simplified model of the average turbulence profile above the site Mauna Kea, Hawaii. He assumed a constant C_n^2 distribution from ground level at Mauna Kea (altitude 4.2 km above sea level) to a altitude of $10km$ above the ground level ($14.2km$ above sea level). Only observations close to the zenith were considered so the effects of the zenith angle were ignored.

In Beckers' model, he sectioned the atmosphere into N equal layers of thickness h_i. He then defined Fried's parameter, r_0, for each each layer , r_i, as shown in equation 4.1.

$$r_i = 0.185\ \lambda^{6/5} \left(\int_{h_i} C_n^2(h) dh \right)^{-3/5} (i = 1, ..., N) \tag{4.1}$$

r_0 can be expressed in terms of r_i as :

$$r_0^{-5/3} = \sum_i r_i^{-5/3} \tag{4.2}$$

with a constant C_n^2 distribution and equal height sections of atmosphere the above sum simplifies to :

$$r_0 = N^{-3/5} r_i \tag{4.3}$$

For each layer, the deformable mirror was considered to be at the mid point of the layer so the maximum lateral displacement of the rays within each layer is $\theta_i * (h_i/2)$ Since θ_i must be the same for all layers, θ_i is equal to θ_0 , the isoplanatic angle for the system. In a single deformable mirror pupil conjugate system the average displacement for the rays, at the average height of the turbulence, in terms of the correlation length r_0 is $0.314\,r_0$ as given in equation 2.7. Beckers assumed that a value of $0.63\,r_0$, twice the average displacement, would be acceptable for the maximum permissible lateral displacement of the rays in a section of atmosphere. He also assumed that the lateral displacement of the rays when assigned to each layer are less than the total permissible lateral displacement by $N^{-3/5}$ so the maximum permissable wavefront difference for each layer is $0.63\,r_i\,N^{-3/5}$. The predicted gain in isoplanatic angle as predicted by Beckers is found by equating the maximum lateral displacement of the rays to the maximum permissible lateral displacement :

$$\theta_0 * (h_i/2) = 0.63\,r_i\,N^{-3/5} \tag{4.4}$$

By Substituting equation 4.3 and h/N for h_i the expression becomes:

$$\theta_0 = 2N0.63r_0/h \tag{4.5}$$

Comparing equation 4.5 to equation 2.7 the predicted gain of $2N$ in isoplanatic angle, or $4N^2$ in isoplanatic area for Beckers' model is found. The gain in area in terms of the number of deformable mirrors is quadratic. The configuration of the deformable mirrors in a serial arrangement in the atmosphere in Beckers' model provides a substantial gain over a parallel arrangement (A parallel arrangement of single conjugate adaptive optics systems is a number of complete independent adaptive optics systems working beside each other to increase the field of view). where the gain is linear in terms of the number of deformable mirrors.

Beckers calculated the total number of actuators needed for the adaptive optics system as described in his model for the case of an 8 meter telescope. He assumed that there would be one actuator for each element of area with a diameter equal to the multiconjugate Fried's parameter defined for each layer, r_i, as given in equation 4.1. The increase in area of the deformable mirrors due to the distance from the pupil was also accounted for in his calculation. Beckers found that the total number of actuators was almost independent of the number of layers, N. The increase in r_i off sets the increase in beam size and number of deformable mirrors in the multiconjugate system.

The $2N$ gain in isoplanatic angle for a constant C_n^2 has been confirmed using a more detailed method of calculation by Wallner [64]. Wallner also calculated the gain in isoplanatic angle for the cases of exponential and Hufnagel-Valley-Boundary average C_n^2 profiles. It was found that the gain in isoplanatic angle was slightly better than N.

This reduction in gain in isoplanatic angle from the $2N$ in the constant C_n^2 profile to N is expected because in the exponential and Hufnagel-Valley-Boundary profiles there is a large concentration of turbulence at the low level and a large distance from the average height to the turbulence. No detailed analysis of the expected gain in isoplanatic angle for a strongly layered atmosphere has been done but it is expected [4, 25] that the gain would be greater than the case with the constant C_n^2 profile if the deformable mirrors were place in optimal locations.

4.2 Atmospheric Tomography

The problem of determining the three dimensional wavefront distortions has been explored by several researchers [4, 6, 5, 9, 25, 26, 27, 37, 52, 56, 57, 58, 65]. The

first method proposed was by Dicke[9] in 1975. He proposed to treat the atmosphere as a two layer system and to use the differential wind velocities of the low and high layers to deconvolve the turbulence profile. This method of deconvolution using the temporal characteristics is only viable when there is sufficient differential velocities between the layers. Beckers [4, 6, 5] proposed using the spacial characteristics of the atmosphere to deconvolve the three dimensional turbulence profile. By observing a number of guide stars at various angles from the ground a set of data consisting of position in the telescope pupil and angle can be accumulated. If the measurements are made so a sufficient number of rays from different object points pass through each coherent patch in each layer in which a deformable mirror in the multiconjugate adaptive optics system is placed the turbulence at each layer can be determined. The problem of determining the atmospheric turbulence profile is then reduced to solving a system of equations. This method of determining the three dimensional turbulence profile is similar to what is used in ultrasonic medical imaging where it is termed tomographic mapping.

Sodium laser guide stars are considered to be the best source for reference objects for determining the three dimensional turbulence profile because of the low probability of finding a sufficient number of natural guide stars. Tallon [56, 57, 58] analyzed the problem of using laser guide stars as the reference objects to determine the three dimensional profile of the atmospheric turbulence.

When laser guide stars are used as the reference objects the finite distance to the "star" which is ionization in the atmospheric sodium layer must be considered. The light from the $95km$ sodium layer propagates as a cone of light from the height of the sodium layer to the entrance aperture of the telescope. This property of conical propagation is termed focal anisoplanatism in the literature. Focal anisoplanatism results in two problems with the measurement of the turbulence in the atmosphere.

These are magnification of wavefront distortions and the reduced coverage of the atmosphere at high levels.

The magnification of the wavefront distortions results from the expansion of the beam as it propagates from the sodium layer. When the divergent beam is imaged in the wavefront sensor a wavefront distortion at the mid point between the ground level and the sodium level would appear magnified a factor of two with respect to a wavefront distortion at the entrance to the telescope. This magnification scales linearly between the entrance aperture and the sodium layer and must be factored into the system of equations used to determine the three dimensional atmospheric turbulence profile.

The reduced coverage due to focal anisoplanatism is a severe restriction on the maximum field of view which the laser guide stars can provide wavefront information. The beam diameter reduces with the height from the ground which reduces the maximum area that can be wavefront sensed. To compensate for this effect multiple laser guide stars must be used. The guide stars are arranged to provide full coverage of the volume above the telescope for wavefront sensing, compensating for the focal anisoplanatism. This effect of reduced coverage is also present in single conjugate adaptive optics systems which use laser guide stars. For wavefront sensing over the full aperture with a single conjugate adaptive optics system a minimum of three laser guide stars must be used.

Tallon [56, 57, 58] studied the optimal configurations of laser guide stars for the cases of three and four laser guide stars. For the case of three laser guide stars the optimal configuration is a equilateral triangle with the three stars at the vertices of the triangle. The position of each of these vertices must be at the edge of the conical volume mapped out by the telescope field of view. Tallon [58] calculated the optimal angular distance θ from the center of the field to each of the guide stars as :

$$\theta = 0.29\left(\frac{1}{h_m} - \frac{1}{H}\right) D \tag{4.6}$$

Where h_m is the maximum level of turbulence to be sensed, H is the height of the laser guide star, and D is the diameter of the aperture of the telescope. The geometry constrains h_m to a maximum value of :

$$h_m < 0.13\, H \tag{4.7}$$

For a given h_m that is in agreement with equation 4.7 with the guide stars placed at the angular distance as given in equation 4.6 the maximum un-vignetted field of view, α, is given by:

$$\alpha = \left(\frac{0.155}{h_m} - \frac{1.155}{H}\right) D \tag{4.8}$$

For a $8\,m$ telescope on top of Mauna Kea, Hawaii, with a maximum level of turbulence, h_m, of $9\ km$ the guide stars must be placed at an angular distance of $\theta = 48\ arcseconds$ and the un-vignetted field of view is $\alpha = 7\ arcseconds$.

When four laser guide stars are used the optimal configuration is with the four stars placed at the vertices of a square. Again, the position of each of these vertices must be at the edge of the conical volume mapped out by the telescope field of view. The corresponding equations for the four star configuration as derived by Tallon[58] is :

$$\theta = 0.5\left(\frac{1}{h_m} - \frac{1}{H}\right) D \tag{4.9}$$

$$\alpha = \left(\frac{0.41}{h_m} - \frac{1.41}{H}\right) D \tag{4.10}$$

$$h_m < 0.29\, H \tag{4.11}$$

With four laser guide stars and an 8 m telescope on top of Mauna Kea, Hawaii, with a maximum level of turbulence, h_m, of 9 km the guide stars must be placed at an angular distance of $\theta = 83\ arcseconds$ and the un-vignetted field of view is $\alpha = 50\ arcseconds$.

The wavefront sensor must be designed to view the laser guide stars which are at the angle θ which is significantly greater than the un-vignetted field of view of the system, α . This separation between the laser guide stars and the un-vignetted field of view of the system is an advantage because the laser guide stars will not interfere with faint objects in the science field.

By using laser guide stars a sufficient number of measurements can be made of the atmospheric turbulence over a number of pupil positions and object angles so a system of equations can be formed. In the inversion of the equations to determine the atmospheric turbulence profile it has been assumed that the system of equations is a linear system [25, 26, 27, 37, 56, 57, 58]. The methods of inversion which have been investigated are minimum-variance reconstruction [26, 27], and digital demodulation [37]. It is unclear which method is the best method of reconstruction. Further work is needed in this area to determine the best method for the inversion of the system.

4.3 The Optimal Placement of the Deformable Mirrors

For a given distribution of atmospheric turbulence there is an optimal sectioning of the atmosphere with the deformable mirrors for the largest isoplanatic angle. The problem of the optimal sectioning has been studied by two researchers, Wallner[64] and Yan[66].

Wallner derived an expression for the optical path difference of a ray which passes through an atmosphere sectioned by deformable mirrors as a function of the boundaries of the sections and the positions of the deformable mirrors within the sections. The boundaries of the sections and the positions of the deformable mirrors within the boundaries was then optimized for the minimum optical path difference by differentiation of the expression with respect to the variables and setting the expression equal to zero.

The result of his derivation is a system of integral equations which are satisfied when the atmosphere is optimally sectioned. These equations are :

$$\int_{h_i}^{H_i} C_n^2(h)(h-h_i)^{2/3}dh = \int_{H_{i-1}}^{h_i} C_n^2(h)(h_i-h)^{2/3}dh \tag{4.12}$$

$$H_i = \frac{h_i + h_{i+1}}{2} \tag{4.13}$$

Where h_i is the height of the deformable mirror in the layer i and H_i is the boundary between layers i and $i+1$. The optimal layering is found by setting $H_0 = 0$ and guessing h_1. The right side of equation 4.12 is evaluated, then the left side is integrated from h_1 until it is equal to the right hand side, thus determining H_1. The height of the second deformable mirror, h_2, is found using equation 4.13. The evaluation of the right side of equation 4.12, integration of the left side, and evaluation of equation 4.13 is repeated for each of the layers until H_m is reached. If H_m is equal to the upper limit of the turbulence profile the optimal layering is determined, if not, the value of h_1 is adjusted and the procedure is repeated.

Yan[66] derived a system of equations for the optimal sectioning of the atmosphere based on the criteria that the residual wavefront error is the same in each layer. The system of equations is :

$$h_i = \left[\left(\sum_{i=1}^{N} h_i^{-5/3} \right) \frac{\int_{h_i} C_n^2(h)dh}{\int_0^H C_n^2(h)dh} \right]^{-3/5} \quad \text{for } i = 1, \ldots, N \tag{4.14}$$

Where h_i is the thickness of each layer. Yan's derivation did not include the optimization of the position of the deformable mirrors within each layer. It was assumed that the deformable mirror would be placed in the mid point of each layer. From Wallner's work we know that this is not true for the first and last layers. Yan's system of equations does not in fact find the optimal sectioning of the atmosphere.

Wallner's equations for optimizing the locations of the deformable mirrors is currently the best method for sectioning the atmosphere. For the optimal sectioning to be determined the $C_n^2(h)$ distribution must be measured using a method such as SCIDAR[14]. With the $C_n^2(h)$ measured the optimal location of the deformable mirrors can be found using Wallner's method, and the deformable mirrors can be positioned for the optimal configuration.

4.4 The Multiconjugate Adaptive Optics System

The multiconjugate adaptive optics system solves the problem of the limited isoplanatic angle of the single conjugate system. The ideal multiconjugate adaptive optics system would have many deformable mirrors which could be independently positioned at any conjugate altitude. As multiconjugate adaptive optics is a new and unproven field, it is best to design a simple multiconjugate system to test the principles of multiconjugate adaptive optics.

The simplest multiconjugate adaptive optics system has two deformable mirrors. These deformable mirrors could be fixed in position, but this would limit the versatility of the system. Ideally the deformable mirrors should be able to be positioned

independently over the full range of conjugate altitudes. This would allow the systems to adapt to atmospheric conditions so the atmosphere would be sectioned to provide the largest isoplanatic angle.

If the atmosphere is characterized by a Hufnagel-Valley Boundary average C_n^2 profile then the gain in field of view for a system with two deformable mirrors would be approximately 2 times in isoplanatic angle [64]. Using the predicted gain for a constant C_n^2 distribution as calculated by Beckers[4] the isoplanatic angle would be 4 times larger. With the strong layering that has been observed in the atmosphere[8, 35, 57, 58] the gain in isoplanatic angle may be larger than Beckers' prediction [4, 25]. The multiconjugate adaptive optics system should be designed with a field of view at least as large as the improved isoplanatic angle predicted by Beckers.

The source of wavefront information would have to come from laser guide stars because of the lack of suitable natural guide stars in the sky. The system would also have to measure the tip-tilt of a natural guide star because of the inability of the laser guide stars to measure this. It may be possible to eliminate the natural guide star by using polychromatic artificial stars [19, 22], but this technique is still unproven in the field.

The focal anisoplanatism of the laser guide stars limits the field of view over which wavefront information can be determined. If a constellation of 3 laser guide stars is used, the field of view over which wavefront information can be determined is 7 *arcseconds* for an 8 m telescope. This field of view is only large enough for work in the visible band where the isoplanatic angle is small. With 4 laser guide stars the field of view for which wavefront information can be found is increased to 50 *arcseconds* for a 8 m telescope. The four laser guide star configuration provides a field of view which is only restrictive in the far infrared region for a multiconjugate system with 2 deformable mirrors. Four laser guide stars is the minimum number of laser guide

stars for a multiconjugate system which works in the visible and near infrared.

There would have to be two wavefront sensor systems in the multiconjugate adaptive optics system. One wavefront sensor system would sense the tip-tilt of the natural guide star. The second wavefront sensor system would sense wavefront information from the laser guide stars.

The natural guide star wavefront sensor system should be designed as a Shack-Hartman wavefront sensor without the lenslet array so the tip-tilt over the whole aperture would be sensed. The wavefront sensor would be fed with a beam splitter placed after the deformable mirrors. The sensor should be designed to be able to measure the tip-tilt of several natural guide stars over the field of view of the system. The light from the natural guide star would have the higher order aberrations corrected by the laser guide star system so the asymmetrical aberrations of the image would be removed. With the asymmetrical aberrations removed the tip-tilt measurements from several stars can be added to reduce the error in the measurement of the tip-tilt [33].

The best method to feed the laser guide star wavefront sensor is to use the angular separation between the position of the laser guide stars, θ, and the un-vignetted field of view of the system, α. Pick off mirrors can be placed around the natural guide star wavefront sensor to steer the light from the laser guide stars into the laser guide star wavefront sensor system.

The design should also have a system to measure the $C_n^2(h)$ distribution. A SCIDAR system is the best method of measuring the $C_n^2(h)$ for this design. A SCIDAR system requires a camera which is able to take high speed images of the pupil of the telescope. The camera would only be used when the deformable mirrors are repositioned to their optimal location. The camera would be fed with light only at these times by a steering mirror inserted into the optical path, directing the light into the

SCIDAR camera.

A suitable adaptive optics system to test the principles of multiconjugate adaptive optics is composed of a system with two deformable mirrors. The deformable mirrors would be able to be independently positioned over the full range of conjugate altitudes. The mirrors would be positioned for optimal correction of the turbulence using SCIDAR measurements. There would be two wavefront sensor systems, one that would measure the tip-tilt using natural guide stars, and the other would measure the wavefront information from the array of four laser guide stars.

Chapter 5

The Optical design of Adaptive Optics Systems

The optical design of an adaptive optics system must provide an arrangement of optics which: images the atmosphere onto the deformable mirror(s), provides the light feed to the wavefront sensor(s), corrects for atmospheric dispersion, and produces near diffraction limited images for the science instrument. When the adaptive optics system is permanently mounted on the telescope there should be minimal interchange time between adaptive optics mode and normal mode. The standard arrangement is to insert a pair of diagonal mirrors into the beam to redirect the light through the adaptive optics system and back to the original optical path of the telescope so the beam returns to the same focal position with the same focal ratio and exit pupil location. This configuration allows the adaptive optics system to be used with existing science instruments, with a minimal setup time between normal telescope operation and adaptive optics mode. When the adaptive optics system is a stand alone instrument the system should be designed with a minimum of surfaces to maximise the optical transmission and decrease scattered light.

5.1 Main Beam Optics

The main beam optics must: image the turbulence onto the deformable mirror(s), provide a feed of light for the wavefront sensor(s), and re-image the light for the science instrument. The best method is to use reflective mirrors as the principal optical elements in the design. Adaptive optics systems have been designed using refractive optical components, but these systems have been limited in success due to chromatic aberrations of the beam [45].

The optimal arrangement is found by using off-axis conics with the focal points of the system coincident with the foci of the conics on the axes of symmetry of the conics [38]. The axes of symmetry of the conics are all parallel, but may be displaced laterally for systems with different input and output focal ratios. The input light beam is tilted with respect to the axes of symmetry of the conics. The image surface and exit beam are also tilted with respect to the axes of symmetry of the conics, but the image surface remains perpendicular to the beam upon exiting the system.

There is an arrangement which has been used in a number of adaptive optics systems where the beam is parallel to the axis of the conic, but displaced from the axis of symmetry [13, 17, 38]. The most common form of this arrangement is to use one large paraboloid. The beam is directed parallel to the axis of symmetry of the paraboloid but displaced off axis. The radius of curvature and position of the paraboloid is selected so that the pupil of the system is imaged at the point the beam (reflected from the paraboloid) intersects the axis of symmetry of the paraboloid. The deformable mirror is placed at this point, reflecting the beam back onto the paraboloid which forms the final focus at a point displaced from the axis of symmetry equal to the displacement of the input beam. This arrangement is termed the double pass paraboloid. It has the advantage of a simple, economical arrangement

of optics because it requires only one paraboloid mirror. A severe disadvantage of this system is the tilting of the image surface with respect to the beam. With this system the detector must be tilted. The resolution of this system is inferior to systems where the input and output beams are tilted with respect to the axes of symmetry of conics.

5.1.1 CFHT Adaptive Optics Bonnette

The CFHT adaptive optics bonnette is permanently mounted above the f/8 Cassegrain focus of the 3.6 m CFHT telescope [18, 24]. The word "bonnette" is used in the instrument name because "bonnette" is the French word for the instrument support structure at the Cassegrain focus of the telescope. When the system is in use, diagonal mirrors are inserted into the telescope beam to redirect the light into the adaptive optics bonnette, and back to the original focal location as shown in figure 5.1. The adaptive optics system magnifies the focal ratio of the beam from f/8 to f/20. The optics are designed to operate with a resolution of 0.06 *arcseconds* over a 1.5 *arcminute* field in the wavelength region from 400 nm to 1000 nm.

The system is a single conjugate adaptive optics system with the deformable mirror placed at the pupil of the telescope. The deformable mirror is a 19 electrode bimorph deformable mirror. The f/20 mirror is used as a tip-tilt mirror for the correction of image motion which is outside the range of the bimorph deformable mirror. The wavefront sensor is a 19 sub-aperture curvature wavefront sensor.

The adaptive optics bonnette main optics are shown in figure 5.1. The optics are designed to fit in a 1040 mm diameter, 280 mm thick enclosure which is mounted at the Cassegrain focus of the telescope. A simplified figure with only the off-axis paraboloidal mirrors is show in figure 5.2.

The diagonal mirrors are mounted on a slide which allows the diagonal mirrors to

be inserted into the beam and the light is directed in to the adaptive optics bonnette. The final image location is unchanged when the diagonal mirrors are inserted. When the adaptive optics bonnette is in use the image is magnified to F/20 from F/8. This magnification was made to provide a larger image scale so the improved resolution, from the adaptive optics, could be sampled by the CCD detectors. This change in focal ratio is a disadvantage when instruments such as spectrographs are used with the system. These instruments are designed for a specific focal ratio and require optics to be inserted to compensate for the change in focal ratio when the telescope is in adaptive optics mode. The location of the exit pupil of the system is also changed with the use of the adaptive optics bonnette. The change in location of the exit pupil is a problem for infrared instruments which have a cold stop in the instrument to remove stray heat from the image.

The optics in the adaptive optics bonnette consist principally of two off-axis paraboloidal mirrors as show in figure 5.2. The F/8 beam from the telescope comes to an intermediate focus after being directed into the adaptive optics bonnette with the first diagonal mirror. The intermediate focus is used in the system as a location to insert reference sources for calibration. After the intermediate focus a F/8 off-axis paraboloid collimates the beam. The collimated beam then passes through the ADC (Atmospheric Dispersion Corrector) and then hits the deformable mirror. The position of the F/8 off-axis mirror is selected so the pupil of the telescope is formed on the deformable mirror. The F/20 off-axis paraboloid re-images the light to form the F/20 focus which is directed to the original image plane of the telescope.

The off-axis paraboloidal mirrors are positioned so the intermediate F/8 focus and the final F/20 focus are coincident with the foci on the axes of symmetry of the off-axis paraboloidal mirrors. The axes of symmetry of the two paraboloidal mirrors are parallel to each other and displaced a distance proportional to the square of the ratio

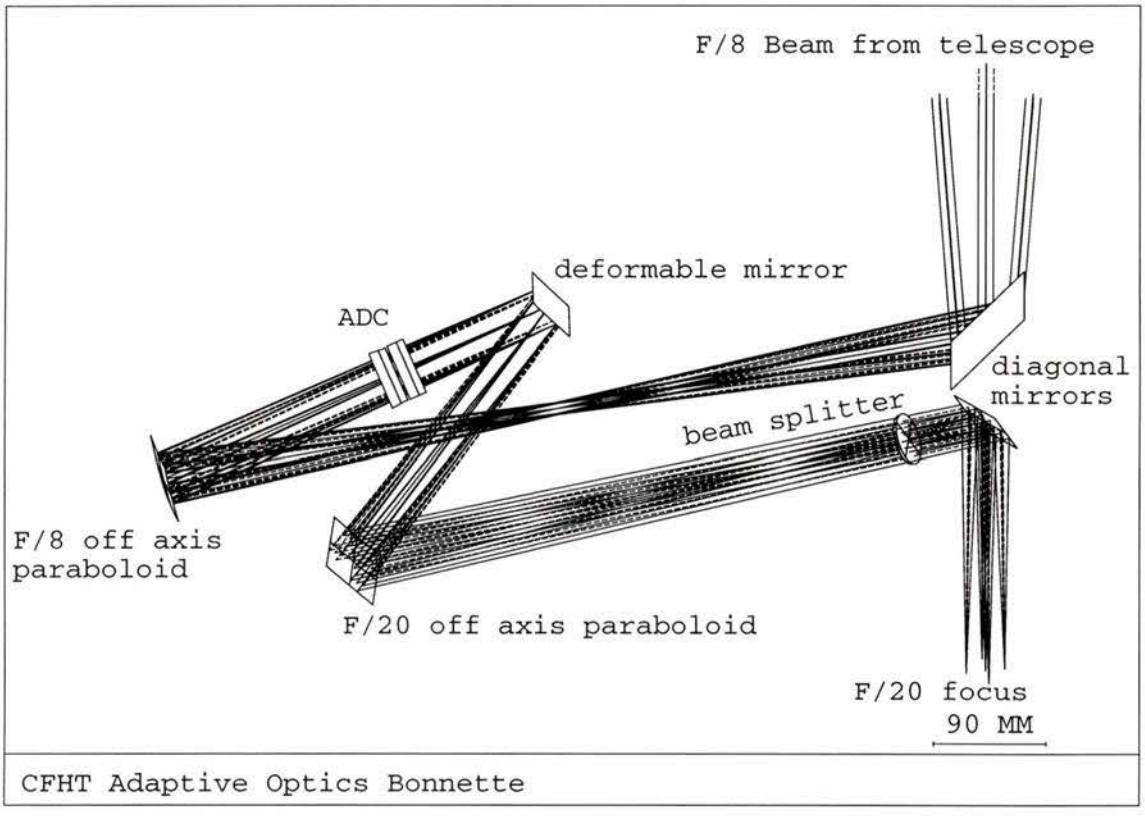

Figure 5.1: CFHT adaptive optics bonnette

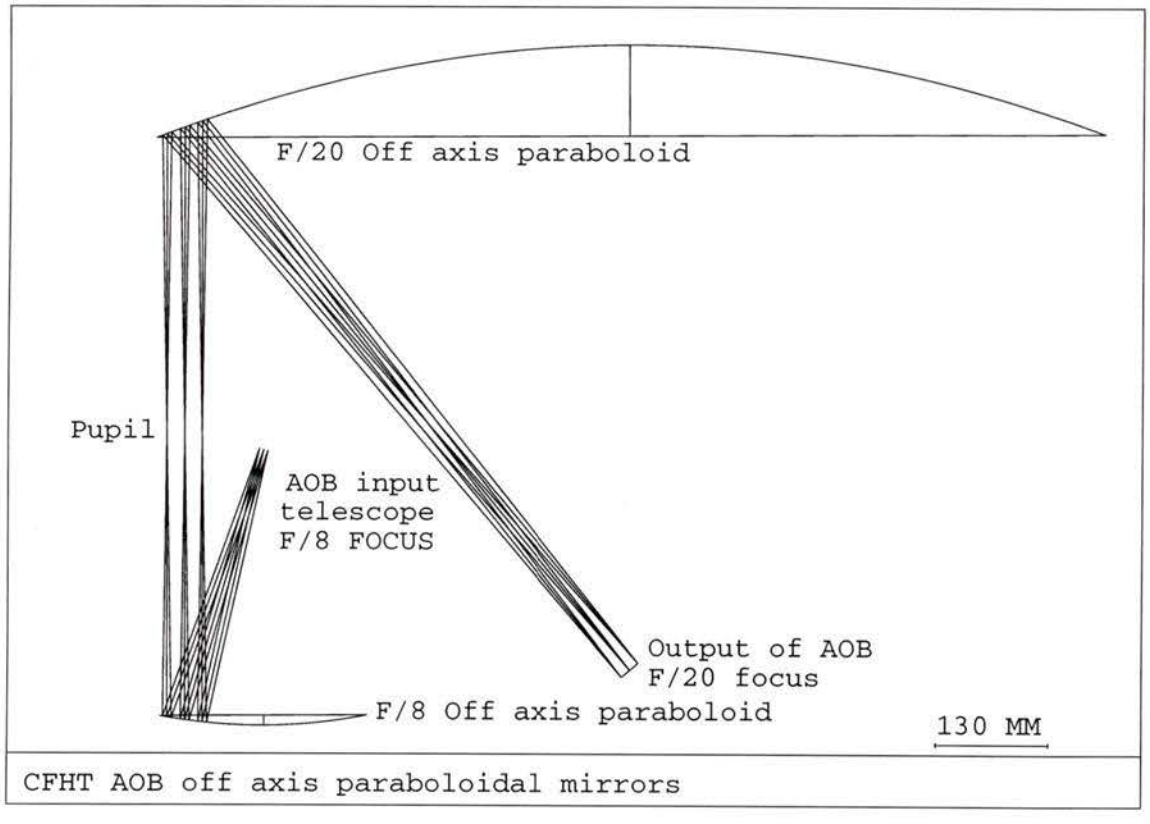

Figure 5.2: CFHT AOB off-axis paraboloidal mirrors

of the change of focal ratios [24]. The axes of symmetry are displaced such that the astigmatism introduced by the F/8 off-axis paraboloid is removed, by an opposite and equal amount of astigmatism introduced by the F/20 off-axis paraboloid, resulting in an image free from astigmatism.

A beam splitter between the F/20 off-axis paraboloidal mirror and the final diagonal mirror feeds a percentage of the light into the wavefront sensor module. The wavefront sensor module is not show in figure 5.1. There are four different beam splitters which have been made to be used in the adaptive optics bonnette system [18]. Three are true beam splitters which have transmissions to the science instrument of 10%, 45% and 85%, and reflectances to the wavefront sensor of 85% , 45%, and 10% respectively. The forth beam splitter is a dichroic which transmits the light above $1\mu m$ to the science instrument and reflects light between $0.5\,\mu m$ and $1\,\mu m$ to the wavefront sensor.

The surface on the beam splitter which reflects the light into the wavefront sensor has a concave radius to make the reflected beam telecentric. The telecentric feed into the wavefront sensor allows guide stars from anywhere in the field of view of the adaptive optics bonnette to be selected without pupil miss-alignment between the wavefront sensor and the pupil of the adaptive optics bonnette because both pupils are placed at infinity.

The wavefront sensor module is shown in figure 5.3. The wavefront sensor is a curvature wavefront sensor where the local curvature is measured by measuring the irradiance distribution before and after an image of the pupil (which is the image of the primary mirror). The wavefront sensor module is able to move, as a unit, relative to the beam splitter to allow the wavefront sensor module to select guide stars from anywhere in the field of view.

The first element in the wavefront sensor module, a convex toroid, intercepts the

portion of the beam reflected from the beam splitter which contains the light from the guide star of interest. The convex toroid produces a F/100 beam which is focused on the oscillating membrane mirror. The oscillating membrane mirror is used to move the location of the image of the pupil relative to the lenslet array to allow the irradiance distribution before and after the image of the pupil to be measured. The beam is then reflected by a concave toroid, then a small convex toroid, then a paraboloidal mirror. A $26mm$ diameter image of the pupil (which is the image of the primary mirror) is formed after the paraboloid. A lenslet array is located at the image of the pupil, which sections the image of the pupil onto 19 separate photo-avalanche diodes. The photo-avalanche diode is a high speed, and high sensitivity, light detector.

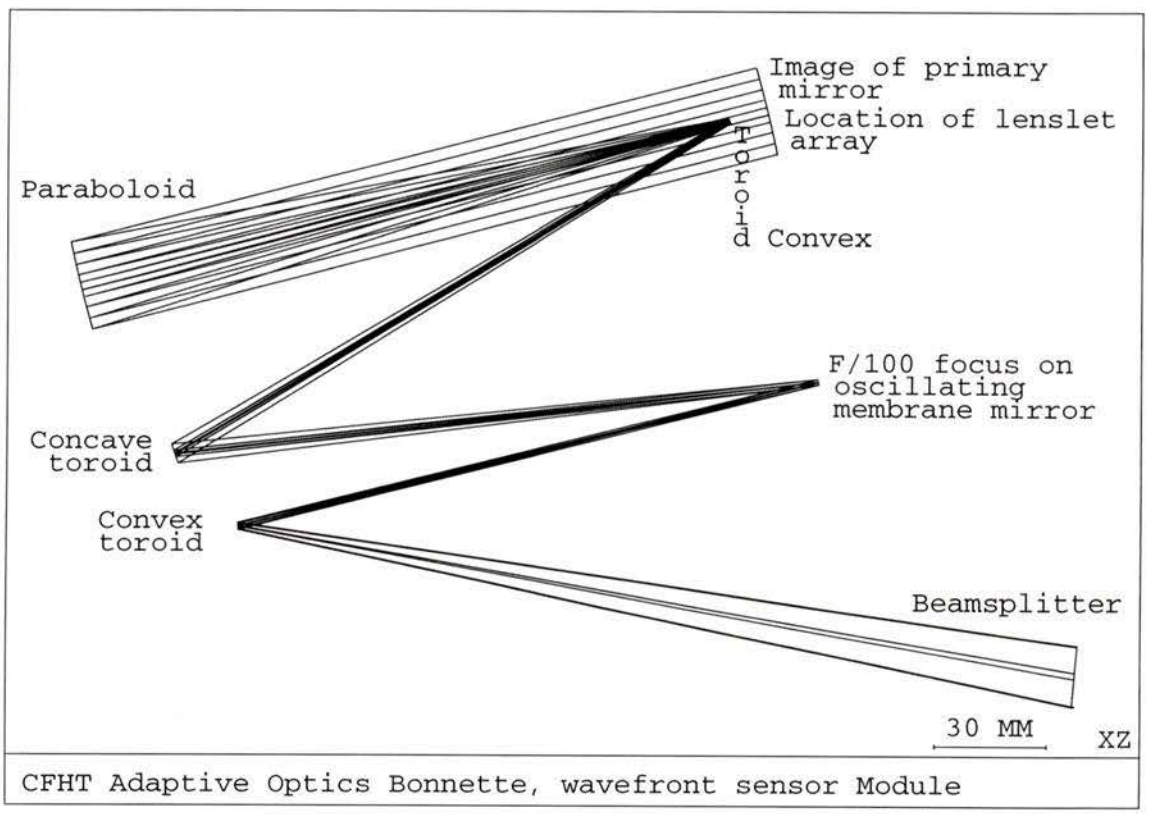

Figure 5.3: CFHT AOB wavefront sensor module

The CFHT adaptive optics bonnette is constructed. The first engineering runs

with the adaptive optics bonnette were completed in the end of March, 1996. The preliminary results have shown that the system is a success and images with a resolution of 0.068 *arcseconds* were obtained [43]. The CFHT adaptive optics bonnette will be the first adaptive optics system which will be commissioned for use by all observers subscribing to the CFHT telescope.

5.1.2 Gemini Adaptive Optics Module

The Gemini adaptive optics module is planned to be permanently installed above the F/16 Cassegrain focus of the $8\,m$ Gemini telescopes. The Gemini telescopes are two 8 meter telescopes which will be installed at Mauna Kea, Hawaii and Cerro Pachon, Chile under an international project between Canada, United States, the United Kingdom, Chile, Argentina, and Brazil. The planned completion for the telescopes is 1998–2000.

The Gemini adaptive optics system is designed to be a low order adaptive optics system with a relatively wide field at near IR wavelengths [44]. The design is unique because the final focal ratio of the telescope with the adaptive optics system in place is the same (F/16) as with the adaptive optics system removed. The goal of the adaptive optics system is to provide seeing of better than 0.5 Strehl ratio in the infrared ($1.6\,\mu m$) and better than 0.2 Strehl ratio in the red ($0.7\,\mu m$) [32].

The adaptive optics module has undergone three major revisions in its optical design. An overview of these three revisions will be given for an insight into the evolution of the system. Work is continuing on this adaptive optics system and a fourth design revision may occur.

The adaptive optics module is to be installed in the ISS (Instrument Support Structure), a $2\,m$ square, $1\,m$ thick steel hexagonal box. The ISS is attached to

the bottom of the mirror cell of the telescope 0.3 m above the Cassegrain focus with a 2 m diameter rolling element bearing. The Gemini telescope mounting is an alt-azimuth design. With this type of telescope mounting the image of the stars rotates as the telescope follows the motion of the stars over the night. This field rotation of the image must be removed by an image derotator. The ISS is rotated on the 2 m diameter bearing to de-rotate the image[23].

The first version of the adaptive optics module was designed, as a single conjugate adaptive optics system, with the deformable mirror conjugate to the pupil of the telescope [34]. The system was designed with a resolution of 0.1 *arcseconds* over a 1.5 *arcminute* field in the wavelength region from 400 nm to 1000 nm. The chief aberration of the image is curvature of the focal surface. The focal surface has a convex curvature with a radius of 529 mm. This can be corrected using a weak field flattener lens located before the focal surface. With a field flattener the image quality is improved to 0.017 *arcseconds* over the 1.5 *arcminute* field.

The optical design of the first version of the adaptive optics module is shown in figure 5.4. The main beam optics consists of a diagonal mirror which launches the light into the adaptive optics module. The light is directed into an off-axis hyperboloidal mirror which forms an image of the pupil of the telescope on the deformable mirror. Between the hyperboloidal mirror and the deformable mirror there is an intermediate focus which can be used as a location to insert reference sources for calibrating the system. The light is then re-imaged by an off-axis ellipsoidal mirror which forms a F/16 image. A flat mirror and diagonal mirror are used to steer the beam to the original focal location and satisfy the packaging constraints of fitting the adaptive optics module within the ISS. The last diagonal mirror is also a beam splitter to feed the wavefront sensor module which would be located behind the diagonal mirror. In this configuration the main path of the adaptive optics module is all reflecting so

chromatic aberrations in the main optical path are eliminated.

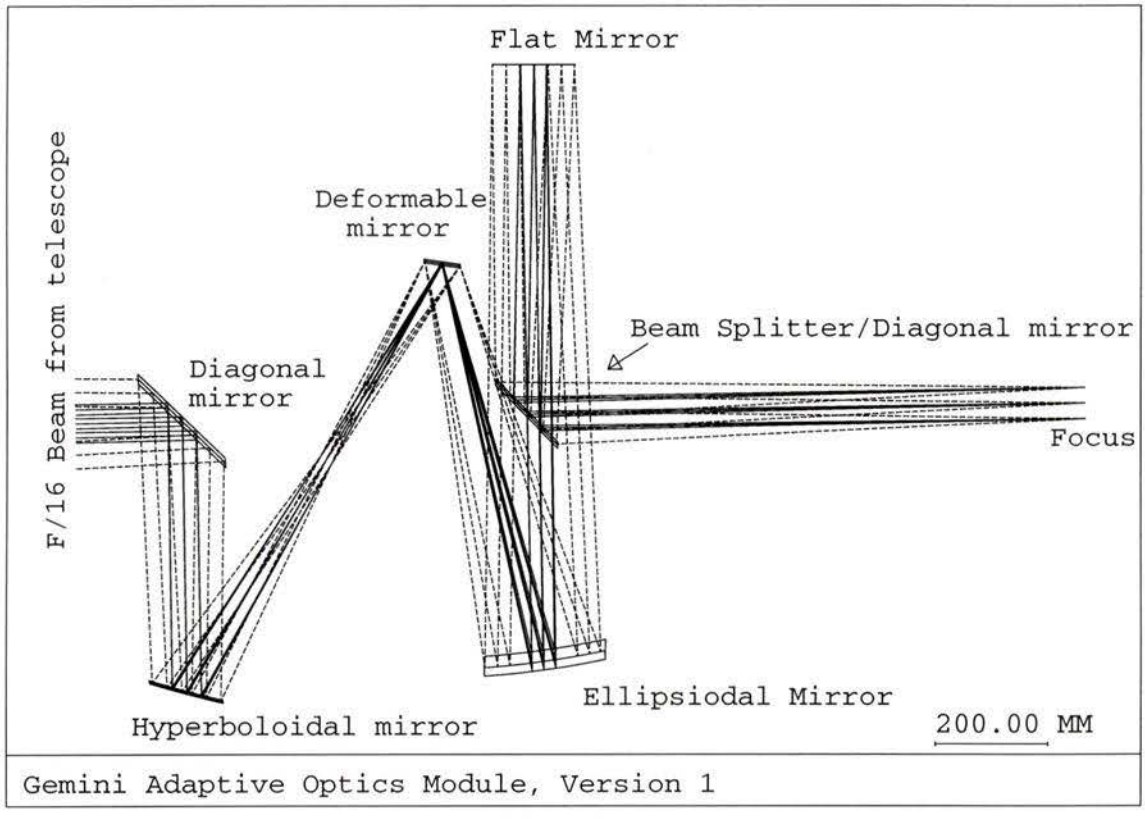

Figure 5.4: Gemini adaptive optics module, version 1

The off-axis conics are placed so the axes of symmetry of the conics are coincident. The foci of the system are also coincident with the axes of symmetry. The first powered mirror, a hyperboloidal mirror, is located before the light from the telescope comes to focus. A virtual focal point exists behind the hyperboloidal mirror where the light would have come to focus. This virtual focus behind the hyperboloidal mirror is also coincident with the axes of symmetry of the conics. As with the CFHT adaptive optics bonnette, the light beam is tilted with respect to the axes of symmetry of the conics in this design. The axes of symmetry of the two conics are coincident because the input and output focal ratios of the system are the same whereas in the CFHT adaptive optics bonnette the axes are displaced because the input and output focal

ratios of this system were different.

The second version of the Gemini adaptive optics system is shown in figure 5.5. This system was designed with several differences from the first version [39]. The system is a multiconjugate system with two deformable mirrors. The image quality requirements for this version are more stringent than the previous version and the field of view is twice as large. The system was required to have a resolution of 0.01 *arcseconds* at the center of the field and a resolution of 0.07 *arcseconds* at the edge of the 3 *arcminute* field in the wavelength region 400 nm to 1000 nm. The exit pupil was required to be unchanged when the adaptive optics module is inserted in the beam. This was required to prevent problems with infrared instruments used with the adaptive optics system. A change in the exit pupil would cause more stray heat in infrared instruments designed with cold stops. The packaging constraint was also changed for this system. The adaptive optics system was constrained so all the optics were on one side of the ISS cube but the optical elements were allowed to protrude outside the ISS cube. It was required that no elements were closer than $800mm$ or further than $2300mm$ from the original optical axis of the telescope without the adaptive optics system in use.

The two deformable mirrors in this system are designed to be able to scan a range of conjugate altitudes of the atmosphere. The two deformable mirrors are to be fixed to a single slide with the two mirrors separated by 523 mm and held at a constant angle of incidence to the light of 15.3 *degrees*. The mirrors slide as a unit, remaining in the same relative position to each other. In the lower position, the deformable mirrors image atmospheric layers at $0km$ for the low altitude deformable mirror, and $4.2km$ for the high altitude deformable mirror. At the upper position, the deformable mirrors image atmospheric layers at $5.4km$ for the low altitude deformable mirror, and $12.2km$ for the high altitude deformable mirror. The system in figure 5.5 is shown

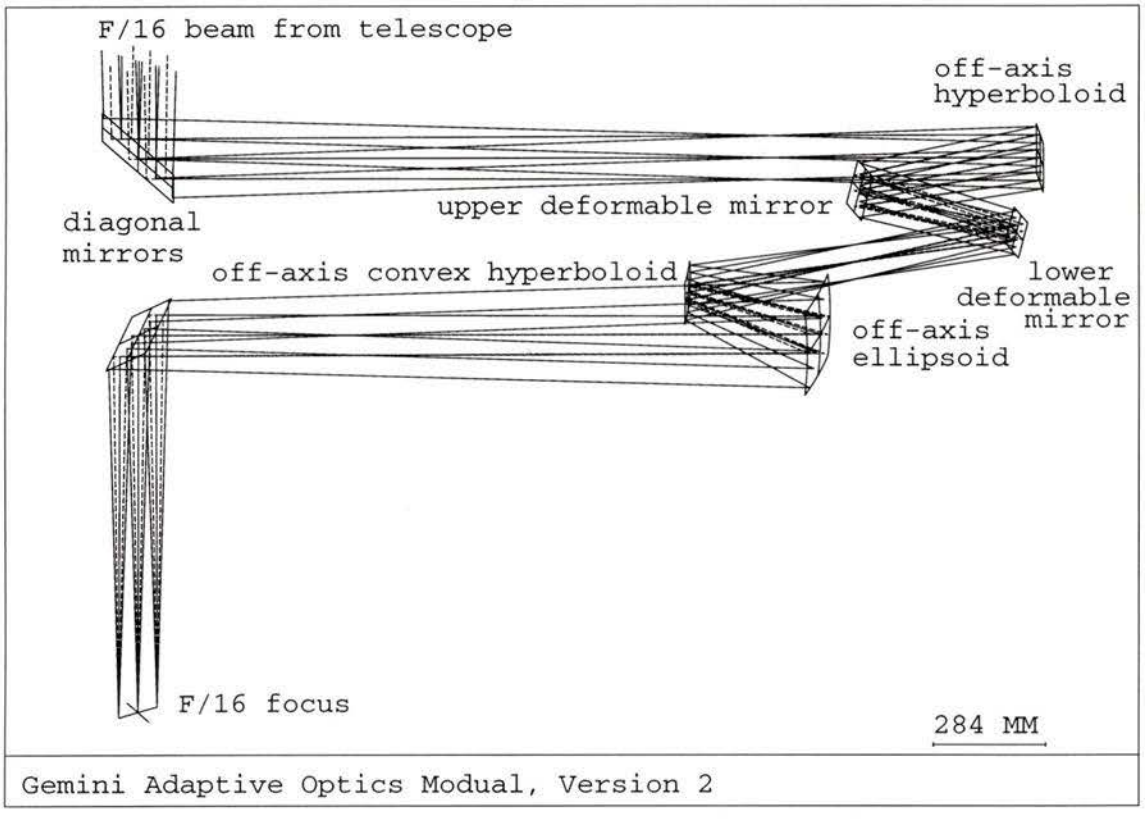

Figure 5.5: Gemini adaptive optics module, version 2

with the deformable mirrors in the upper position. When the deformable mirrors are in the lower position the two deformable mirrors are closer to the off-axis convex hyperboloidal mirror. The scanning of the mirrors, over their range of conjugate altitudes, as a unit causes no missalignment of the optics or degradation of the image quality.

The system in figure 5.5 is shown without a beam splitter to feed the wavefront sensor. A beam splitter is to be inserted between the off-axis hyperboloid and the diagonal mirror. If the membrane beam splitter is used, the image quality for the system is 0.004 *arcseconds* at the center of the field, and 0.032 *arcseconds* at the edge of the 3 *arcminute* field. No field flattener is required because a system of three off-axis conics are used. With three off-axis conics the Petzval sum of the system can be minimized to allow a flat focal surface. The disadvantage of the membrane beam splitter is that surface irregularities on the surface of the membrane will degrade the beam reflected to feed the wavefront sensors.

When a glass beam splitter rather than a membrane is used the image quality of the final image is degraded with astigmatism and chromatic aberrations. The image quality for the system with the glass beam splitter is 0.01 *arcseconds* at the center of the field and 0.04 at the edge of the 3 *arcminutefield* . The glass beam splitter has the advantage of being able to be manufactured with less surface irregularities which would result in less image degradation of the reflected beam to the wavefront sensor.

The main beam optics, shown in figure 5.5, consist of a diagonal mirror which launches the light into the adaptive optics module. The light is directed into an off-axis concave hyperboloidal mirror after coming to focus at a point between the diagonal mirror and the off-axis conic. This intermediate focal point can be used as a point to insert reference sources for calibration. The off-axis hyperboloidal mirror is followed by the two deformable mirrors which are designed to be mounted on a single

slide and scan a range of conjugate altitudes. Following the deformable mirror is a pair of off-axis conics: an off-axis convex hyperboloidal mirror, followed by an off-axis concave ellipsoidal mirror. This pair of mirrors function as a reverse telephoto lens system bringing the system to focus at the original focal location with a focal ratio of $F/16$. The off-axis concave hyperboloidal mirror is followed by the final diagonal mirror which steers the beam to the original focal location.

The positions and radii of the three off-axis mirrors must be selected so the final focal ratio is F/16 and the exit pupil of the system is unchanged. The Petzval sum of the three mirrors is also minimized to provide a flat focal surface. The axes of symmetry of the three conics are almost coincident and the foci of the system are almost on the axes of symmetry of the three conics. Small deviations of the positions of the axis and foci , from a coincident arrangement, are allowed during optimization to permit greater degrees of freedom in the system.

The third version of the Gemini adaptive optics system is show in figures 5.6 and 5.7. This version has several differences from the previous version [41]. The system has two deformable mirrors, like the previous version, but the mirrors are fixed in conjugate altitude. The deformable mirrors are fixed at conjugate altitudes of $6.5\,km$ for the upper deformable mirror, and $0\,km$ for the pupil deformable mirror. Another difference of this version is that the beam splitter transmits the beam to feed the wavefront sensor module and reflects the main beam. With the beam being reflected from the beam splitter for the main beam optics the science image is not degraded by the action of the beam spitter. The required image quality is the same as in the previous version, a resolution of 0.01 *arcseconds* at the center of the field and a resolution of 0.07 *arcseconds* at the edge of the 3 *arcminute* field. The actual image quality achieved for the system is 0.007 *arcseconds* at the center of the field and 0.042 *arcseconds* at the edge of the 3 *arcminute* field.

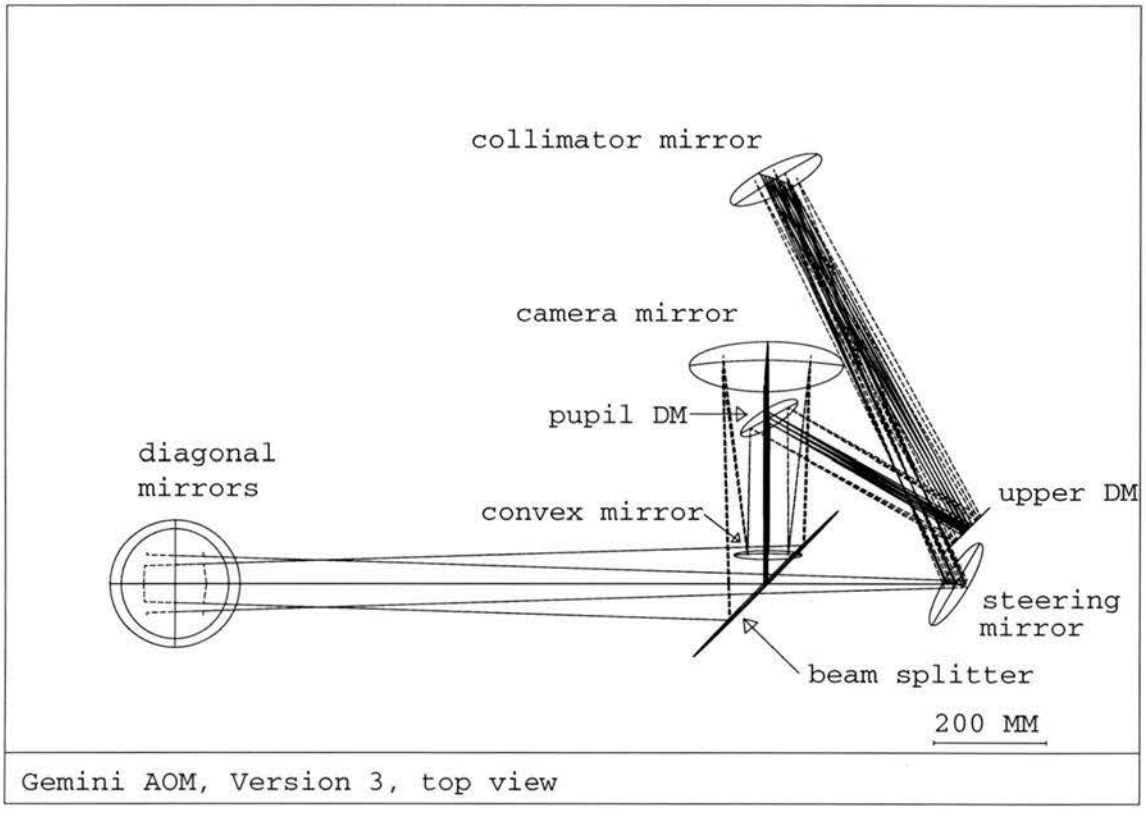

Figure 5.6: Gemini adaptive optics module, version 3, top view

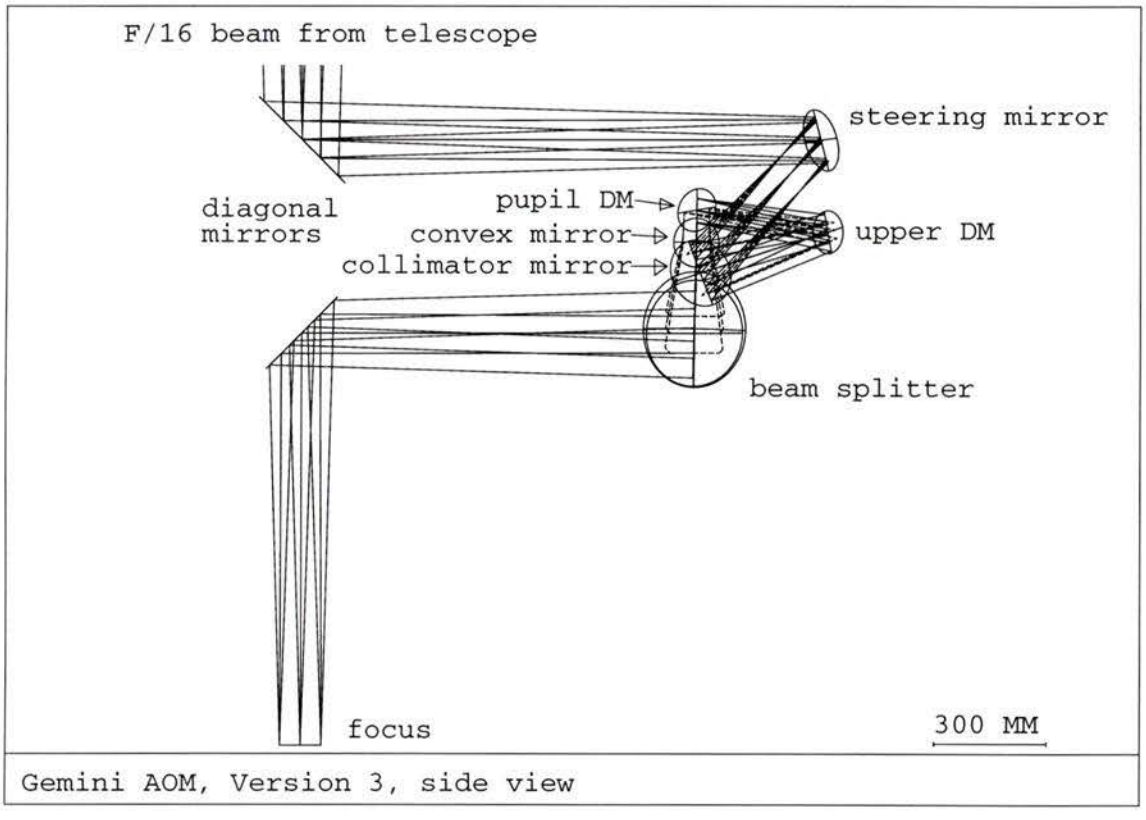

Figure 5.7: Gemini adaptive optics module, version 3, side view

The two deformable mirrors are fixed, rather than permitted to scan in this system, to simplify the design and construction of the system. It is planned to install only the upper deformable mirror for the initial configuration. A flat mirror will be placed at the location of the pupil mirror. The system will then be upgraded by installing the second deformable mirror. The final configuration is planned to be a $82\,mm$ diameter continuous faceplate deformable mirror at the pupil ($0\,km$) and $60\,mm$ diameter membrane mirror at the upper deformable mirror position ($6.5\,km$). The upper deformable mirror is undersized, only as large as a beam from a single star. The area outside this single beam diameter will be outside the adaptive area of the deformable mirror, this will either be reflected by a mirror placed around the membrane deformable mirror or removed by an annular stop being placed around the deformable mirror. The upper deformable mirror is intended to correct the slower low order aberrations of the image with the pupil deformable mirror correcting the fast high order aberrations. The upper deformable mirror, a membrane mirror, is better suited to the low order aberrations because this mirror has a longer stroke length to correct the low order aberrations which are larger in amplitude than the high order aberrations. The continuous faceplate mirror does not have the stroke length to correct low order aberrations but is faster than the membrane mirror.

The beam at the upper deformable mirror position was made small because of the limited size which membrane deformable mirrors can be constructed. The system will not use multiple guide stars to deconvolve the vertical atmospheric profile so no information will be avaliable for a correction of an upper deformable mirror larger than what would be illuminated by a single star. If a mirror is placed around the undersized upper deformable mirror the ability of the upper deformable mirror to enlarge the isoplanatic patch will be limited by the annulus of uncorrected light reflected by this mirror. If an annular stop is placed around the upper deformable

mirror the isoplanatic patch of the system will be enlarged, but the light gathering capability of the system will be reduced.

The main beam optics, shown in figures 5.6 and 5.7, consist first of a diagonal mirror which launches the light into the adaptive optics module. The light is then directed by a steering mirror to the collimator, an off-axis concave hyperboloidal mirror. The collimator mirror is followed by the upper deformable mirror, at a conjugate altitude of 6.5 km. The pupil deformable mirror is next, followed by the convex mirror. The convex mirror is a small convex off-axis hyperboloidal mirror. The convex mirror works with the camera mirror, a concave off-axis ellipsoidal mirror, to expand the beam for the correct focal ratio and exit pupil location. The curvatures of the collimator, camera, and convex mirror are selected so the Petzval sum of the curvatures is a minimum for a flat focal surface. The beam splitter follows the camera mirror. The science beam is reflected, by the beam splitter, while the feed to the wavefront sensor is transmitted. The quality of the main beam is not degraded by the beam splitter but astigmatism is introduced into the beam transmitted through the beam splitter for the wavefront sensor. The astigmatism introduced by the beam splitter can be corrected by using a tilted cylindrical lens between the beam splitter and the wavefront sensor.

5.2 Optimizing and Simulation of the Optical Design

The optical design must be optimized and simulated using computer modeling before the instrument is constructed. Several commercial lens design software packages are avaliable. Most of the lens design software is geared to the design of on axis refractive systems such as a standard camera lens. The lens design software *CodeV*, produced

by Optical Research Associates Pasadena, California, USA, is the most advanced of the commercial lens design software and is best suited to designing off-axis systems such as adaptive optics systems.

The optimization and simulation is initially carried out using ray based simulations of the system. Rays of light are traced through the system such that the rays follow the laws of reflection or refraction for geometric optics at each surface defined in the system. Final simulation and, if necessary, optimization must be done using diffraction analysis. Diffraction analysis is necessary in the final stages for adaptive optics systems because the image quality is near diffraction limited. Diffraction effects can cause the ray based simulation to be inaccurate. Diffraction analysis is much more computationally intensive than ray based simulations and analysis, thus using ray based simulations in the initial stages of design is more efficient. The *CodeV* software is able to optimize and simulate the system using ray based and diffraction analysis.

The lens design software uses the damped least square method of optimization with the constraints controlled by the Lagrangian multiplier method. Global optimization using the method of simulated annealing is avaliable in the *CodeV* lens design software [28, 54].

An adaptive optics system can be designed by first defining the required optical parameters and constraints for the system. The chief optical parameters are the telescope specifications, the final focal ratio and exit pupil location, the conjugate altitude and size of the deformable mirror(s), the spectral range for the system, and the image quality requirement. Some constraints are the packing volume, location, the required transmission for the system, and the system cost.

A series of preliminary layouts which meet the system optical parameter and constraints are calculated for the system. These preliminary layouts can be made without

the folding and deformable mirrors, and the packing constraints can be omitted until the latter design stages. These preliminary systems are then entered into the lens design software and the systems are optimized to determine the actual performance which each design will yield. The systems are constrained so the foci of the conics are on the axis of symmetry with the axes parallel in the initial stages of optimization. These constraints ensure the system does not fall into a local sub-minimum in the initial stages of optimization. The off-axis elements in the system are constrained to conics. Generalized aspheric surfaces are not used because of the manufacturing difficulties in producing these types of surfaces.

The optimized preliminary systems, which meet the target image quality for the system, are then packaged into the allocated volume for the system. The folding mirrors, deformable mirrors, and beam splitters are added as required for the system. During packing the designer must define constraints which ensure the main beam is not vignetted by the mirrors and off-axis conics.

The systems which meet the image and packing requirements, as well as the other required parameters are then evaluated for cost, and transmission. Then the system which best satisfies the optical parameters and system constraints is selected for the detailed design. In the detailed design the manufacturing and construction tolerances are determined. An ADC (Atmospheric Dispersion Corrector) is designed for the system, as well as the wavefront sensor(s).

The system is finally simulated using diffraction analysis to determine the image performance over the required spectral range and over the field of view of the system. The field distortion for the system is also mapped for the system field of view. The system design is then exported from the lens design software as an initial graphics exchange specification file for importing into the computer aided design software for the design of the lens mounting structure.

5.3 The Design of the Atmospheric Dispersion Corrector

The ADC (Atmospheric Dispersion Corrector) corrects for the optical dispersion caused by the air. The refractive index of the air varies as a function of wavelength, thus the air is an optically dispersive medium. The earth's atmosphere acts as a prism on the light being observed by the telescope, dispersing the light. The amount of dispersion observed is dependent on the variation in the index of refraction and the zenith distance of the telescope. The zenith distance is the angle between the object being observed and point directly overhead (the zenith). At a zenith angle of 45 degrees atmospheric dispersion will result in the light from $400nm$ and $1000nm$ to be spread into a spectrum over 1 arcsecond long.

The atmospheric dispersion can be modeled by treating the air as a flat slab over the telescope, ignoring the curvature of the earth [49]. The atmospheric dispersion as a function of the refractive index of the air and the zenith angle is given by equation 5.1:

$$\delta_\lambda = (n_1 - n_2)tan(Z) \tag{5.1}$$

Where $(n_1 - n_2)$ is the difference in refractive index of air at wavelengths λ_1 and λ_2, the zenith distance is given by Z, and the atmospheric dispersion observed is δ_λ.

The refractive index of the air as a function of wavelength has been modeled by Edlen[1]. The Edlen dispersion equation for air at 760 Torr and 15 degrees Celsius is given in equation 5.2 :

$$(n_\lambda - 1) \times 10^8 = 6432.8 + \frac{2949810}{146 - 1/\lambda^2} + \frac{25540}{41 - 1/\lambda^2} \tag{5.2}$$

Where n_λ is the refractive index of the air and λ is the wavelength of the air in microns. This equation can be used for the design of an ADC or, if greater precision is required, measurements can be made of the dispersion at the telescope site.

The atmospheric dispersion is corrected by introducing a prism, with an equal but opposite amount of dispersion to the atmospheric dispersion into the main beam of light. Because the atmospheric dispersion varies with zenith angle the dispersion of the prism must be made variable to allow the atmospheric dispersion to be corrected at all parts of the sky. This is done by using two prism that are counter-rotated to vary the dispersion. The ADC should also be made so the beam is not deviated in direction after passing through the prisms. The dispersion of the prism is made variable by using a pair of prisms which are counter rotated with respect to each other to vary the dispersion.

An ADC designed using two prism pairs is show in figure 5.8. Each prism consists of a low dispersion and high dispersion glass. The prism pairs are mounted so that they can be rotated with respect to the sky and with respect to each other. The amount of dispersion is controlled by the orientation of the prisms to each other. In figure 5.8 the ADC is shown in the off position with the prisms rotated so the dispersion caused by the first prism is compensated by the second prism.

The glass type and the wedge angle of the glass for the two prisms is selected so the dispersion of the atmosphere at the maximum zenith angle is compensated when the prisms are rotated for maximum dispersion. If one of the prisms is rotated 180 degrees the prism pair will be at maximum dispersion.

Some glass pairs which closely match the dispersion of the atmosphere are LAFN21 and KF9, FK54 and BAK5, UBK7 and LLF6, BK7 and F2, FK5W and LLF6W [1, 11, 39]. The pair LAFN21 and KF9 matches the atmospheric dispersion the closest, but has colour dependent aberration if it is not in a perfectly collimated

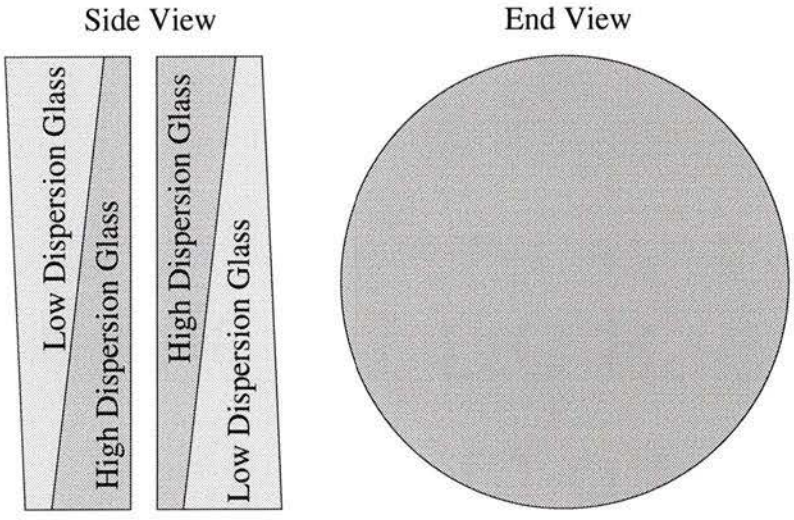

Figure 5.8: Atmospheric dispersion corrector

beam when the ADC is in the off position. The glass pair BK7 and F2 is the least expensive of the glass sets but does not provide the best performance.

The ADC performs best when inserted into a collimated or near collimated beam. If the ADC is placed in a converging beam the ADC will introduce chromatic and spherical aberrations into the system. The ADC also changes the transmission characteristics of the telescope due to absorption and reflection losses in the ADC. Reflection losses can be reduced by putting oil between the prisms rather than an air space.

To simulate the dispersion of the atmosphere in lens design software, a prism must be inserted before the optical system. The atmosphere can be simulated, without loss of accuracy, by using a thin wedge prism in front of the lens system. The refractive index, dispersion, and wedge angle of the prism are selected so the dispersion is equal to the dispersion of the atmosphere. The refractive indices of the glass 'atmos' in the lens file in appendix A were selected to simulate the atmospheric dispersion at a zenith angle of 45 degrees using a $100mm$ thick prism with a 1 degree wedge angle.

5.4 The Design of the Shack-Hartman Wavefront Sensor

The Shack-Hartman wavefront sensor requires the least amount of processing to determine the wavefront which is needed for the atmospheric tomography. This criteria has been used to select the Shack-Hartman wavefront sensor as the sensor of choice for the multi-conjugate adaptive optics system in this thesis.

In designing the wavefront sensor the selection of the sub-aperture size for the sensor is very important in the design of the adaptive optics system. The lower limit for the sub-aperture size is given by the variance error. The variance error for the Shack-Hartman wavefront sensor is inverse-square proportional to the signal to noise as shown in equation 2.18. The signal to noise ratio for each sub-aperture is proportional to the area of the sub-aperture. There is an additional lower limit on the sub-aperture size based on the diffraction limit of the sub-aperture. The sub-aperture must be made large enough so the diffraction limit of the sub-aperture is smaller than the isoplanatic patch. For typical atmospheric conditions at wavelengths longer than $0.39\mu m$ the sub-aperture will be able to resolve the isoplanatic patch when it is made equal to or larger than the coherence length (r_0).

The upper limit on the size of the sub-aperture is set by the actuator spacing of the deformable mirror. The sub-aperture must be smaller than the actuator spacing on the mirrors. If full correction is to be made the sub-aperture should be made equal to the coherence length (r_0). There is an additional limit on the sub-aperture size caused by the high order aberrations. It has been shown that the sub-aperture size should be smaller than $0.16\lambda/s$ where s is the angular size of the object being observed [60] . This limit is important with laser guide stars, which are larger than real stars, due to the method of producing the stars.

The image quality in each sub-aperture should be as close as economically possible to the diffraction limit to reduce the signal to noise of the system. Asymmetrical aberrations, such as coma and astigmatism, must be minimized in the sub-aperture as these will cause a field dependent error in the measurement of the tilt of the sub-aperture.

The effect of alignment and flexure errors must be considered in the design of the Shack-Hartman wavefront sensor. Methods such as a modulated reference beam to calibrate the senor or a nutating mirror with a modulated reference beam (such as in the I-cubed sensor) or an integrated lenslet array and CCD system (such as the 'micro Shack-Hartmann' developed by LASERDOT[16]) can be used to reduce the effects of alignment and flexure in the wavefront sensor.

5.5 Tolerancing of Adaptive Optics Systems

Tolerancing an optical design is one of the most important stages in the design process. Poor tolerancing can result in a final system which does not meet the required performance criteria, or a system which is unnecessarily expensive because of overly strict tolerances. It is very important that the tolerances be written in a clear and concise manner.

Typically for an astronomical adaptive optics system only one complete system is built. The statistical tolerancing methods normally used for commercial optical systems, where many systems are built, are not applicable to astronomical adaptive optics systems. The errors must be summed linearly, not using the statistical method of summing the square of each error and taking the square root. The linear summing of errors greatly increases the manufacturing costs for astronomical adaptive systems.

Several methods are used to maximize the tolerances in adaptive optics systems.

The most important is the use of compensators in the design. The mountings of the optical elements should be made adjustable. These adjustable parameters of position and tilt are allowed to vary over a specific range to compensate aberrations caused by the imperfect manufacture of the non-adjustable parameters. These mounts must have a movement resolution which matches or is better than the sensitivity of the movement of the element to the system performance. The gravitational flexure and thermal expansion of the mounting of the element must also be considered in the tolerancing of the system.

Special consideration, because the powered elements are off-axis conics, is necessary when calculating the sensitivity of the system performance to element movement. The element's position in the software is specified to the pole of the conic, not the center of the used aperture of the element. The translation and rotation of the element for the positional sensitivities must be specified to the center of the used aperture of the element. This requires a rotation and translation of the de-centers, and translations to a coordinate system placed at the center of the used aperture, oriented normal to the surface. This ensures the sensitivities are directly mapped to the movements of the mount holding the optical element.

The surface accuracy is not adjustable for the mirrors in the system. The deformable mirror can compensate for some aberrations caused by the surface errors in the mirror but it is limited to errors which change slowly over the surface of the mirror. Errors which change rapidly over short distances can not be compensated by the deformable mirror. These errors must be minimized during manufacture for mirrors used in adaptive optics systems. Two tolerances can be used when tolerancing the surface accuracy of the mirrors in the system, one tolerance for the errors which change slowly and can be compensated by the deformable mirrors and another for the errors which change rapidly and can not be compensated.

The design process can be improved by using an iterative method of design. As each surface is manufactured the surface parameters are measured and entered into the design software. The system is re-optimized using these surface parameters to determine the optimal parameters for the surfaces yet to be manufactured. Another surface is then manufactured to the new prescription until all the surfaces have been made. At this point, a final optimization is made to determine the optimal positions of the elements. The order of manufacture of the elements is done using the sensitivity table, with the element with the most sensitive parameters being manufactured first.

In summary, the tolerancing procedure for an adaptive optics system is best done by dividing the system parameters into compensators, or parameters which are adjustable during the manufacture and fixed parameters. The sensitivities of the compensators are then calculated as well as the required resolution of movement for each parameter. Tolerances and sensitivities for the fixed parameters are determined taking into account the ability of the deformable mirror to correct for errors which change slowly over the surface. The elements are then manufactured starting with the most sensitive element and working to the least sensitive element, re-optimizing the design with the actual parameters for each surface.

Chapter 6

A Multiconjugate Adaptive Optics System

This is a proposed design for a multiconjugate adaptive optics system imaging two selectable atmospheric layers. This instrument is intended to serve as a test bed to test the principles of multiconjugate adaptive optics, and to develop the new control algorithms need for multiconjugate adaptive optics. This instrument has been designed to be used with the $3.58m$ Canada-France-Hawaii Telescope (CFHT). This telescope was chosen as the telescope for this design because this is the most suitable Canadian telescope for adaptive optics work. The superb site, Mt. Mauna Kea in Hawaii, provides excellent seeing conditions, which combined with adaptive optics significantly increase the scientific productivity of the telescope. This proposed instrument is a natural extension of the current CFHT adaptive optics bonnette project.

6.1 Design Overview

This design will implement the multiconjugate adaptive optics system described in section 4.4. A schematic diagram of the proposed system is given in figure 6.1. The system will have a SCIDAR camera, two deformable mirrors, laser guide star wavefront sensors, and a natural guide star tip-tilt sensor.

The SCIDAR camera is used to measure the $C_n^2(h)$ distribution in the atmosphere for the optimal placement of the deformable mirrors. The SCIDAR camera is a camera which takes high speed images of the pupil of the telescope. Because the SCIDAR camera is only needed when the deformable mirrors are repositioned to their optimal locations, the camera will be fed by a steering mirror which will be inserted into the optical path, directing all the light into the SCIDAR camera. At other times, the steering mirror will be retracted and the light will pass through the main optical path.

This adaptive optics system will have two deformable mirrors which will be able to be placed independently in conjugate altitude. The positioning of the deformable mirrors must not affect the image quality for the system. The type of deformable mirror will not be defined in this design. The final selection depends on the final size of the mirrors, and the avaliable deformable mirrors at the time of manufacture. It will be assumed that a clearance of a volume equal to a cylinder, with a diameter equal to twice the clear aperture and a depth equal to the clear aperture, will be sufficient for the deformable mirrors.

The system will use laser guide stars for the source of the wavefront information. To compensate for focal anisoplanatism an array of four guide stars will be used as described by Tallon [56, 57, 58]. The array of four laser guide stars will provide wavefront information for a field of view of 22 *arcseconds* with the $3.58m$ telescope aperture, $90km$ laser guide star height above Mauna Kea, and $9km$ maximum level

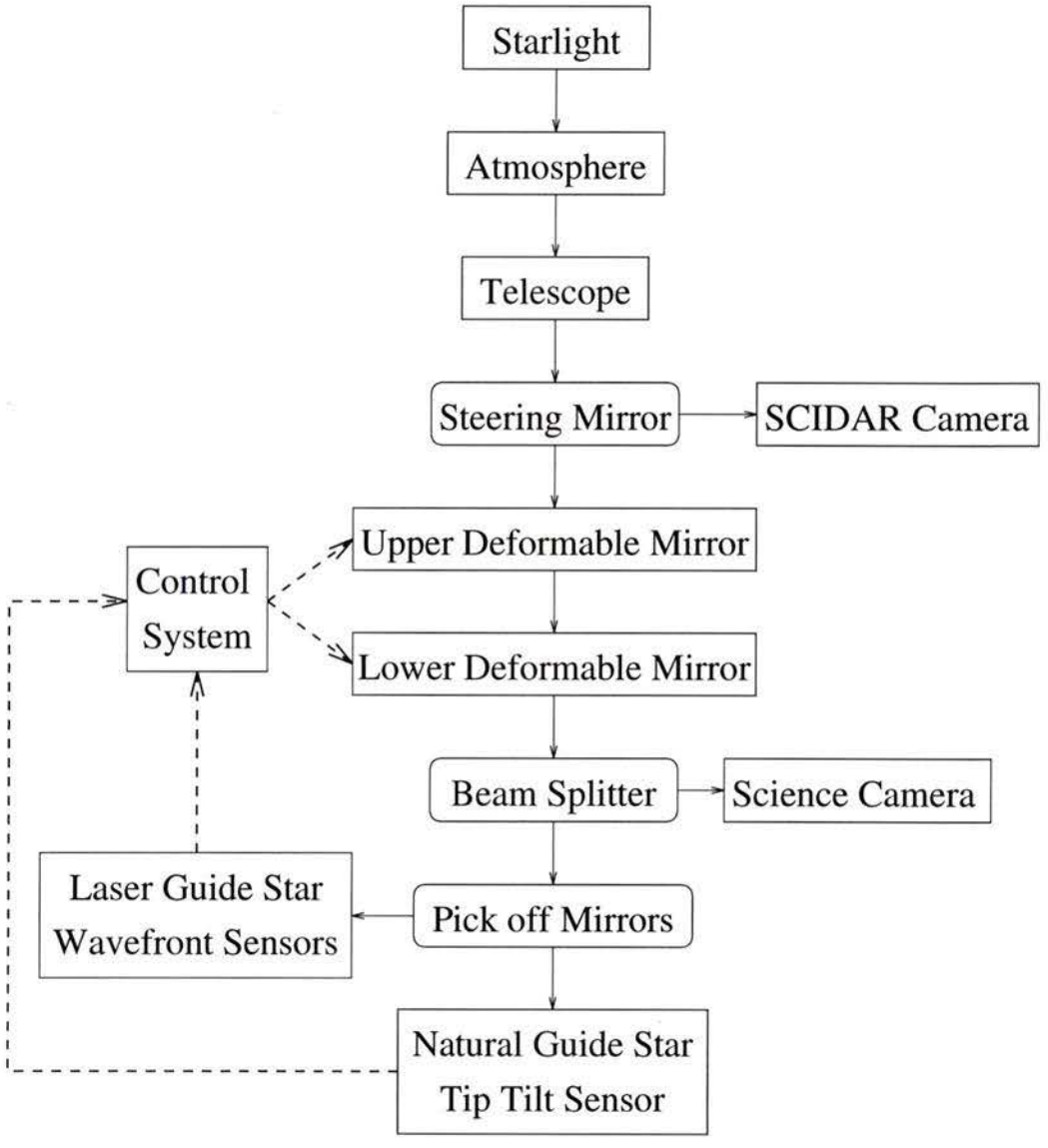

Figure 6.1: Schematic of the proposed multiconjugate adaptive optics system

of turbulence. In this configuration the laser guide stars are placed at an angle of 37 *arcseconds* from the center of the field.

The system will use a natural guide star tip-tilt sensor and four laser guide star wavefront sensors. The natural guide star tip-tilt sensor will be designed as a Shack-Hartman wavefront sensor without the lenslet array, so the tip-tilt (or the oscillating motion of the stellar image) over the whole aperture will be sensed. The natural guide star tip-tilt sensor will be designed with a field of view equal to the 22*arcsecond* field of view over which the laser guide star array will provide information. The sensor will be able to measure the tip-tilt of any suitable natural guide stars over the 22 *arcsecond* field of view. The measurement of multiple guide stars will allow the tip-tilt measurements from several stars to be added to reduce the error in the measured tip-tilt.

It will be assumed that the laser guide star wavefront sensors will be an array of four Shack-Hartman integrated CCD and lenslet arrays (see section 2.5.1). The model for these wavefront sensors will be the micro Shack-Hartman wavefront sensors produced by LASERDOT[16]. Each laser guide star wavefront sensor will be placed to sense one laser guide star, which will be at an angle of 37 *arcseconds* from the center of the field of view. The method of using separate wavefront sensors was selected over a single wide field wavefront sensor because of the large angle between the laser guide stars and the reduced alignment and flexure errors with the micro Shack-Hartman wavefront sensor. The laser guide star wavefront sensors will be fed using small pick off mirrors placed around the natural guide star tip-tilt sensor.

The system will also have an ADC (Atmospheric Dispersion Corrector) to correct for the optical dispersion caused by the air. The ADC will be placed into the system where the beam is collimated (or near collimated) and where there is ample room for the mounting of the prisms. The final placement of the ADC will be made after

the main optics have been designed and packaged in the defined volume.

The image quality target for the system will be a Strehl ratio of 0.9 or greater over the 22 *arcsecond* field of view of the science camera. The focal ratio of the system will be set to allow the images to be sampled by the science camera at the Nyquist sampling frequency. The Nyquist sampling frequency is two samples for each resolution element (the resolution element is the Rayleigh resolution criterion in this case), and is the minimum sampling rate without loss of information [50]. The science camera pixel size will be assumed to be $15\mu m$, thus the final focal ratio of the system must be $F/45$. This focal ratio will make the pixel size equal to half the Rayleigh resolution criteria. Astronomical grade image detectors with $15\mu m$ pixels are currently in use in many astronomical instruments.

The system will be mounted at the CFHT Cassegrain focus. As it is a test instrument, to test the principles of multiconjugate adaptive optics, it will be designed as an independent instrument. No constraint will be made on the position of the final focus as in the case of the Gemini adaptive optics module and the CFHT adaptive optics bonnette. The final focal ratio will be set to $F/45$ (as defined above) and the exit pupil of the system will not be constrained. The Cassegrain focus was selected over the Coude focus because the scattered light is less and the optical transmission is higher at the Cassegrain focus. The $F/8$ secondary will be used because the $F/16$ secondary at CFHT has an optical defect, a turned edge, which reduces the image quality.

Using the predicted gain in isoplanatic angle of 4 times larger for 2 deformable mirrors as calculated by Beckers[4], the $22 arcsecond$ field of view provided by the array of 4 laser guide stars becomes limiting at wavelengths longer than $1.3\mu m$. At $4.2\mu m$ the isoplanatic angle without multiconjugate optics becomes equal to the 22 *arcsecond* field of view provided by the array of laser guide stars. These values are found by

interpolating the values given in table 2.3. The field of view provided by the four laser guide stars is sufficient for work in the visible and near infrared.

6.2 Preliminary Design

In this design the deformable mirrors will be able to be independently positioned in conjugate altitude over a range of $0km$ to $9km$. The method devised to achieve this is shown in figure 6.2. The system uses three slides and a steering mirror along with the two deformable mirrors. Figure 6.2 shows the deformable mirror slide assembly in two configurations: one with the deformable mirrors at their maximum separation, and the second with the deformable mirrors positioned with both mirrors at the lowest positions.

The upper deformable mirror, DM 1, is mounted on a large slide which moves in the direction of the incoming beam. The lower deformable mirror, DM 2, is mounted on a slide, which is mounted on the large slide that the upper deformable mirror, DM 1, is mounted on. The direction of motion of the slide that DM 2 is mounted on is in the direction of the beam reflected from the upper deformable mirror, DM1. The steering mirror is mounted on an independent slide which moves the steering mirror in the direction of the outgoing beam.

The angle of incidence of the deformable mirrors and the steering mirror is fixed at 30 degrees which causes the beam to be deviated at an angle of 60 degrees at each reflection. The 30 degree angle of incidence was selected because it provides a good median between the elongation of the beam on the deformable mirror and the smallest distance between the two deformable mirrors without vignetting the beam. The net deviation of the beam after passing through the deformable mirror slide assembly is 60 degrees at the intersection of the input and output beam.

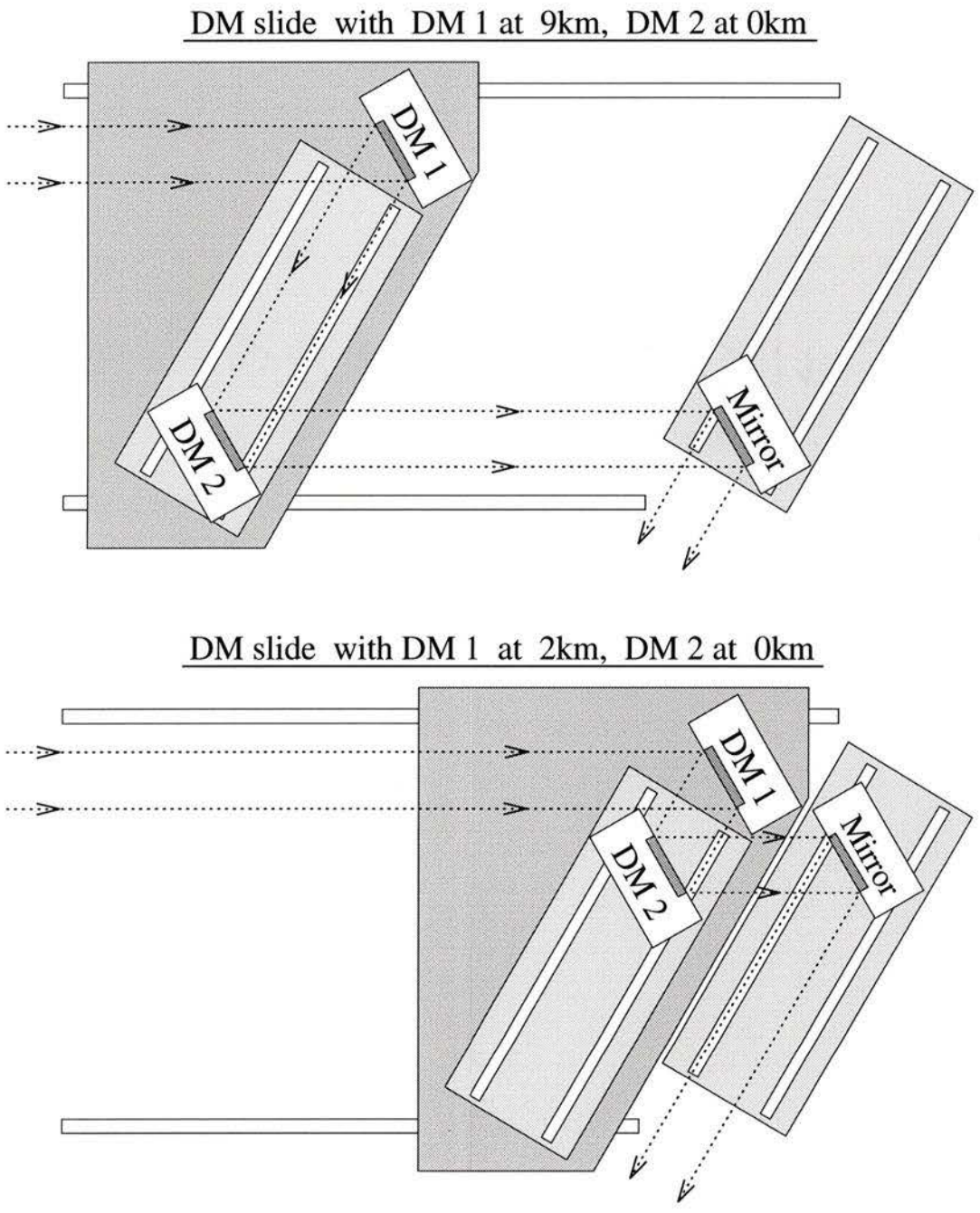

Figure 6.2: Schematic of the deformable mirror slide assembly

The deformable mirrors are moved so that the distance from the entrance to $DM1$ plus the distance from $DM2$ to the steering mirror is constant, and the distance from $DM1$ to $DM2$ plus the distance from the steering mirror to the exit is constant. When these constraints are satisfied the position of the input and output beam does not change. The positions of the two deformable mirrors can be independently selected with the only constraint being the minimum distance between the two deformable mirrors. The minimum distance between the two mirrors is $1.73D$ for a collimated beam of a diameter D and a 30 degree angle of incidents of the mirrors with clearance around the deformable mirrors as specified in section 2.4.

The main beam optics must image the $9km$ and $0km$ (pupil) layers of the atmosphere onto the deformable mirrors when the deformable mirror slide assembly is in the configuration shown in the top diagram in figure 6.2. The separation between the images of the $9km$ layer and the $0km$ layer is determined by the size of the deformable mirrors and the field of view. A first order approximation of the separation is derived by the fact that the axial magnification (the magnification of the axial separation of the images of two objects) is proportional to the square of the lateral magnification, and the lateral magnification is proportional to the ratio of the sizes of the exit and entrance pupils of the system. Since the lower deformable mirror diameter is equal to the exit pupil diameter of the system, a first order approximation of the separation is given by the distance $9km$ times the square of the ratio of the lower deformable mirror diameter and the primary mirror diameter.

The telescope alone, without additional optics, forms a real image of the $9km$ layer but not of the $0km$ layer. To image the $0km$ layer on a deformable mirror a positive element must be added to make a real image of the $0km$ layer. The deformable mirror slide requires that there are no optical elements between the images of the $9km$ layer and the $0km$ layer. The added element (which also collimates the beam) must be

before the image of the $9km$ layer formed by the telescope alone. The focus of the $9km$ layer, by the telescope alone, is $91mm$ from the telescope focus for an object at infinity (i.e., a star). Preliminary calculations showed that, with one element before the deformable mirror slide assembly, the size of the deformable mirrors would be close to $5mm$ with a separation of approximately $17mm$ between the $9km$ layer and the $0km$ layer. These results indicated that a system with only one element would have too small of a deformable mirror and too small of a separation between the mirrors.

It was decided that a system of two optical elements before deformable mirror slide assembly, and one element after to form the final image, would be the simplest system to satisfy the constraints. With two optical elements before the deformable mirrors the size of the deformable mirrors are not restricted as in the case of one optical element before the deformable mirrors. The curvatures of the three optical elements also gives more control over the Petzval sum of the system making the possibility of better quality images at the final focus.

The first order arrangement for the initial starting point of the design of the main optics are shown in figure 6.3. The optical elements are shown as singlet lenses in this diagram, but in the actual design they will be off-axis mirrors. Singlet lens were used in the diagram for clarity. The deformable mirror slide assembly is not shown in the figure but the positions of the $9km$ layer and $0km$ layer are shown.

The first optical element in the initial starting point is a field lens which is located at the focus of the telescope for a point at infinity. This field lens has a negative focal length equal to the distance between the focus of the telescope for a point at infinity and the focus of the telescope for a point at $9km$. The field lens collimates the light from the point at $9km$ without changing the focus for a point at infinity. This lens has been termed a field lens because it is located at a field (i.e., focus). Normally,

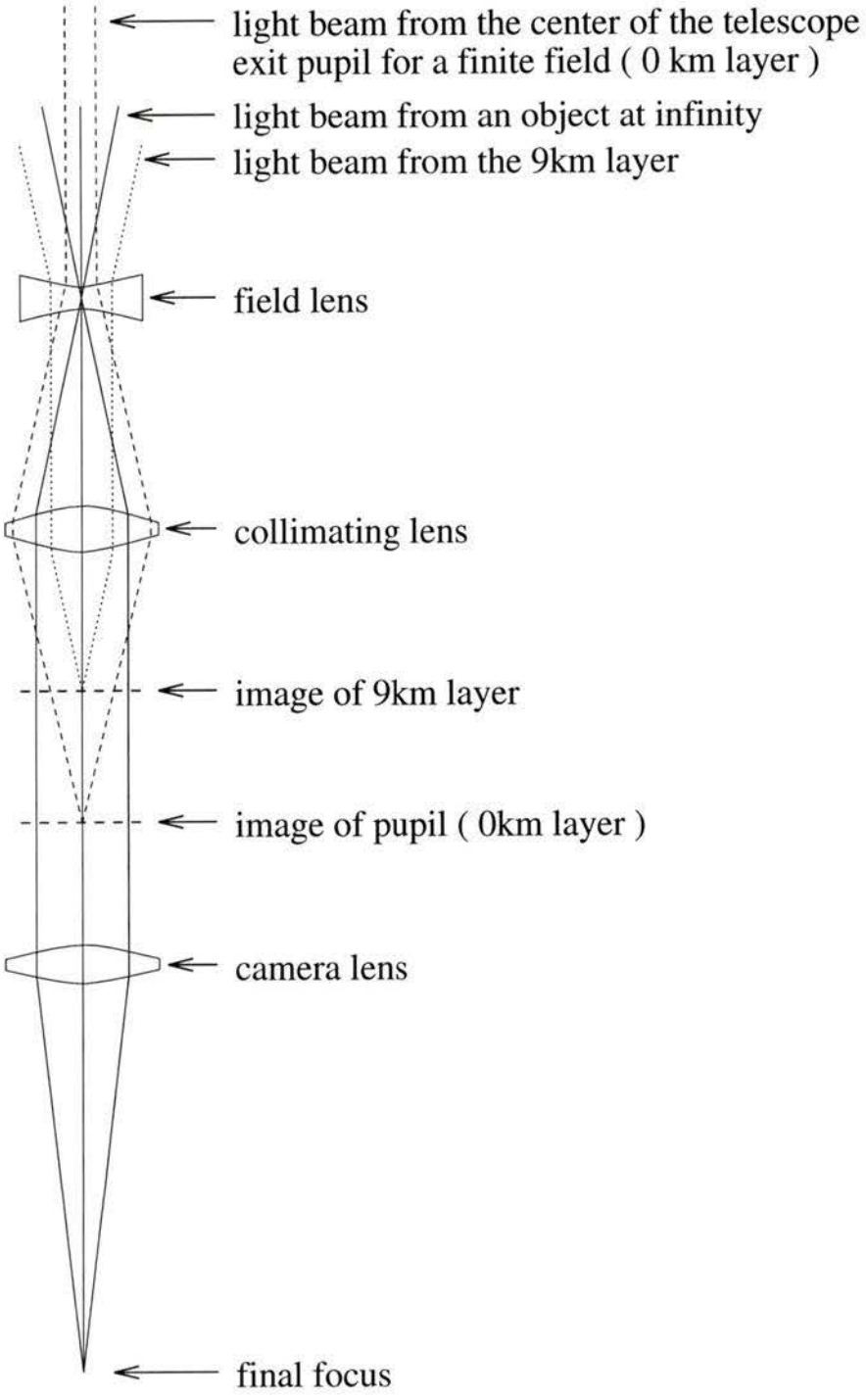

Figure 6.3: First order layout of main beam optics

when the lens is called a field lens in optics it is a positive lens located at, or near, the field and it is used to flatten the field or make a real image of the pupil after the lens. This lens is similar to the standard field lens but it is a negative lens rather than a positive lens, and it makes a virtual image of the pupil rather than a real image.

The next optical element, the collimating lens, collimates the light from the point at infinity. The distance from the collimating lens to the field lens determines the size of the collimated beam exiting the collimating lens. This distance is adjusted to match the collimated beam size to the deformable mirror size.

The image of the $9km$ layer is located at a distance equal to the focal length of the collimating lens, from the collimating lens. The distance from the image of the $9\ km$ layer to the image of the pupil ($0\ km$, layer) is equal to the actual separation in the atmosphere ($9\ km$) times the square of the ratio of the deformable mirror size to the primary mirror size.

The last optical element, the camera lens, re-images the light to make the final focus. The distance from the camera lens to the final focus and the size of the deformable mirrors determines the final focal ratio. The final focal ratio has been set to $F/45$ to allow the final image to be properly sampled using a detector with $15\mu m$ pixels.

This initial configuration was entered into the *CodeV* optical design software as a system of off-axis mirrors. The axis of symmetry of the mirrors were constrained so that they would all be parallel, and the axis of symmetry of the camera mirror was allowed to be displaced laterally in the plane of the other two axes. The system was then analyzed (using simulated ray traces) to determine the actual locations of the $9\ km$ layer and $0\ km$ layer. The optical prescription for the CFHT was also entered into the *CodeV* software to simulate the actual telescope that would be used with the adaptive optics system.

The initial configuration was then optimized to obtain a configuration which would give good clearance between the optical elements as well as good image quality. The 22 *arcsecond* field of view for the system was entered into the software and the beam was slightly de-collimated so the total beam size would not change when the deformable mirrors are scanned over the range of conjugate altitudes.

The beam was slightly de-collimated so the total size of the beam (the diameter of the beam plus the field) for the science field does not change on the deformable mirrors when they are scanned over the range of conjugate altitudes. This was done to use all of the actuators (on the deformable mirrors) at all positions of conjugate altitude. This de-collimation will result in the beam from a single object point expanding (instead of being exactly collimated), and the total beam size expanding after the pupil.

The system had to be optimized in iterative stages because the optimization package in the *CodeV* software was not able to converge on the optimal solution using one set of constraints. The system was optimized by alternating between two sets of constraints with two separate sets of variables. The position of the 9 *km* layer and 0 *km* layer and the size of the deformable mirrors was one set of constraints. These constraints were coupled to the variation of the radii of the first two mirrors in the adaptive optics system (the field mirror and the collimating mirror) and the separation between these two mirrors. The other set of constraints were the image quality and the final focal ratio. These constraints were coupled to: the variation of the conic constants of the three mirrors, the radii of the camera mirror, the lateral displacement of the axis of symmetry of the camera mirror, and the distance from the camera mirror to the final focus.

If the system was optimized in one stage, with all of the above variables and constraints together, the software would satisfy the position of the layer constraint by

varying the conic constants. This would introduce a large amount of image aberrations at the 9 km layer and the 0 km layer. An enhancement to the $CodeV$ lens design software would be to give the user the ability to couple specific constraints to specific variables as an option within the optimization package.

The target values of the constraints were required to be slowly changed from the paraxial values to the final value, optimizing the system at each stage. If the values for the constraints were changed too rapidly the optimization software would lose the configuration and deviate to a solution with the variables becoming values which can not be manufactured, such as very small radii, or very large conic constants.

In the optimization there were three variables that were varied manually. These variables were adjusted to give the necessary clearance between the optical elements, as well as to make the system easier to construct. These variables were: the off-axis angle of the optics, the distance from the field lens to the focus of the telescope (for a point at infinity), and the distance from the 0 km layer to the camera mirror.

A preliminary design which satisfied the system constraints was found. This design is shown in figures 6.4 and 6.5. Figure 6.4 shows the multiconjugate adaptive optics system with the CFHT optics. Figure 6.5 shows only the multiconjugate adaptive optics system's optics.

The deformable mirror size for the preliminary design is $20mm$. With the $20mm$ deformable mirror size the distance between the $9km$ layer and the $0km$ is $238mm$. This deformable mirror size gives a good balance between the deformable mirror size and the distance between the deformable mirrors for the construction of the slide.

The field mirror was located 50mm before the telescope focus for a point at infinity. The field mirror was moved from being at the focus for a point at infinity to reduce the surface tolerance on the field mirror. If it were located at the focus any surface defects on the mirror would be seen at the final image. Moving the field mirror from

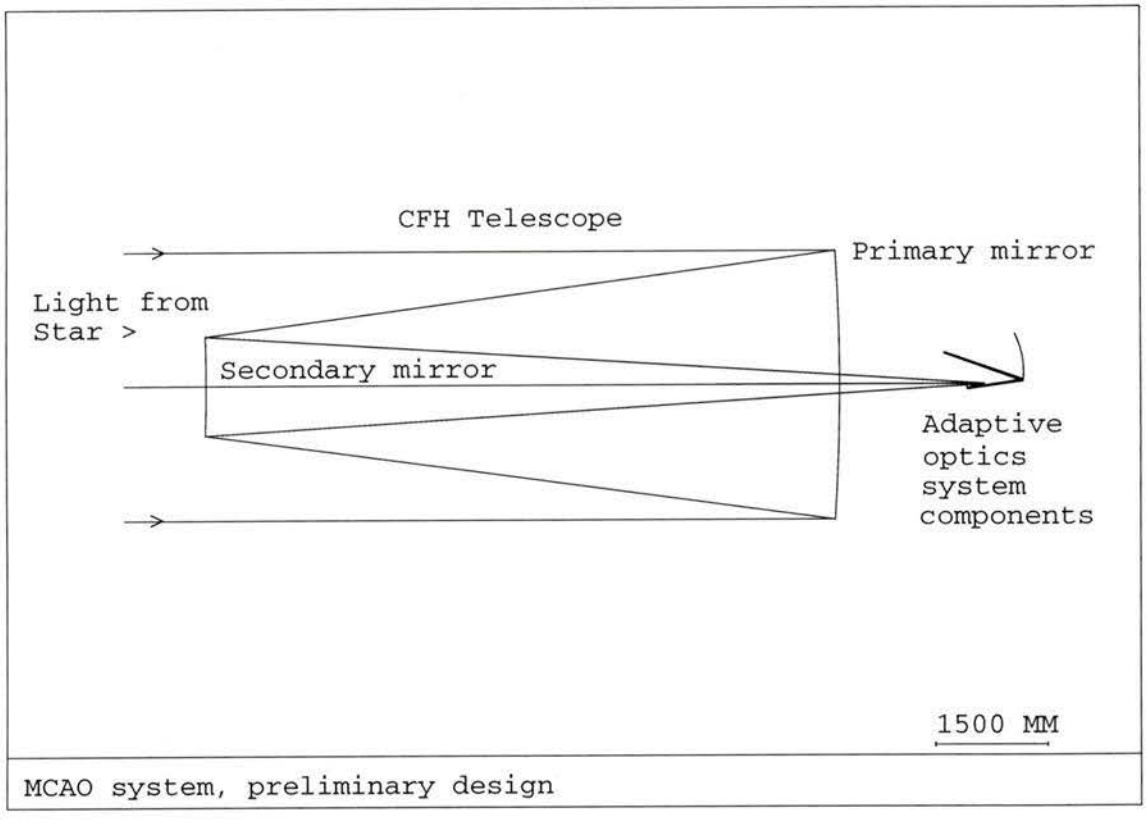

Figure 6.4: Preliminary design shown with telescope

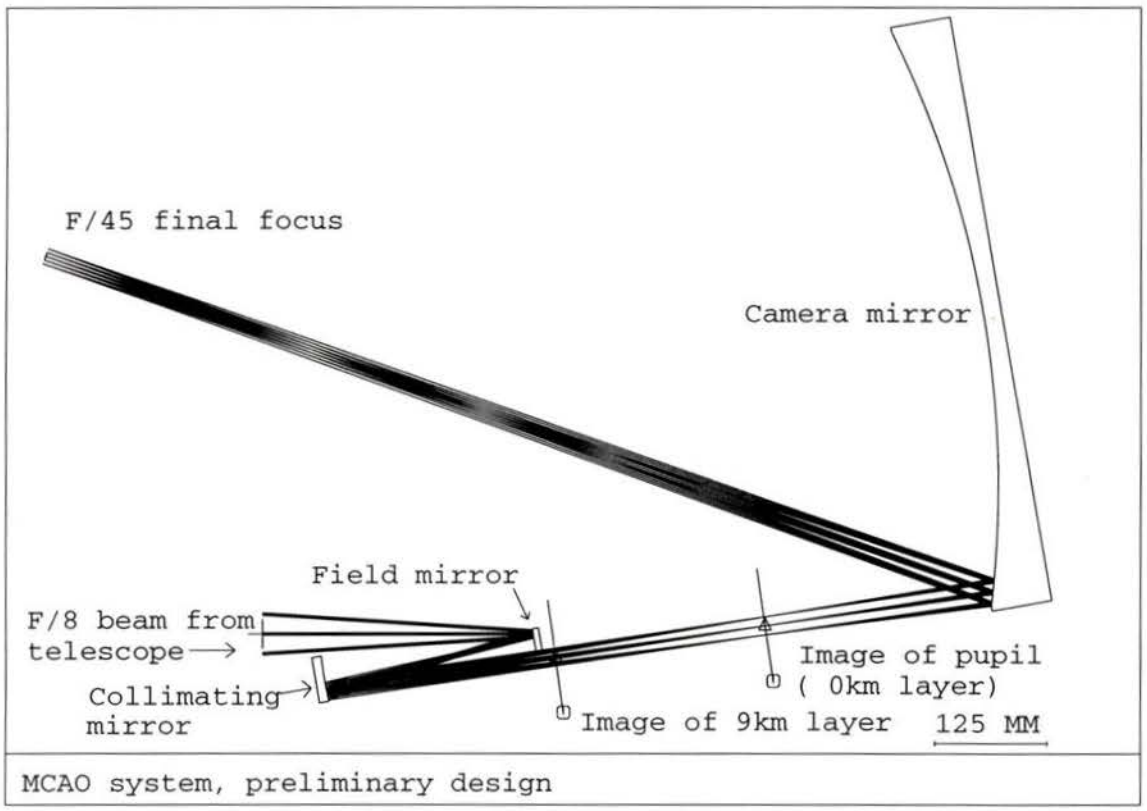

Figure 6.5: Preliminary design shown without the telescope

the focus blurs the image of the surface defects.

The curved mirrors in the design are all conic surfaces. The field mirror and collimating mirror are hyperboloid, and the camera mirror is an ellipsoid. The axis of symmetry of the field mirror and the collimating mirror are congruent. The axis of symmetry of the camera mirror is parallel to the axis of symmetry of the other mirrors but displaced laterally.

The image quality of the preliminary design is very good. Over the whole 22 *arcsecond* field of view the image quality was better than 0.98 Strehl ratio measured at a wavelength of $550nm$. This corresponds to 82% of the light being contained within the Airy disk of $60\mu m$.

6.3 Final Design

The preliminary design was used as the starting point for the final design. The final design is shown in figure 6.6. This figure shows the system complete with the SCIDAR system, natural guide star wavefront sensor, laser guide star wavefront sensor, and the science camera. The steering mirror for feeding the light into the SCIDAR camera is shown inserted into the main beam in the figure but in actual usage this steering mirror would be only inserted into to the beam when the SCIDAR camera is in use, directing all of the light into the SCIDAR camera. The *CodeV* optical prescription for the final design is given in appendix A. The lens file uses the zoom feature in the lens design software to incorporate science camera, SCIDAR camera, and wavefront sensors in one lens file. The science camera is at zoom position 1, the SCIDAR camera is at zoom position 2, the natural guide star wavefront sensor is at zoom position 3, and the laser guide star wavefront sensors are at zoom positions 4, 5, 6, and 7.

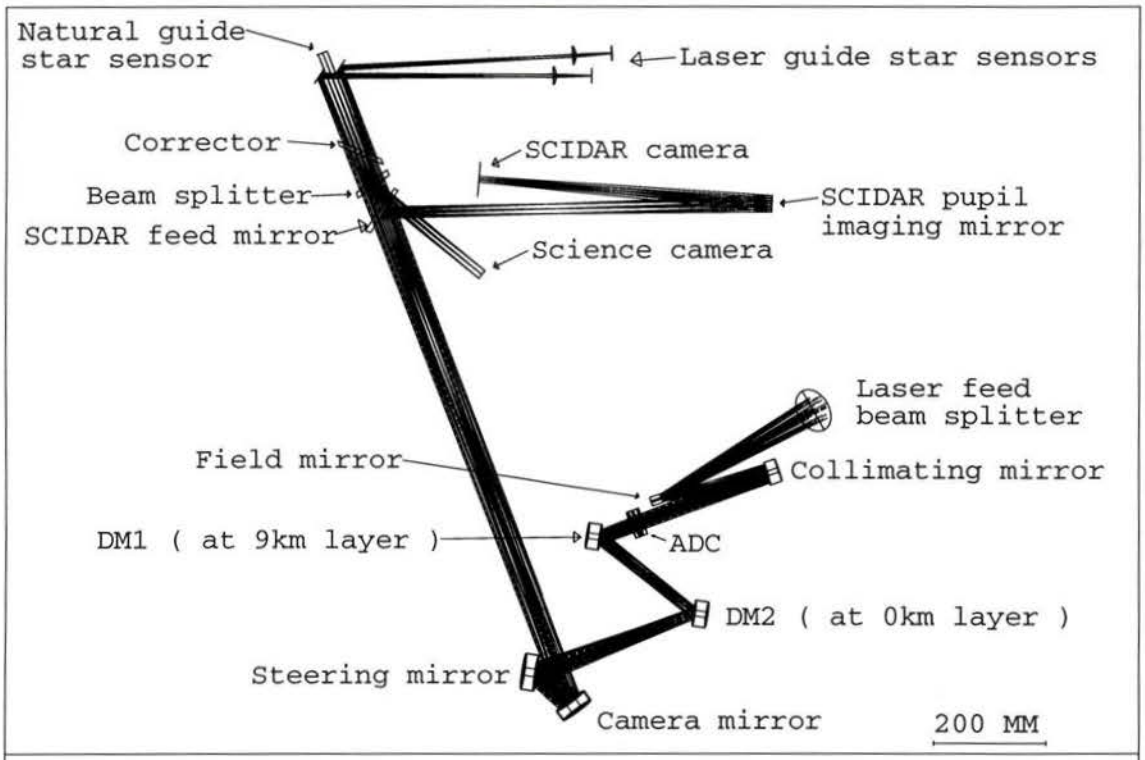

MCAO system, final design, top view

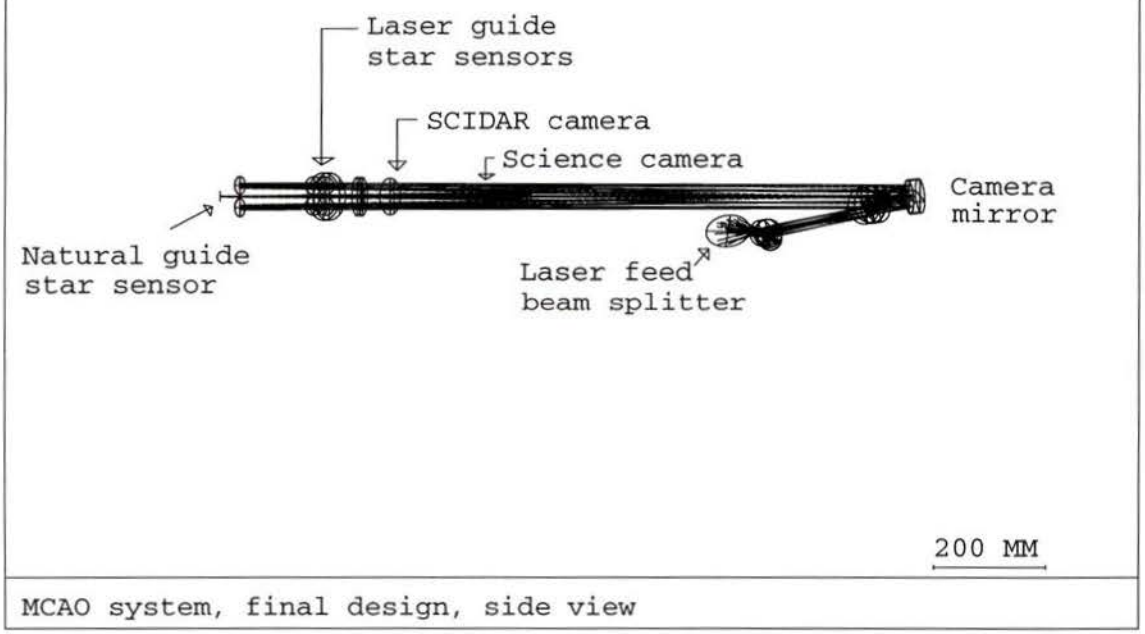

MCAO system, final design, side view

Figure 6.6: Final design, top and side views

6.3.1 Main Beam Optics

The main beam optics are the optics in the adaptive optics system from the telescope to the science detector which the light from the science object passes through. These optics do not include the wavefront sensors or the SCIDAR camera. The main beam optics are shown in figure 6.7. The main beam optics are based on the preliminary design (figure 6.5) with the addition of the deformable mirrors, a steering mirror, the ADC, and two beam splitters.

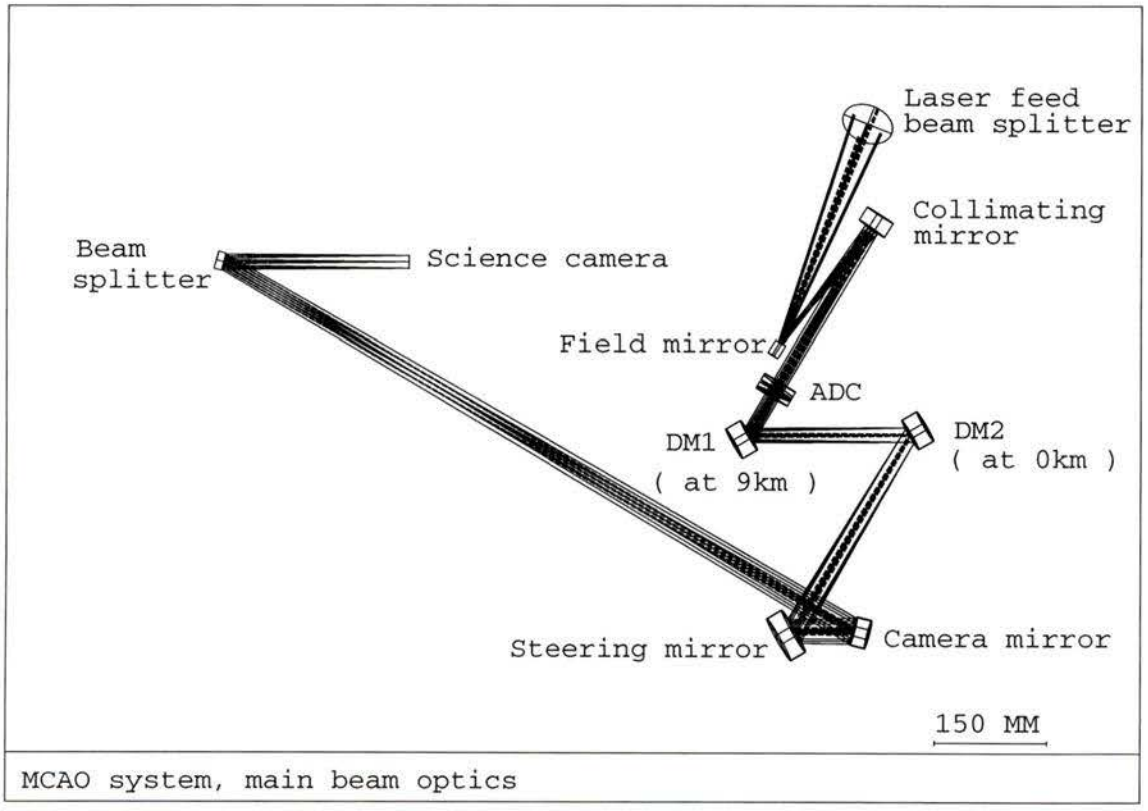

Figure 6.7: Main beam optics

The deformable mirrors were added to the preliminary design as flat mirrors with a size equal to twice the clear aperture of $20mm$, and a thickness equal to the clear aperture to insure that sufficient clearance is provided for the deformable mirrors. The

steering mirror, to complete the deformable mirror slide assemble, was also added to the design.

It was found that the camera mirror in the preliminary design could be replaced with an on-axis toroidal surface rather than the off-axis conic surface because of the long focal ratio, $F/45$, and the small field of view of $22 arcseconds$. The image quality was not degraded by this change and the manufacturability was improved. The other two off-axis mirrors were not able to be changed to toroidal surfaces without a large loss of image quality.

A method to project the laser light onto the sodium layer to make the laser guide stars was added to the system. It was decided to put a beam splitter before the field mirror which would allow the laser light for the laser guide star to be fed up the telescope by passing it through the back of the beam splitter. The light from the sky would be reflected from the front of this beam splitter into the adaptive optics system.

The field mirror was moved to 35mm before the telescope focus for a point at infinity. This change was made to reduce the amount that the field mirror and collimating mirror are off-axis to make the mirrors easier to manufacture. This change also reduced the distance from the field mirror to the collimating mirror, and increased the distance from the collimating mirror to the image of the 9 km layer. The reduced distance between the field mirror and the collimating mirror allows more room for the beam splitter before the adaptive optics system. The increased distance from the collimating mirror to the image of the 9 km layer allows the room needed to put the ADC between the collimating mirror and the upper deformable mirror.

The ADC was designed using the methods described in section 5.3. The values for the atmospheric dispersion were taken from information from CFHT [48]. The atmospheric dispersion was simulated in $CodeV$ by placing a 100 mm thick prism

with a 1 *degree* wedge angle in front of the telescope. The refractive index values for the prism were calculated to give the same dispersion as the atmosphere.

The ADC was designed to operate from the zenith to 45 *degrees* from the zenith over a wavelength range from 400 nm to 1000 nm. All the angles of the glasses for each of the ADC prisms were allowed to vary. The pair of prisms were constrained to be symmetric to allow the dispersion of the first prism to be compensated by the second prism by counter rotating the prisms.

All of the glass pairs listed in section 5.3 were tried for the ADC. The glass pair LAFN21 and KF9 gave the best image performance when the ADC was on, but has significant aberrations when the ADC was in the off position. The glass pair FK54 and BAK5 gave images very close to the latter pair, and gave good images when the ADC was in the off position. This glass pair was chosen as the ADC glass pair for this design.

The range of atmospheric conjugate altitudes which the deformable mirrors can be placed, using the slide in the final design, is 0 km to 7.2 km for the lower deformable mirror and 1.8 km to 9 km for the upper deformable mirror. The mirrors can be placed at any altitude over these ranges with, the only constraint being the minimum distance between the mirrors of 38 mm (which corresponds to an atmospheric altitude difference of 1.8 km).

When the deformable mirrors are adjusted in conjugate altitude they could vignette the beam from the camera mirror to the beam splitter. To prevent this vignetting of the beam two rotations were introduced in the system. These rotations were along the optical axis just before the upper deformable mirror and just after the steering mirror for the deformable mirror slide. An equal, but opposite amount of rotation was introduced at each of the two rotation points to allow the beam from the camera mirror, including the laser guide star light, to clear the deformable mirrors

when they are scanned in conjugate altitude. Because the rotation was equal and opposite the image quality was not effected.

Three additional rotations were made in the system. Two were used to make the optical elements after the camera mirror lay on a plane parallel to the bottom of the primary mirror. One just before the field mirror and the other after the camera mirror. The third rotation was made between the secondary mirror of the telescope and the beam splitter used to feed the laser beam for the guide stars. This rotation was used to align the laser guide star wavefront sensors to the plane parallel to the primary mirror, compensating for the optical rotation effect of the optical components.

The image quality at the science detector was evaluated to consider the effects of diffraction using the point spread function and the modulation transfer function. This system is too close to the diffraction limit for ray based analysis to be used to evaluated the image performance. When ray based analysis is used it is found that 100% of the rays are within a diameter of $9\mu m$ over the whole field. Diffraction theory states that, at most, 84% of the energy should be contained within the airy disk diameter. The airy disk diameter for the system is $60\mu m$, which is much larger than the diameter containing 100% of the rays obtained from the ray based analysis.

The worst and best point spread functions for the image at the science detector with the ADC in place are shown in figure 6.8. The point spread function is the intensity pattern which a perfect infinitely small point object would make. These plots were normalized so a perfect lens would have an intensity of 100. The best point spread function with the ADC in the system (as shown in figure 6.8) was found to be with the telescope pointed at the zenith at the field angle of 5.5 *arcseconds* in the y axis and -5.5 *arcseconds* in the x axis. The worst point spread function with the ADC in the system (as shown in figure 6.8) was also found to be with telescope pointed at the zenith at the field angles of 11 *arcseconds* in the y axis and

0 *arcseconds* in the x axis. The airy rings (which result from the wave nature of light) can be seen in these plots.

The Strehl ratio at the center of the science detector with the ADC in the system and the telescope pointed at a zenith angle of 45 *degrees* is 0.956. The best Strehl ratio for this configuration is 0.958 at the field position of 0 *arcseconds* in the y axis and 11 *arcseconds* in the x axis. The worst Strehl ratio for this configuration is 0.943 at the field position of 11 *arcseconds* in the y axis and 0 *arcseconds* in the x axis. The respective RMS wavefront errors are 0.034 waves, 0.033 waves, and 0.039 waves (the units of RMS waves is $494.9nm$).

With the ADC in the system and the telescope pointed at the zenith the Strehl ratio at the center of the science detector is 0.955. The best Strehl ratio for this configuration is 0.962 at the field position of $5.5arcseconds$ in the y axis and $-5.5arcseconds$ in the x axis. The worst Strehl ratio for this configuration is 0.939 at the field position of 11 *arcseconds* in the y axis , 0 *arcseconds* in the x axis. The respective RMS wavefront errors are 0.034 waves, 0.032 waves, and 0.040 waves (the units of RMS waves is $494.9nm$).

When the ADC is removed from the system, and the effects of atmospheric dispersion are ignored, the Strehl ratio is greater than 0.99 over the whole field. The RMS wavefront error is less than 0.004 waves (the units of RMS waves is $494.9nm$).

The MTF (Modulation Transfer Function) for the system is given in figures 6.9, 6.10, and 6.11. Figure 6.9 shows the MTF with the ADC in the system and a zenith angle of 0 *degrees*. Figure 6.10 shows the MTF with the ADC in the system and a zenith angle of 45 *degrees*. Figure 6.11 shows the MTF with the ADC removed from the system.

The MTF gives a better indication of the ability of the system to resolve extended objects. A description of the MTF is given by Smith [53]. The small upward bump

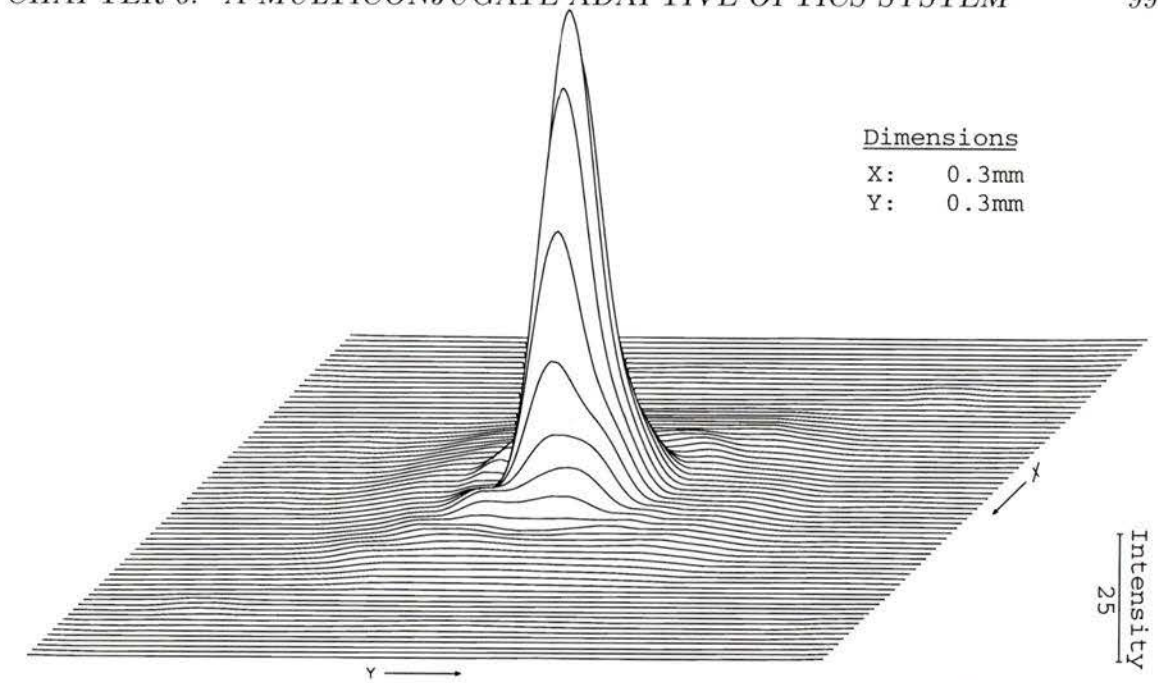

Science camera Best image quality ADC in, Zenith angle=0°	DIFFRACTION INTENSITY POINT SPREAD FUNCTION Peak intensity for perfect lens = 100 FLD(5.5, -5.5) arcseconds	WAVELENGTH WEIGHT 1000.0 NM 1 850.0 NM 1 700.0 NM 1 550.0 NM 1 400.0 NM 1

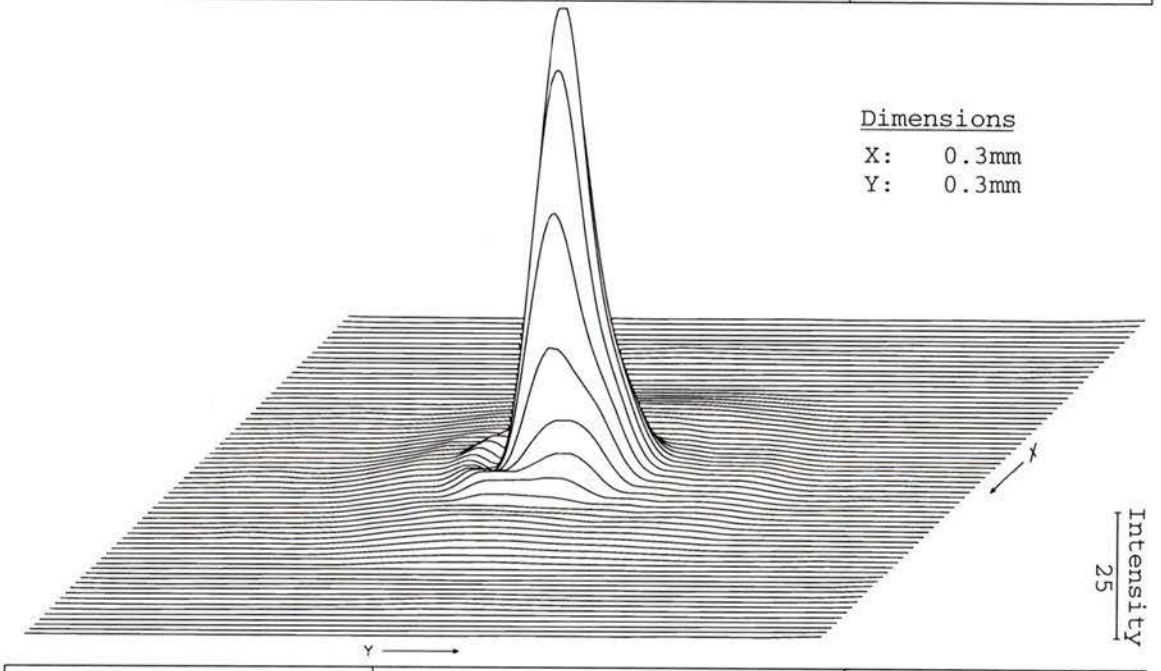

Science camera Worst image quality ADC in, Zenith angle=0°	DIFFRACTION INTENSITY POINT SPREAD FUNCTION Peak intensity for perfect lens = 100 FLD(0, 11) arcseconds	WAVELENGTH WEIGHT 1000.0 NM 1 850.0 NM 1 700.0 NM 1 550.0 NM 1 400.0 NM 1

Figure 6.8: Worst and best point spread functions for the science camera

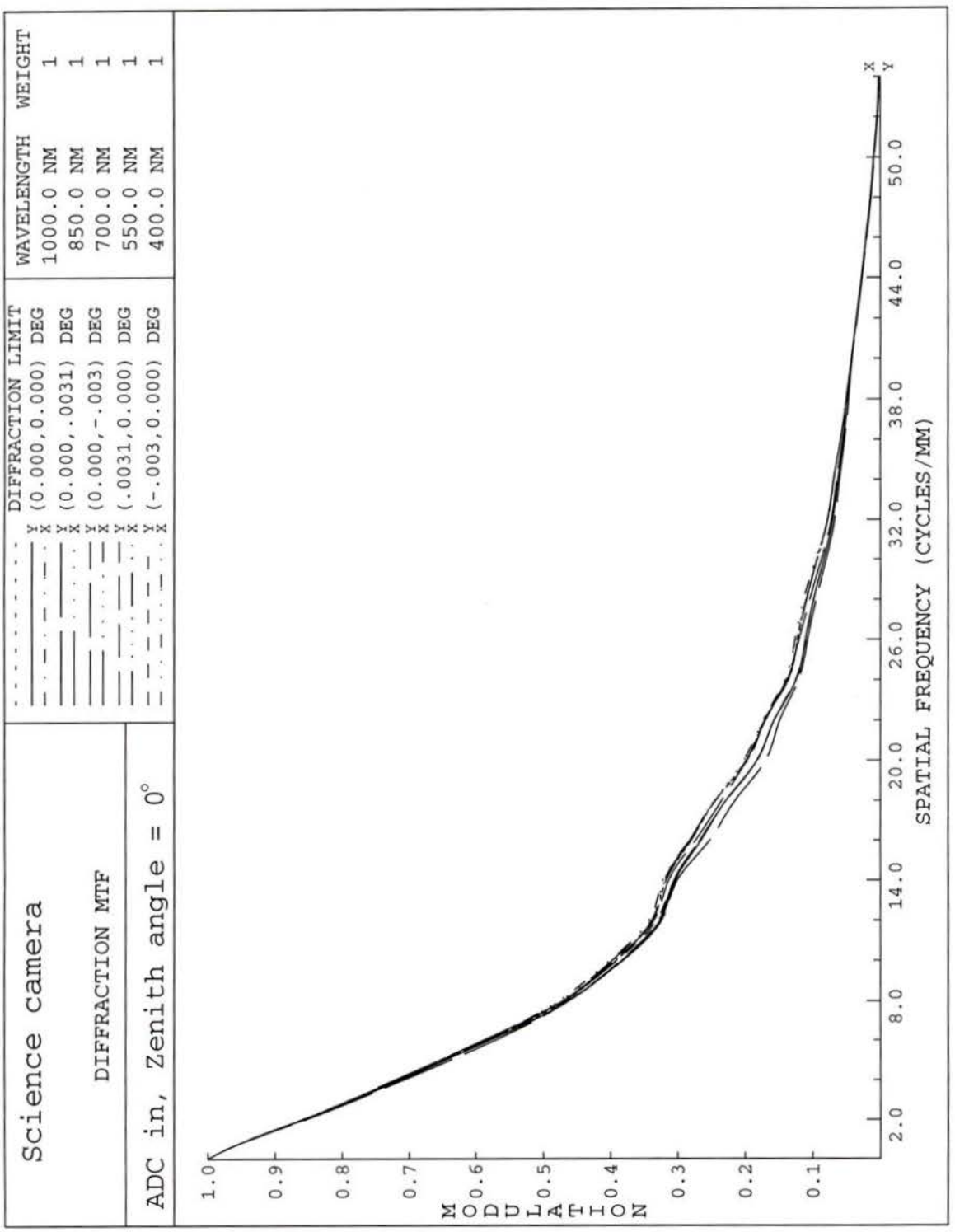

Figure 6.9: MTF with the ADC in, and a zenith angle of 0 *degrees*

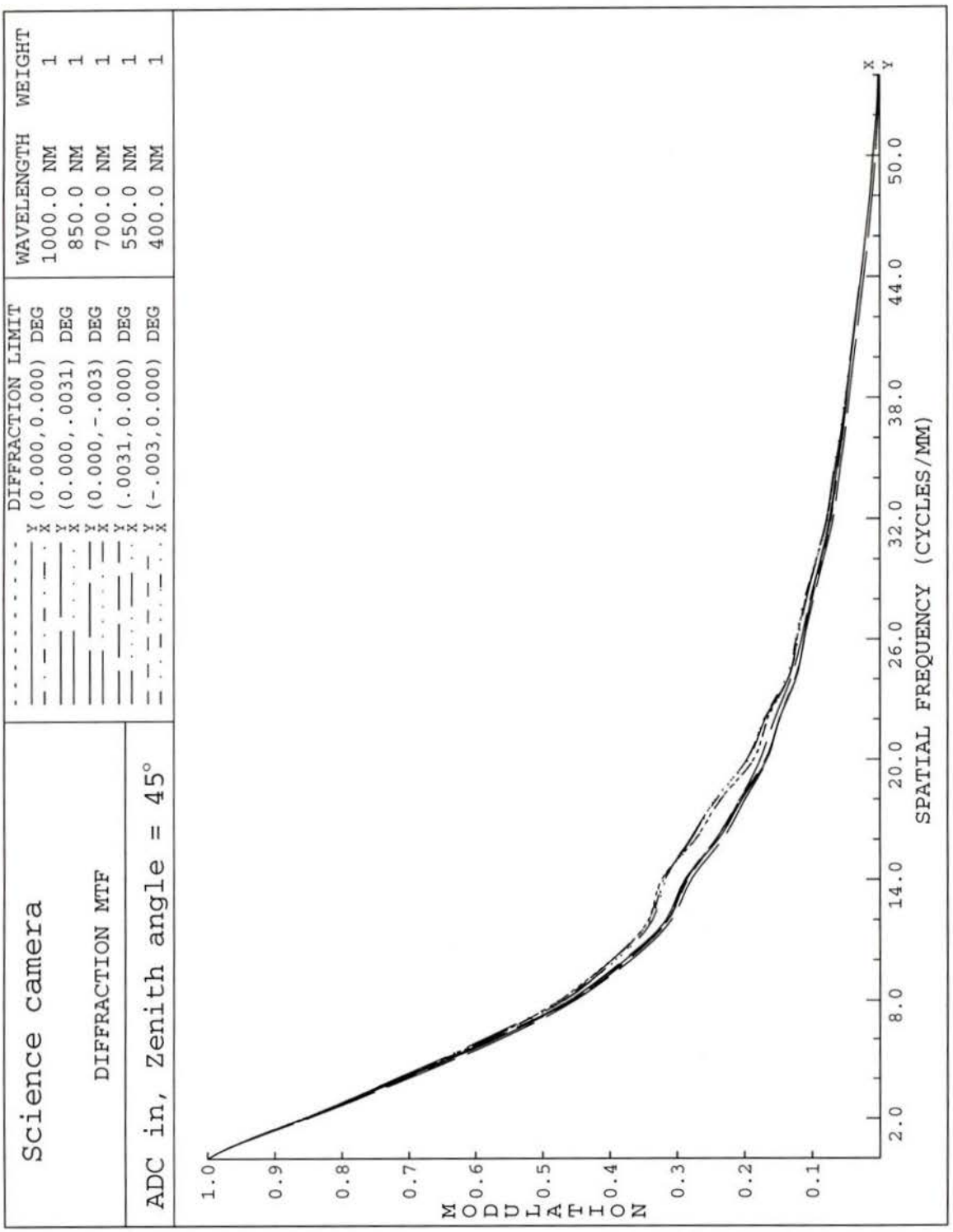

Figure 6.10: MTF with the ADC in, and a zenith angle of 45 *degrees*

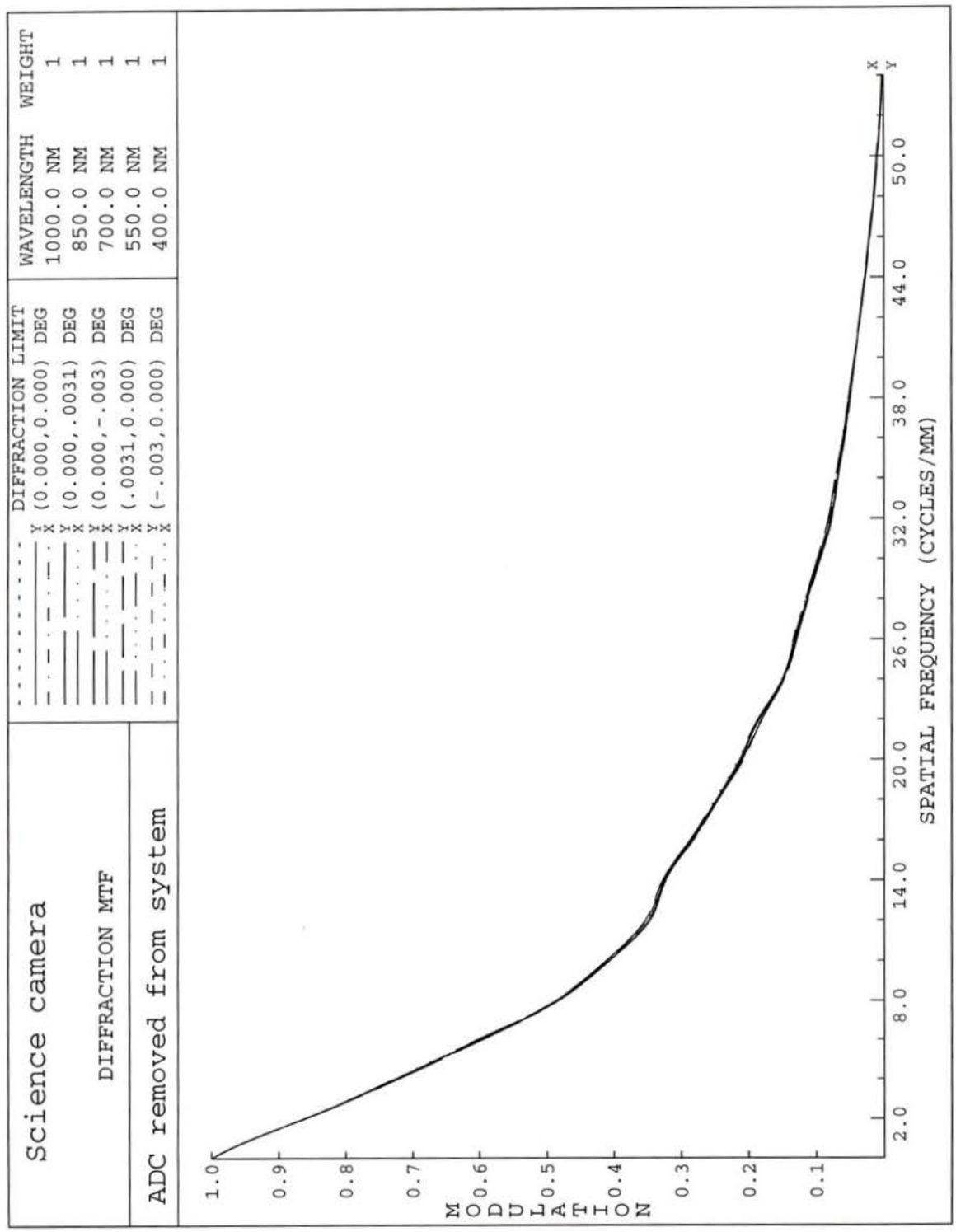

Figure 6.11: MTF with the ADC removed from the system

in the MTF (at a spacial frequency of approximately $15 cycles/mm$) is due to the central obstruction in the CFHT which improved the modulation at this frequency.

The uppermost line in the MTF graphs is the theoretical maximum modulation for the system (the diffraction limit). When the ADC is removed from the system the MTF for the system is almost perfect, as can be seen in figure 6.11. The ADC causes a slight decrease in the modulation at spacial frequencies between 10 and $30 cycles/mm$. The contrast of objects with spacial frequencies in this range would be slightly degraded.

The *CodeV* optical prescription for the main beam optics system is given in appendix A and B. The lens file in appendix A contains the complete adaptive optics system including the wavefront sensors and SCIDAR camera. The main beam optics is zoom position 1 in this lens file. The lens file in Appendix B contains only the main beam optics.

The command scripts for the final optimization of the main beam optics, not including the ADC, is given in appendix C. There are three different command scripts in this appendix. The lens file which was used with these command scripts is in appendix D. The command scripts were run on this lens file, in sequence, until there was no further change in the lens file.

6.3.2 SCIDAR Camera

The SCIDAR camera has been designed to make a high resolution image of the pupil on an image detector. The size of the image of the pupil was set at $10\ mm$. A focal point was put before the detector so a field stop could be put at this point to allow only light from the stars of interest to pass onto the image detector. The SCIDAR camera is shown in figure 6.12.

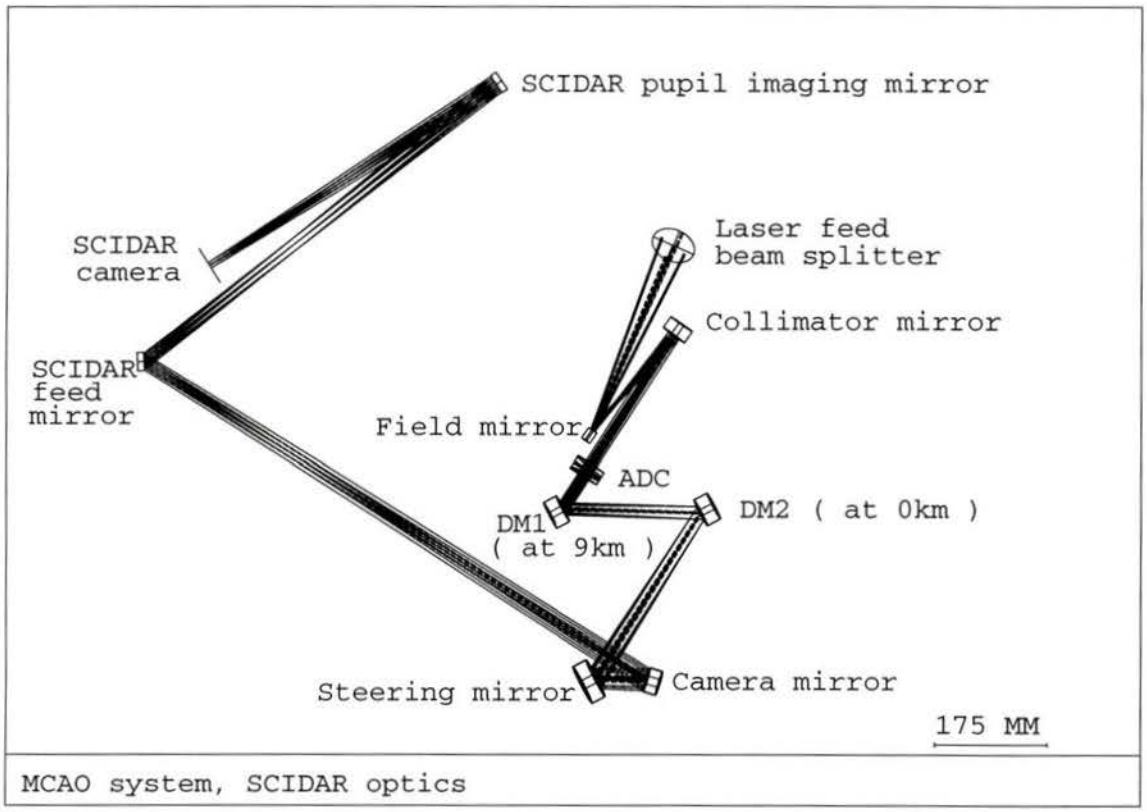

Figure 6.12: SCIDAR optics

The SCIDAR camera was ray traced by removing the atmosphere and tracing rays from the stop of the system to the image plane. The system was traced as a telecentric system with the numerical aperture of the beam set equal to the field of view which would be imaged onto the image detector.

The camera mirror was designed as a spherical mirror placed after the focal point of the system. The curvature of the mirror, the distance from the mirror to the focal point, the distance from the mirror to the detector, and the tilt of the mirror were all adjusted to give a 10 mm diameter image of the pupil with good image quality and clearance. The image quality of the pupil for a 5 *arcsecond* field of sky was found to have a Strehl ratio of greater than 0.9 over the whole pupil. The optical prescription for the SCIDAR camera is given in zoom position 2 in the lens file in appendix A.

6.3.3 Wavefront Sensors

Figure 6.13 shows the layout of the wavefront sensor optics. The wavefront sensors were fed using a beam splitter which reflected the light for the science camera, and transmitted the light for the wavefront sensors. The beam splitter introduced aberrations into the beam which were corrected using a corrector plate after the beam splitter. The corrector plate is a wedge of glass with planar surfaces.

A focus with the same focal ratio and field of view as the science field was provided for the natural guide star tip-tilt sensor. At this point, an image detector designed to measure the position of the natural guide star(s) will be placed. Using this corrector the Strehl at the natural guide star focus was, with the ADC removed from the system, better than 0.98 over the whole field. The image quality was degraded only slightly (by the beam splitter and corrector) as compared to the image quality at the science camera.

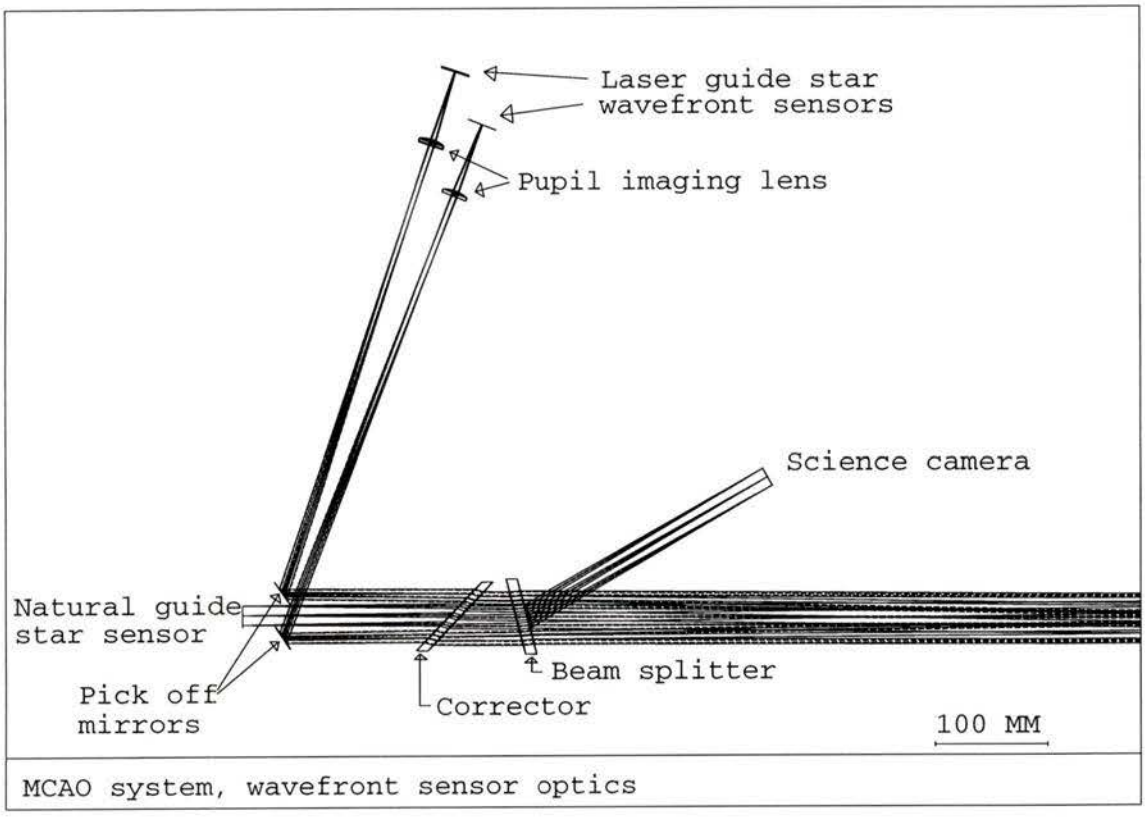

Figure 6.13: Wavefront sensor optics

The four laser guide star wavefront sensors were fed by placing small pick off mirrors around the natural guide star focus. These mirrors were placed so that they would not vignette the natural guide star tip-tilt sensor. The laser guide star wavefront sensors were traced using light with a wavelength equal to the sodium D_2 line ($598nm$) coming from an object point at an altitude of 90 km. For each wavefront sensor a lens was used to make a 1.24 mm diameter image of the pupil. This pupil diameter corresponds to a 18 by 18 array of micro lenses with the same lens diameter, $69\mu m$, as the LASERDOT micro Shack-Hartman lenslet array. This sub-aperture size corresponds to twice the size of the isoplanatic patch size. This sub-aperture size is equal to the r_i defined for each layer by Beckers in equation 4.1 for two deformable mirrors. The pupil size can be easily changed by changing the pupil imaging lens if a different number of sub-apertures or a different micro lens diameter is desired. The image quality for a single sub-aperture with a plano-convex micro lens (made from $BK7$ glass) was tested. The Strehl ratio was found to be 0.99.

The optical prescription for the wavefront sensor optics is given in the lens file in appendix A. The natural guide star wavefront sensor is zoom position 3 in the lens file. The laser guide star wavefront sensors are zoom positions 4, 5, 6, and 7 in the lens file.

6.4 System Tolerances

The inverse image quality sensitivity of main beam optics was calculated and tabulated in table 6.4. These values are calculated over the wavelength range of $400nm$ to $1000nm$. The inverse image quality sensitivity calculated is the amount of variation of a parameter necessary to cause 0.01 RMS wavefront distortion at the image. The

science detector was allowed to move in the direction of the beam (i.e., to focus) as a compensator.

The coordinate system used in the lens design program has the X and Y axis parallel to the optical surface, with the Z axis perpendicular to the surface. For a surface which is not tilted Z is in the direction of the optical axis.

The prism wedge angle for the atmospheric dispersion corrector is the wedge angle for each of the two different glasses which make the prism pair. The prism unit tilt and rotation is the tilt of a prism pair (consisting of the low dispersion and high dispersion glasses) and the rotation of a prism pair around the optical axis. The sensitivities are the same for the two prism pairs.

The toroidal camera mirror radii sensitivity was calculated for the average radii and the difference between the X and Y radii of the toroid. The difference between the X and Y radii is much more sensitive than the average of the X and Y radii.

This sensitivity table can be used to estimate the mounting and fabrication tolerances for the system. The total RMS wavefront distortion can be calculated for a given set of system tolerances by computing the RMS wavefront distortion for each tolerance and summing. The expected Strehl ratio for the system can be found using equation 2.10. The RMS wavefront variance (σ^2) in section 2.6 is equal to 2π times the RMS wavefront distortion given in table 6.4. The expected Strehl ratio for a perfect star image can be found by multiplying the RMS wavefront distortion by 2π and inputing this into equation 2.10. The expected performance for the adaptive optics system to correct distorted images can be estimated by using the other equations in section 2.6.

variation in parameter for 0.01 RMS wavefront distortion		
Laser feed beam splitter		
decenter	Z axis	0.18 mm
tilt	X/Y axis	0.092 degrees
Field mirror		
radii		1 mm
Conic constant		0.73
decenter	X/Y axis	0.41 mm
	Z axis	0.28 mm
tilt	X/Y axis	0.18 degrees
	Z axis	3.7 degrees
Collimating mirror		
radii		1.5 mm
Conic constant		0.23
decenter	X/Y axis	0.74 mm
	Z axis	1.8 mm
tilt	X/Y axis	0.069 degrees
	Z axis	2.9 degrees
Atmospheric dispersion corrector		
prism wedge angle		0.023 degrees
prism unit tilt		1.8 degrees
prism unit rotation		0.74 degrees
DM 1		
decenter	Z axis	0.75 mm
tilt	X/Y axis	0.029 degrees
DM 2		
decenter	Z axis	0.75 mm
tilt	X/Y axis	0.023 degrees
Steering mirror		
decenter	Z axis	0.75 mm
tilt	X/Y axis	0.017 degrees
Camera mirror		
average radii		6.1 mm
difference between X and Y radii		0.46mm
decenter	X/Y axis	0.79 mm
	Z axis	2.8 mm
tilt	X/Y axis	0.032 degrees
	Z axis	0.138 degrees
Beam splitter		
tilt	X/Y axis	0.017 degrees

Table 6.1: Main beam sensitivity table

Chapter 7

Summary

From the survey of literature in chapters 3 and 4 is was found that, theoretically, the isoplanatic angle (defined in the glossary in appendix E) could be enlarged using multiconjugate adaptive optics. The predicted gain in isoplanatic angle was found to be up to 2 times the number of deformable mirrors used in the multiconjugate adaptive optics system. The simplest multiconjugate adaptive optics system would have two deformable mirrors, with such a system the predicted gain in isoplanatic angle would be up to 4 times. A system composed of two deformable mirrors, a SCIDAR camera, a natural guide star wavefront sensor, four laser guide stars with wavefront sensors, and a atmospheric dispersion corrector was determined to be a suitable system to test the theory of multiconjugate adaptive optics.

A design for a multiconjugate adaptive optics system with two independently selectable layers has been presented. This design incorporated the necessary optical components for a multiconjugate adaptive optics system. A novel method of positioning the deformable mirrors so they could be independently positioned at any conjugate altitude was used in the design. The system was designed to have a field of view of 22 *arcseconds* with the four laser guide stars positioned at an angle of

37 *arcseconds* from the center of the field. The link between the separation of the deformable mirrors and the ratio of the entrance pupil to the deformable mirror size was also found to be an important constraint in the design of multiconjugate adaptive optics systems. The optical design utilized a new arrangement of two off-axis conics and a toroidal mirror to image the main beam. The image quality of a Strehl ratio better than 0.93 over the whole field of view was achieved at the science camera (including the effects of the atmosphere being corrected by an atmospheric dispersion corrector).

The design was made for use at the $F/8$ Cassegrain focus of the $3.58m$ Canada-France-Hawaii telescope. The design can be readily adapted to other telescopes with similar apertures and focal ratios. A change of focal ratio is more easily accommodated than a change of aperture because a change of aperture will result in a change in the size and separation of the deformable mirrors.

The design demonstrated that an optical design can be found which incorporates the necessary optical components for a multiconjugate adaptive optics system with a very good image quality. Further work is now needed to determine the best control system algorithms which would couple the information from the wavefront sensors to the deformable mirrors. These algorithms should be tested using a computer simulation of the system which incorporates the optical design presented here. Such a computer simulation would include the effects of the optical aberrations and the central obstruction caused by the secondary mirror in the telescope. The sensitivities of the components to the construction parameters can also be integrated into the computer simulation to include the effects of alignment and manufacturing tolerances on the system performance. After the computer simulation of the control algorithms with the proposed optical design has been completed the results of these simulations can be used to redesign the optical design to optimize the design to the control

algorithms.

Bibliography

[1] E. Atad, J.W. Harris, and C.M. Humphries. Optical design and imaging performance of the UK large telescope - part 1. Technical report, Royal Observatory Edinburgh, Royal Observatory, Blackford Hill, Edinburgh, U.K., September 1990. UNITED KINGDOM LARGE TELESCOPE PROJECT Technical Report No 13.

[2] H. W. Babcock. The possibility of compensating astronomical seeing. *PASP*, 65:229–36, 1953.

[3] Raffaele Barletti and Guido Ceppatelli. Mean vertical profile of atmospheric turbulence relevant for astronomical seeing. *J. Opt. Soc. Am.*, 66(12):1380–1383, December 1976.

[4] Jacques M. Beckers. Increasing the size of the isoplanatic patch with multiconjugate adaptive optics. In M.-H. Ulrich, editor, *ESO Conference on Very Large Telescopes and Their Instrumentation*, volume 2, pages 693–703. European Southern Observatory, March 1988. ESO Conference and Workshop Proceedings No. 30.

[5] Jacques M. Beckers. Detailed compensation of atmospheric seeing using multiconjugate adaptive optics. In *Active Telescope Systems*, volume 1114, pages 215–217. SPIE, 1989.

[6] Jacques M. Beckers. Solar image restoration by adaptive optics. In R.J. Rutten and G. Severino, editors, *Solar and Stellar Granulation: 1988 June 21-25, Capri, Italy. (OAC Workshop #3) (NATO Advance Research)*, pages 43–53, Cargese, France, 1989. NATO, Kluwer Academic Publishers, Dordrecht, The Netherlands.

[7] Jaucques M. Beckers. Adaptive optics for astronomy : Principles, performance and applications. *Annual Review of Astronomy and Astrophysics*, 31:13–62, 1993.

[8] J.-L. Caccia, J. Vernin, and M. Azouit. Structure function C_n^2 profiling by two-color stellar scintillation with atmospheric dispersion. *Applied Optics*, 27(11):2229–35, June 1988.

[9] Robert H. Dicke. Phase-contrast detection of telescope seeing errors and their correction. *Astrophysical Journal*, 198:605–615, June 1975.

[10] Mark A. Ealey. Active and adaptive optical components: The technology and future trends. In *Active and Adaptive Optical Components*, volume 1543, pages 2–33. SPIE, 1991.

[11] Harland W. Epps. Construction optical design for the 3.6-m C.F.H.T. wide-field cassegrain corrector (CADC). Technical report, University of California Santa Cruz, Santa Cruz, California, July 1992.

[12] Bruce Jacobsen et al. Field evaluation of two new continuous dye laser systems optimized for sodium beacon excitation. In *Adaptive Optics in Astronomy*, volume 2201, pages 342–351. SPIE, 1994.

[13] D. Wittman et al. Optical sensing of infrared wavefronts for adaptive control: A new CCD detector and MMT experiments. In *ESO Conference on Progress in Telescope and Instrumentation Technologies*, pages 453–60, Garching, Germany, 1992. ESO.

[14] F. Roddier et al. Seeing at Mauna Kea: a joint UH-UN-NOAO-CFHT study. In *Advanced Technology Optical Telescopes IV*, volume 1236, pages 485–91. SPIE, 1990.

[15] Jack L. Bufton et al. Measurements of turbulence profiles in the troposphere. *Journal of the Optical Society of America*, 62(9):1068–70, September 1972.

[16] Jean-Jacques Roland et al. Adaptive optics : A general purpose system for astronomy. In *Adaptive Optics in Astronomy*, volume 2201, pages 58–76. SPIE, 1994.

[17] M.J. Northcott et al. The UH curvature based adaptive optics instrument. In F. Merkle, editor, *Proceedings of the ICO-16 Satellite Conference on Active and Adaptive Optics*, pages 41–46, Garching, Germany, 1993. European Southern Observatory.

[18] R. Arsenault et al. "PUEO", the Canadian-France-Hawaii telescope adaptive optics bonnette I: System description. In *Adaptive Optics in Astronomy*, volume 2201, pages 833–842. SPIE, 1994.

[19] R. Foy et al. Atlas status report and tilt sensing using multicolour laser reference star. In M.-H. Ulrich, editor, *ESO Conference on Progress in Telescope and Instrumentation Technologies*, pages 437–441, Garching, Germany, April 1992. European Southern Observatory. ESO Conference and Workshop Proceedings No. 42.

[20] Robert D.McClure et al. An image-stabilization, high resolution camera for the Canada-France-Hawaii telescope. *PASP*, 101(646), December 1989.

[21] R. Foy and A. Labeyrie. Feasibility of adaptive telescope with laser probe. *Astronomy and Astrophysics*, 152:L29–L31, 1985.

[22] R. Foy, A. Migus, F. Biraben, G. Grynberg, P.R. McCullough, and M. Tallon. The polychromatic artificial sodium star: a new concept of the correcting the atmospheric tilt. *Astron. Astrophys. Suppl. Ser.*, 111, June 1995.

[23] Gemini Instrument Group. Mounting of Cassegrain instruments. Technical report, Association of Universities for Research in Astronomy, Inc (AURA), Tucson, Arizona, May 1992. Internal publication.

[24] W. A. Grundman and E. H. Richardson. Design of the adaptive optics system for the CFHT Cassegrain focus. In *ESO Conference on Progress in Telescope and Instrumentation Technologies*, page 547, Garching, Germany, 1992. ESO.

[25] Andrew J. Jankevics. Wide field adaptive optics. In *Active and Adaptive Optical Components*, volume 1543, pages 438–448. SPIE, 1991.

[26] Dustin C. Johnston and Byron M. Welsh. Atmospheric turbulence sensing for a multiconjugate adaptive optics system. In *Active and Adaptive Optical Systems*, volume 1542, pages 76–87. SPIE, 1991.

[27] Dustin C. Johnston and Byron M. Welsh. Analysis of multiconjugate adaptive optics. *J. Opt. Soc. Am. A*, 11(1), January 1994.

[28] Richard C. Juergens, editor. *Code 5 reference manual volume II version 8.0*, pages 3.69–3.108. Optical Research Associates, Pasadena, California, U.S.A., 1995.

[29] R. B. Leighton. The amateur scientist, concerning the problem of making sharper photographs of the planets. *Scientific American*, pages 156–167, June 1956.

[30] L.C. Martin. *Technical Optics*, volume 2, pages 280–83. Sir Isaac Pitman & Sons, LTD., London, 1950.

[31] Fritz Merkle. Adaptive optics. *Physics World*, pages 33–38, January 1991.

[32] Gemini Project Office. Gemini science requirements version 1.0. Technical report, Association of Universities for Research in Astronomy, Inc (AURA), Tucson, Arizona, October 1992. Internal publication.

[33] Scot S. Olivier and Donald T. Gavel. Tip-tilt compensation for astronomical imaging. *J. Opt. Soc. Am. A*, 11(1), January 1994.

[34] John S. Pazder, E. Harvey Richardson, and Gregory Barrick. Optical designs of adaptive optics modules for the Canada-France-Hawaii and Gemini telescopes. In F. Merkle, editor, *Proceedings of the ICO-16 Satellite Conference on Active and Adaptive Optics*, pages 59–64, Garching, Germany, 1993. European Southern Observatory.

[35] René Racine. Profiles of night-time atmospheric turbulence above Mauna Kea. private communications, February 1994.

[36] E. N. Ribak. Deformable mirrors. In D.M. Alloin and J.-M. Mariotti, editors, *Proceedings of the NATO Advanced Study Institute on Adaptive optics for Astronomy*, pages 149–161, Cargese, France, 1994. NATO, Kluwer Academic Publishers, Dordrecht, The Netherlands.

[37] Erez N. Ribak, Yael Baharav, and Joseph Shamir. Compensated imaging over arcminutes with fringes in the sodium layer. In *Adaptive Optics in Astronomy*, volume 2201, pages 381–392. SPIE, 1994.

[38] E. H. Richardson. Integrated adaptive optics systems. In D.M. Alloin and J.-M. Mariotti, editors, *Proceedings of the NATO Advanced Study Institute on Adaptive optics for Astronomy*, pages 227–236, Cargese, France, 1994. NATO, Kluwer Academic Publishers, Dordrecht, The Netherlands.

[39] E. H. Richardson. Report on optical design of Gemini adaptive optics module. Technical report, EHR Optical Systems, Victora, B.C., August 1994.

[40] E. H. Richardson and C.L.Morbey. Optical design of an all-reflecting, high resolution camera for active-optics on ground-based telescopes. In *Adaptive Optics*, volume 551, pages 26–31. SPIE, 1985.

[41] E. H. Richardson and John Stanley Pazder. Optical design of Gemini adaptive optics module. Technical report, EHR Optical Systems, Victora, B.C., April 1995.

[42] F. Rigaut. Astronomical reference sources. In D.M. Alloin and J.-M. Mariotti, editors, *Proceedings of the NATO Advanced Study Institute on Adaptive optics for Astronomy*, page 168, Cargese, France, 1994. NATO, Kluwer Academic Publishers, Dordrecht, The Netherlands.

[43] Francois Rigaut, Olivier Lai, and Jean-Pierre Veran. PUEO's performance : image quality improvement. Internal publication, May 1996.

[44] David Robertson and Matt Mountain. Gemini instrumentation. In *Instrumentation in Astronomy VIII*, volume 2298, pages 143–152. SPIE, 1994.

[45] F. Roddier. Adaptive optics at the University of Hawaii I: Current performance at the telescope. In *Adaptive Optics in Astronomy*, volume 2201, pages 2–9. SPIE, 1994.

[46] F. Roddier and C. Roddier. Curvature sensing and compensation: A new concept in adaptive optics. In M.-H. Ulrich, editor, *ESO Conference on Very Large Telescopes and Their Instrumentation*, volume 2, pages 667–73. European Southern Observatory, March 1988. ESO Conference and Workshop Proceedings No. 30.

[47] G. Rousset. Wavefront sensing. In D.M. Alloin and J.-M. Mariotti, editors, *Proceedings of the NATO Advanced Study Institute on Adaptive optics for Astronomy*, pages 115–137, Cargese, France, 1994. NATO, Kluwer Academic Publishers, Dordrecht, The Netherlands.

[48] Derrick Salmon. Memorandum: Atmospheric refraction at Mauna Kea. Internal publication, August 1991.

[49] Daniel J. Schroeder. *Astronomical Optics*, pages 26–27. Academic Press, California, U.S.A., 1987.

[50] Daniel J. Schroeder. *Astronomical Optics*, pages 309–10. Academic Press, California, U.S.A., 1987.

[51] R. V. Shack and B.C. Platt. Production and use of lenticular Hartmann screen. *J. Opt. Soc. America*, 61:656, 1971. Abstract.

[52] Joseph Shamir, Devon G. Crowe, and James W. Beletic. Improved compensation of atmospheric turbulence effects by multiple adaptive mirror systems. *Applied Optics*, 32(24):4618–28, August 1993.

[53] Warren J. Smith. *Modern Optical Engineering : the design of optical systems*, pages 345–361. McGraw-Hill, U.S.A., second edition, 1990.

[54] Warren J. Smith. *Modern Lens Design : A Resource Manual*, pages 5–10. McGraw-Hill, U.S.A., 1992.

[55] C. L. Strong, editor. *The Scientific America Book of Projects for the Amateur Scientist*, pages 26–37. Simon and Schuster, Inc., New York, N.Y., U.S.A., 1960.

[56] M. Tallon and R. Foy. Adaptive telescope with laser probe: isoplanatism and cone effect. *Astron. Astrophys*, 235:549–557, 1990.

[57] M. Tallon, R. Foy, and J. Vernin. 3-d wavefront sensing for multiconjugate adaptive optics. In *ESO Conference on Progress in Telescope and Instrumentation Technologies*, page 517, Garching, Germany, 1992. ESO.

[58] M. Tallon, R. Foy, and J. Vernin. Wide field adaptive optics using an array of laser guide stars. In Robert Q. Fugate, editor, *Laser Guide Star Adaptive Optics Workshop*, Albuquerque, New Mexico, March 1992. Starfire Optical Range, Phillips Laboratory.

[59] Robert K. Tyson. Adaptive optics system performance approximations for atmospheric turbulence correction. *Optical Engineering*, 29(10), October 1990.

[60] Robert K. Tyson. *Principles of Adaptive Optics*. Academic Press Inc., 1991.

[61] Robert K. Tyson. The status of astronomical adaptive optics systems. *OE Reports*, pages 11–13, January 1993.

[62] Gleb Vdovin and P.M. Sarro. Flexible mirror micromachined in silicon. *Applied Optics*, 34(16):2968–72, June 1995.

[63] J. Vernin and C. Muñoz-Tuñón. Optical seeing at La Palma Observatory I. general guidelines and preliminary results at the Nordic optical telescope. *Astron. Astrophys*, 257:811–816, 1992.

[64] Edward P. Wallner. Optimizing the locations of multiconjugate wavefront correctors. In *Adaptive Optics in Astronomy*, volume 2201, pages 110–116. SPIE, 1994.

[65] R. W. Wilson and C. R. Jenkins. Theoretical point spread function for modal adaptive optics. In *Adaptive Optics in Astronomy*, volume 2201, pages 117–128. SPIE, 1994.

[66] Jixiang Yan, Renzhong Zhou, and Xin Yu. Problems with multiconjugate correction. *Optical Engineering*, 33(9), September 1994.

Appendix A

lens file for the final design

```
                RDY             THI      RMD        GLA
> OBJ:         INFINITY        INFINITY
    1:         INFINITY      100.000000         'atmos'
      XDE:     0.000000    YDE:     0.000000    ZDE:     0.000000    DAR
      ADE:     1.000000    BDE:     0.000000    CDE:     0.000000

    2:         INFINITY        0.000000
    3:         INFINITY        0.000000
      XDE:     0.000000    YDE:     0.000000    ZDE:     0.000000
      ADE:     0.010195    BDE:     0.000000    CDE:     0.000000

    4:         INFINITY     8553.000000         AIR
      XDE:     0.000000    YDE:     0.000000    ZDE:     0.000000
      ADE:     0.000000    BDE:     0.000000    CDE:     0.000000

  STO:     -27067.00000    -8552.820225  REFL AIR
      CON:
      K   :   -1.000000

    6:     -18880.00000     8552.820225  REFL AIR
      CON:
      K   :   -7.790000

    7:     -27067.00000     1591.000000         AIR
    8:         INFINITY       50.000000
```

```
 9:        INFINITY          0.000000
   XDE:     0.000000   YDE:     0.000000   ZDE:     0.000000
   ADE:     0.000000   BDE:     0.000000   CDE:    -7.242393

10:        INFINITY          0.000000  REFL
   XDE:     0.000000   YDE:     0.000000   ZDE:     0.000000   BEN
   ADE:     0.000000   BDE:    45.000000   CDE:     0.000000

11:        INFINITY       -350.000000
   XDE:     0.000000   YDE:     0.000000   ZDE:     0.000000
   ADE:     0.000000   BDE:     0.000000   CDE:   -12.271648

12:        INFINITY         -0.000000
   XDE:     0.000000   YDE:     0.000000   ZDE:     0.000000
   ADE:   -11.000000   BDE:     0.000000   CDE:     0.000000

13:        INFINITY         35.000000
14:       -160.61582       195.785851  REFL
   CON:
   K   :  -11.517956
   CUM:     0.000000   THM:    20.000000

15:       -366.13072         -0.000000  REFL
   CON:
   K   :   -3.277802
   CUM:     0.000000   THM:    20.000000

16:        INFINITY         -0.000000
   XDE:     0.000000   YDE:   -14.515198   ZDE:     0.000000
   ADE:     1.678189   BDE:     0.000000   CDE:     0.000000

17:        INFINITY       -241.241880
   XDE:     0.000000   YDE:     0.000000   ZDE:     0.000000
   ADE:     0.000000   BDE:     0.000000   CDE:    19.514041

18:        INFINITY         -5.000000        FK54_SCHOTT
   XDE:     0.000000   YDE:     0.000000   ZDE:     0.000000   DAR
   ADE:    -0.535701   BDE:     0.000000   CDE:     0.000000

19:        INFINITY         -5.000000        BAK5_SCHOTT
   XDE:     0.000000   YDE:     0.000000   ZDE:     0.000000   DAR
   ADE:    -5.898478   BDE:     0.000000   CDE:     0.000000
```

```
20:         INFINITY          0.000000
   XDE:     0.000000   YDE:     0.000000   ZDE:     0.000000   DAR
   ADE:    -1.735761   BDE:     0.000000   CDE:     0.000000

21:         INFINITY         -2.000000
22:         INFINITY         -5.000000         BAK5_SCHOTT
   XDE:     0.000000   YDE:     0.000000   ZDE:     0.000000   DAR
   ADE:     1.735761   BDE:     0.000000   CDE:     0.000000

23:         INFINITY         -5.000000         FK54_SCHOTT
   XDE:     0.000000   YDE:     0.000000   ZDE:     0.000000   DAR
   ADE:     5.898478   BDE:     0.000000   CDE:     0.000000

24:         INFINITY          0.000000
   XDE:     0.000000   YDE:     0.000000   ZDE:     0.000000   DAR
   ADE:     0.535701   BDE:     0.000000   CDE:     0.000000

25:         INFINITY        -60.000000
   XDE:     0.000000   YDE:     0.000000   ZDE:     0.000000
   ADE:     0.000000   BDE:     0.000000   CDE:     5.485959

26:         INFINITY         -0.000000  REFL
   XDE:     0.000000   YDE:     0.000000   ZDE:     0.000000   BEN
   ADE:   -30.000000   BDE:     0.000000   CDE:     0.000000
   CUM:     0.000000   THM:    23.100000

27:         INFINITY        220.472354
28:         INFINITY         -0.000000  REFL
   XDE:     0.000000   YDE:     0.000000   ZDE:     0.000000   BEN
   ADE:    30.000000   BDE:     0.000000   CDE:     0.000000
   CUM:     0.000000   THM:    23.100000

29:         INFINITY        -305.000000
30:         INFINITY         -0.000000  REFL
   XDE:     0.000000   YDE:     0.000000   ZDE:     0.000000   BEN
   ADE:   -30.000000   BDE:     0.000000   CDE:     0.000000
   CUM:     0.000000   THM:    23.100000

31:         INFINITY         82.000000
   XDE:     0.000000   YDE:     0.000000   ZDE:     0.000000
   ADE:     0.000000   BDE:     0.000000   CDE:   -25.000000
```

```
32:     -1375.15232       -0.000000  REFL
   XTO:
   RDX: -1272.89670
   XDE:    0.000000   YDE:    0.000000   ZDE:    0.000000   BEN
   ADE:  -15.891946   BDE:    0.000000   CDE:    0.000000
   CUM:    0.000000   THM:   20.000000

33:         INFINITY     -934.353471
   XDE:    0.000000   YDE:    0.000000   ZDE:    0.000000
   ADE:    0.000000   BDE:    0.000000   CDE:   19.497427

34:         INFINITY      -50.000000        AIR
   XDE:    0.000000   YDE:    0.000000   ZDE:    0.000000   BEN
   ADE:    0.000000   BDE:    0.000000   CDE:    0.000000

35:         INFINITY       -0.000000        AIR
   XDE:    0.000000   YDE:    0.000000   ZDE:    0.000000   DAR
   ADE:    0.000000   BDE:    0.000000   CDE:    0.000000

36:         INFINITY       -0.000000
   XDE:    0.000000   YDE:    0.000000   ZDE:    0.000000   DAR
   ADE:    0.000000   BDE:    0.000000   CDE:    0.000000

37:         INFINITY       -0.000000        AIR
   XDE:    0.000000   YDE:    0.000000   ZDE:    0.000000   DAR
   ADE:    0.000000   BDE:    0.000000   CDE:    0.000000

38:         INFINITY       -0.000000
   XDE:    0.000000   YDE:    0.000000   ZDE:    0.000000   DAR
   ADE:    0.000000   BDE:    0.000000   CDE:    0.000000

39:         INFINITY       -0.000000
   XDE:    0.000000   YDE:    0.000000   ZDE:    0.000000
   ADE:    0.000000   BDE:    0.000000   CDE:    0.000000

40:         INFINITY       -0.000000
   XDE:    0.000000   YDE:    0.000000   ZDE:    0.000000
   ADE:    0.000000   BDE:    0.000000   CDE:    0.000000

41:         INFINITY       -0.000000  REFL
   XDE:    0.000000   YDE:    0.000000   ZDE:    0.000000   BEN
```

```
      ADE:    15.000000   BDE:     0.000000   CDE:     0.000000

   42:         INFINITY       -0.000000
   43:         INFINITY       -0.000000        AIR
   44:         INFINITY       -0.000000
   45:         INFINITY       -0.000000
   46:         INFINITY       -0.000000
   47:         INFINITY      250.000000
  IMG:         INFINITY       -0.000000

SPECIFICATION DATA
   EPD      3592.00000
   DIM             MM
   WL         1000.00    850.00    700.00    550.00    400.00
   REF              3
   WTW              1         1         1         1         1
   INI            JSP
   XAN        0.00000       0.00000       0.00000
   YAN        0.00000       0.00306      -0.00306
   VUX        0.00000       0.00000       0.00000
   VLX        0.00000       0.00000       0.00000
   VUY        0.00000       0.00000       0.00000
   VLY        0.00000       0.00000       0.00000

APERTURE DATA/EDGE DEFINITIONS
   CA
   CIR S4   OBS L'sec'    790.000000
   CIR S14  EDG             8.000000
   ADY S14  EDG             6.800000
   CIR S15  EDG            21.000000
   ADY S15  EDG           -14.700000
   CIR S18  EDG            25.000000
   CIR S19  EDG            25.000000
   CIR S20  EDG            25.000000
   CIR S21  EDG            25.000000
   CIR S22  EDG            25.000000
   CIR S23  EDG            25.000000
   CIR S24  EDG            25.000000
   CIR S26  EDG            23.100000
   CIR S28  EDG            23.100000
   CIR S30  EDG            32.500000
```

PRIVATE CATALOG

PWL	1000.00	850.00	700.00	550.00	400.00
'atmos'	1.009895	1.009918	1.009952	1.010027	1.010204

REFRACTIVE INDICES

GLASS CODE	1000.00	850.00	700.00	550.00	400.00
BK7_SCHOTT	1.507502	1.509840	1.513064	1.518522	1.530849
FK54_SCHOTT	1.431533	1.432874	1.434771	1.438031	1.445373
BAK5_SCHOTT	1.546333	1.548797	1.552386	1.558736	1.573540
'atmos'	1.009895	1.009918	1.009952	1.010027	1.010204

No solves defined in system

No pickups defined in system

ZOOM DATA

	POS 1	POS 2	POS 3	POS 4	POS 5	POS 6	POS 7
YAN F1	0.00000	0.00000	0.00000	0.01028	0.01028	0.01028	0.01028
YAN F2	0.00306	0.00306	0.00306	0.01028	0.01028	0.01028	0.01028
YAN F3	-0.00306	-0.00306	-0.00306	0.01028	0.01028	0.01028	0.01028
RSL	DEF	DEF	DEF	DEF	DEF	DEF	DEF
THI S0	INFINITY	INFINITY	INFINITY	0.9e8	0.9e8	0.9e8	0.9e8
CDE S4	0.00000	0.00000	0.00000	45.000	135.000	225.000	315.000
THI S34	-50.000	300.000	-50.000	-50.000	-50.000	-50.000	-50.000
RMD S34	REFR	REFL	REFR	REFR	REFR	REFR	REFR
ADE S34	0.00000	35.000	0.00000	0.00000	0.000	0.000	0.000
THI S35	0.00000	400.000	-10.000	-10.000	-10.000	-10.000	-10.000
RMD S35	REFR	REFR	REFR	REFR	REFR	REFR	REFR
ADE S35	0.00000	0.00000	15.000	15.000	15.000	15.000	15.000
THI S36	0.00000	0.00000	-50.000	-50.000	-50.000	-50.000	-50.000
ADE S36	0.00000	0.00000	15.000	15.000	15.000	15.000	15.000
THI S37	0.00000	0.00000	-10.000	-10.000	-10.000	-10.000	-10.000
RMD S37	REFR	REFR	REFR	REFR	REFR	REFR	REFR
ADE S37	0.00000	0.00000	-43.6507	-43.6507	-43.6507	-43.6507	-43.6507
ADE S38	0.00000	0.00000	-43.88826	-43.88826	-43.88826	-43.88826	-43.88826
THI S39	0.00000	0.00000	0.00000	-150.000	-150.000	-150.000	-150.000
YDE S39	0.00000	0.00000	1.42141	1.42141	1.42141	1.42141	1.42141
ADE S39	0.00000	0.00000	0.67850	0.67850	0.67850	0.67850	0.67850
ADE S40	0.00000	0.00000	0.00000	0.05281	-1.02676	-1.04326	0.05253
BDE S40	0.00000	0.00000	0.00000	-0.52956	-0.53978	0.55590	0.52999

XDE S40	0.00000	0.00000	0.00000	-20.02791	-19.44371	19.97498	20.02791
YDE S40	0.00000	0.00000	0.00000	-18.77294	20.49425	21.01839	-18.77294
RMD S41	REFL	REFL	REFR	REFL	REFL	REFL	REFL
ADE S41	15.0000	-3.000	0.00000	34.000	36.000	36.000	34.000
THI S41	0.00000	0.00000	0.00000	357.98323	356.07762	356.07257	357.98323
RDY S41	INFINIT	-879.2615	INFINITY	INFINITY	INFINITY	INFINITY	INFINITY
THI S42	0.00000	0.00000	0.00000	64.04904	64.57176	65.02870	64.03846
RMD S43	REFR	REFR	REFR	REFR	REFR	REFR	REFR
THI S43	0.00000	0.00000	0.00000	5.000	5.000	5.000	5.000
THI S44	0.00000	0.00000	0.00000	64.04904	64.57176	65.02870	64.03846
RDY S44	INFINITY	INFINITY	INFINIT	-32.35083	-32.55813	-32.69915	-32.34561
THI S47	250.00	-530.5798	-185.83403	0.00000	0.00000	0.00000	0.00000
GL1 S41	AIR	AIR	AIR	AIR	AIR	AIR	AIR
GP1 S41	AIR	AIR	AIR	AIR	AIR	AIR	AIR
GL1 S43	AIR	AIR	AIR	BK7	BK7	BK7	BK7
				_SCHOTT	_SCHOTT	_SCHOTT	_SCHOTT
GP1 S43	AIR	AIR	AIR	BK7	BK7	BK7	BK7
				_SCHOTT	_SCHOTT	_SCHOTT	_SCHOTT
GL1 S35	AIR	AIR	BK7	BK7	BK7	BK7	BK7
			_SCHOTT	_SCHOTT	_SCHOTT	_SCHOTT	_SCHOTT
GP1 S35	AIR	AIR	BK7	BK7	BK7	BK7	BK7
			_SCHOTT	_SCHOTT	_SCHOTT	_SCHOTT	_SCHOTT
GL1 S37	AIR	AIR	BK7	BK7	BK7	BK7	BK7
			_SCHOTT	_SCHOTT	_SCHOTT	_SCHOTT	_SCHOTT
GP1 S37	AIR	AIR	BK7	BK7	BK7	BK7	BK7
			_SCHOTT	_SCHOTT	_SCHOTT	_SCHOTT	_SCHOTT
GL1 S34	AIR	AIR	AIR	AIR	AIR	AIR	AIR
GP1 S34	AIR	AIR	AIR	AIR	AIR	AIR	AIR

This is a decentered system. If elements with power are decentered or tilted, the first order properties are probably inadequate in describing the system characteristics.

	POS 1	POS 2	POS 3	POS 4	POS 5	POS 6	POS 7
INFINITE CONJUGATES							
EFL	-0.176E+06	0.586E+06	0.176E+06	47745.824	48423.298	48595.813	47738.213
BFL	342.5952	1022.0729	-279.3770	16.0757	16.3102	16.2659	16.0706
FFL	-0.143E+08	0.221E+09	-0.14E+08	-0.15E+09	-0.15E+09	-0.15E+09	-0.15E+09
FNO	-49.0982	-163.2437	-49.0982	13.2923	13.4809	13.5289	13.2901
AT USED CONJUGATES							
RED	0.0000	0.0000	0.0000	-0.0008	-0.0008	-0.0008	-0.0008

FNO	-49.0982	-163.2437	-49.0982	-20.6801	-20.6058	-20.7154	-20.6767
OBJ DIS	0.1E+21	0.100E+21	0.100E+21	0.900E+08	0.900E+08	0.900E+08	0.900E+08
TT	0.1E+21	0.100E+21	0.100E+21	0.900E+08	0.900E+08	0.900E+08	0.900E+08
IMG DIS	250.00	-530.5798	-185.8340	0.0000	0.0000	0.0000	0.0000
OAL	8864.6629	9614.6629	8794.6629	9135.7442	9134.8840	9135.7928	9135.7230
PARAXIAL IMAGE							
HT	9.4052	31.2709	9.4052	13.3249	13.2770	13.3477	13.3228
THI	342.5952	1022.0729	-279.3770	-23.3283	-23.5093	-23.9081	-23.3206
ANG	0.0031	0.0031	0.0031	0.0103	0.0103	0.0103	0.0103
ENTRANCE PUPIL							
DIA	3592.0000	3592.0000	3592.0000	3592.0000	3592.0000	3592.0000	3592.0000
THI	8652.0146	8652.0146	8652.0146	8652.0146	8652.0146	8652.0146	8652.0146
EXIT PUPIL							
DIA	44.2420	9.5345	44.2420	1.1599	1.1682	1.1732	1.1597
THI	-1829.6051	-534.3747	1892.8233	0.6582	0.5620	0.3944	0.6581
STO DIA	3592.0	3592.0	3592.0	3592.0	3592.0	3592.0	3592.0

Appendix B

lens file for the main beam optics

```
                RDY              THI      RMD       GLA
OBJ:          INFINITY         INFINITY
  1:          INFINITY       100.000000        'atmos'
    XDE:      0.000000    YDE:     0.000000    ZDE:     0.000000    DAR
    ADE:      1.000000    BDE:     0.000000    CDE:     0.000000

  2:          INFINITY         0.000000
  3:          INFINITY         0.000000
    XDE:      0.000000    YDE:     0.000000    ZDE:     0.000000
    ADE:      0.010195    BDE:     0.000000    CDE:     0.000000

  4:          INFINITY      8553.000000         AIR
    XDE:      0.000000    YDE:     0.000000    ZDE:     0.000000
    ADE:      0.000000    BDE:     0.000000    CDE:     0.000000

STO:      -27067.00000     -8552.820225  REFL AIR
    CON:
    K  :    -1.000000

  6:      -18880.00000      8552.820225  REFL AIR
    CON:
    K  :    -7.790000

  7:      -27067.00000      1591.000000         AIR
  8:          INFINITY        50.000000
  9:          INFINITY         0.000000
    XDE:      0.000000    YDE:     0.000000    ZDE:     0.000000
    ADE:      0.000000    BDE:     0.000000    CDE:    -7.242393
```

```
10:        INFINITY          0.000000  REFL
   XDE:    0.000000   YDE:     0.000000   ZDE:     0.000000   BEN
   ADE:    0.000000   BDE:    45.000000   CDE:     0.000000

11:        INFINITY       -350.000000
   XDE:    0.000000   YDE:     0.000000   ZDE:     0.000000
   ADE:    0.000000   BDE:     0.000000   CDE:   -12.271648

12:        INFINITY          0.000000
   XDE:    0.000000   YDE:     0.000000   ZDE:     0.000000
   ADE:  -11.000000   BDE:     0.000000   CDE:     0.000000

13:        INFINITY         35.000000
14:      -160.61582        195.785851  REFL
   CON:
   K   :  -11.517956
   CUM:    0.000000   THM:    20.000000

15:      -366.13072          0.000000  REFL
   CON:
   K   :   -3.277802
   CUM:    0.000000   THM:    20.000000

16:        INFINITY          0.000000
   XDE:    0.000000   YDE:   -14.515198   ZDE:     0.000000
   ADE:    1.678189   BDE:     0.000000   CDE:     0.000000

17:        INFINITY       -241.241880
   XDE:    0.000000   YDE:     0.000000   ZDE:     0.000000
   ADE:    0.000000   BDE:     0.000000   CDE:    19.514041

18:        INFINITY         -5.000000        FK54_SCHOTT
   XDE:    0.000000   YDE:     0.000000   ZDE:     0.000000   DAR
   ADE:   -0.535701   BDE:     0.000000   CDE:     0.000000

19:        INFINITY         -5.000000        BAK5_SCHOTT
   XDE:    0.000000   YDE:     0.000000   ZDE:     0.000000   DAR
   ADE:   -5.898478   BDE:     0.000000   CDE:     0.000000

20:        INFINITY          0.000000
   XDE:    0.000000   YDE:     0.000000   ZDE:     0.000000   DAR
```

```
   ADE:   -1.735761   BDE:    0.000000   CDE:    0.000000

21:        INFINITY       -2.000000
22:        INFINITY       -5.000000        BAK5_SCHOTT
   XDE:    0.000000   YDE:    0.000000   ZDE:    0.000000   DAR
   ADE:    1.735761   BDE:    0.000000   CDE:    0.000000

23:        INFINITY       -5.000000        FK54_SCHOTT
   XDE:    0.000000   YDE:    0.000000   ZDE:    0.000000   DAR
   ADE:    5.898478   BDE:    0.000000   CDE:    0.000000

24:        INFINITY        0.000000
   XDE:    0.000000   YDE:    0.000000   ZDE:    0.000000   DAR
   ADE:    0.535701   BDE:    0.000000   CDE:    0.000000

25:        INFINITY      -60.000000
   XDE:    0.000000   YDE:    0.000000   ZDE:    0.000000
   ADE:    0.000000   BDE:    0.000000   CDE:    5.485959

26:        INFINITY        0.000000  REFL
   XDE:    0.000000   YDE:    0.000000   ZDE:    0.000000   BEN
   ADE:  -30.000000   BDE:    0.000000   CDE:    0.000000
   CUM:    0.000000   THM:   23.100000

27:        INFINITY      220.472354
28:        INFINITY        0.000000  REFL
   XDE:    0.000000   YDE:    0.000000   ZDE:    0.000000   BEN
   ADE:   30.000000   BDE:    0.000000   CDE:    0.000000
   CUM:    0.000000   THM:   23.100000

29:        INFINITY     -305.000000
30:        INFINITY        0.000000  REFL
   XDE:    0.000000   YDE:    0.000000   ZDE:    0.000000   BEN
   ADE:  -30.000000   BDE:    0.000000   CDE:    0.000000
   CUM:    0.000000   THM:   23.100000

31:        INFINITY       82.000000
   XDE:    0.000000   YDE:    0.000000   ZDE:    0.000000
   ADE:    0.000000   BDE:    0.000000   CDE:  -25.000000

32:    -1375.15232        0.000000  REFL
   XTO:
```

```
      RDX: -1272.89670
      XDE:    0.000000   YDE:    0.000000   ZDE:    0.000000   BEN
      ADE:  -15.891946   BDE:    0.000000   CDE:    0.000000
      CUM:    0.000000   THM:   20.000000

   33:        INFINITY     -934.353471
      XDE:    0.000000   YDE:    0.000000   ZDE:    0.000000
      ADE:    0.000000   BDE:    0.000000   CDE:   19.497427

   34:        INFINITY      -50.000000       AIR
      XDE:    0.000000   YDE:    0.000000   ZDE:    0.000000   BEN
      ADE:    0.000000   BDE:    0.000000   CDE:    0.000000

>  35:        INFINITY        0.000000  REFL AIR
      XDE:    0.000000   YDE:    0.000000   ZDE:    0.000000   BEN
      ADE:   15.000000   BDE:    0.000000   CDE:    0.000000

   36:        INFINITY      250.000000
  IMG:        INFINITY        0.000000

SPECIFICATION DATA
   EPD     3592.00000
   DIM             MM
   WL         1000.00    850.00    700.00    550.00    400.00
   REF              3
   WTW              1         1         1         1         1
   INI            JSP
   XAN        0.00000       0.00000       0.00000
   YAN        0.00000       0.00306      -0.00306
   VUX        0.00000       0.00000       0.00000
   VLX        0.00000       0.00000       0.00000
   VUY        0.00000       0.00000       0.00000
   VLY        0.00000       0.00000       0.00000

APERTURE DATA/EDGE DEFINITIONS
   CA
   CIR S4   OBS L'sec'    790.000000
   CIR S14  EDG             8.000000
   ADY S14  EDG             6.800000
   CIR S15  EDG            21.000000
   ADY S15  EDG           -14.700000
   CIR S18  EDG            25.000000
```

```
   CIR S19  EDG            25.000000
   CIR S20  EDG            25.000000
   CIR S21  EDG            25.000000
   CIR S22  EDG            25.000000
   CIR S23  EDG            25.000000
   CIR S24  EDG            25.000000
   CIR S26  EDG            23.100000
   CIR S28  EDG            23.100000
   CIR S30  EDG            32.500000

PRIVATE CATALOG
   PWL          1000.00      850.00      700.00      550.00      400.00
   'atmos'     1.009895    1.009918    1.009952    1.010027    1.010204

REFRACTIVE INDICES
  GLASS CODE    1000.00      850.00      700.00      550.00      400.00
 FK54_SCHOTT   1.431533    1.432874    1.434771    1.438031    1.445373
 BAK5_SCHOTT   1.546333    1.548797    1.552386    1.558736    1.573540
 'atmos'       1.009895    1.009918    1.009952    1.010027    1.010204

No solves defined in system

No pickups defined in system


        This is a decentered system.  If elements with power are
        decentered or tilted, the first order properties are probably
        inadequate in describing the system characteristics.

INFINITE CONJUGATES
   EFL     -0.1764E+06
   BFL        342.5952
   FFL     -0.1431E+08
   FNO        -49.0982
   IMG DIS    250.0000
   OAL       8864.6629
   PARAXIAL IMAGE
    HT           9.4052
   ANG           0.0031
   ENTRANCE PUPIL
    DIA       3592.0000
    THI       8652.0146
```

```
EXIT PUPIL
 DIA       44.2420
 THI    -1829.6051
```

Appendix C

Command scripts for final optimization

```
!-------------------------------------------------------------------------
! Command Script 1  - file dm_position.seq.1
!-------------------------------------------------------------------------


gbl num ^dia ^dmup ^dmlow ^new13
!
! dm_position.seq.1  DM positioning script using real ray tracing
! uses lens file mcao9
!
! defines pupil and 9k layer location from saved file
!
if (cde s11) <> 0 OR (cde s17) <> 0
wri "cde s11 and cde s17 must be zero "
rtn
end if
save
res mcao9
dez 1
yan 0
xan 0
thi s0 9e6
epd 1400
del s12..19
```

```
^old_th11 == (thi s11)
frz sa
thc s11 0
aut
mxc 10
mxt  1e5
mnt -1e5
mne -1e5
mna -1e5
mae -1e5
vli y
rsp n
sur n
chg y
imp 0.01
go
dra s5..i
^new_th11 == (thi s11)
res
thi s11 (^new_th11)
save
dez 1
yan 0
xan 0
nao 0.00009
thi s0 0
del s14..19
^old_th13 == (thi s13)
frz sa
thc s13 0
aut
mxc 10
mxt  1e5
mnt -1e5
mne -1e5
mna -1e5
mae -1e5
vli y
rsp n
sur n
chg y
imp 0.01
```

```
go
dra s5..i
^new13 == (thi s13)
wri ^new13
res
lvr
^old_th15 == (thi s15)
!thi s15 (1.15*20 - ^new13)
thi s13 (^new13)
save
wri " wrote two new files "
wri "old s11" ^old_th11
wri "new s11" ^new_th11
wri "old s13" ^old_th13
wri "new s13" ^new13
wri "old s15" ^old_th15
```

```
!-------------------------------------------------------------------------
! Command Script 2  - file dm_size.seq.1
!-------------------------------------------------------------------------

gbl num ^dia ^dmup ^dmlow
!
! dm_size.seq.1  DM size script
!
! 20mm DM size
!
if (cde s11) <> 0 OR (cde s17) <> 0
wri "cde s11 and cde s17 must be zero "
rtn
end if
frz sa
msg n ! stop beeps
thc s8  0
ccy s9  0
^dia == 20 ! DM size
^dmup == 12  ! upper DM
^dmlow == 14 ! lower DM
```

```
dez 1
thi s0 1e99
yan 0 11/3600 -11/3600 0        0       11/7200 -11/7200 -11/7200  11/7200
xan 0 0        0       11/3600 -11/3600 11/7200  11/7200 -11/7200 -11/7200
aut
mxc 4
mxt  1e5
mnt -1e5
mne -1e5
mna -1e5
mae -1e5
vli y
rsp n
sur n
chg y
err con
! 9k layer
@sizeupf == (x r5 f4 s^dmup z1 )-(x r4 f5 s^dmup z1 )
dsp @sizeupf
@sizeupf = ^dia
!pupilDM
@sizelow == (x r5  f1 s^dmlow z1 )-(x r4 f1 s^dmlow z1 )
@sizelow = ^dia
dsp @sizelow
go
dra s5..i
sur s7
sur s8
```

```
!-------------------------------------------------------------------------
! Command Script 3  - file image.seq.1
!-------------------------------------------------------------------------


gbl num ^dia ^dmup ^dmlow
!
! image.seq.1 -  image script quality optimization script
!                optimizes the final image quality
!
```

```
!
if (cde s11) <> 0 OR (cde s17) <> 0
wri "cde s11 and cde s17 must be zero "
rtn
end if
frz sa
msg n ! stop beeps
! conic constants of first two mirrors
kc s8  0
kc s9  0
!ydc s9 0
! center  chief ray before entering the DM slide
adc s10 0
ydc s10 0
! camera mirror
ccy s18 0
ccx s18 0
adc s18 0
! focus
thc s19 0
^dia == 20 ! DM sizes
^dmup == 12  ! upper DM
^dmlow == 14 ! lower DM
dez 1
yan 0 11/3600 -11/3600 0        0       11/7200 -11/7200 -11/7200  11/7200
xan 0 0         0       11/3600 -11/3600 11/7200  11/7200 -11/7200 -11/7200
aut
!mnc 4
mxc 10
mxt  1e5
mnt -1e5
mne -1e5
mna -1e5
mae -1e5
vli y
rsp n
sur n
chg y
dra s5..i y
imp 0.01
wtf z1 1 1 1 1 1 1 1 1
! 9k layer
```

```
@sizeup  == (x r5 f4 s^dmup z1 )-(x r4 f5 s^dmup z1 )
dsp @sizeup
!pupilDM
@sizelow == (x r5  f1 s^dmlow z1 )-(x r4 f1 s^dmlow z1 )
dsp @sizelow
! fno via image scale
@is == (y r1 f1 si z1)-(y r1 f2 si z1)
@is = 8.62
aoi r1 f1 s10 = 0
y   r1 f1 s10 = 0
go
```

Appendix D

Lens file for final optimization

```
                RDY             THI      RMD        GLA
> OBJ:         INFINITY        INFINITY
    1:         INFINITY     8553.000000        AIR
  STO:     -27067.00000    -8552.792000  REFL AIR
      CON:
      K  :    -1.000000

    3:     -18880.00000     8552.792000  REFL AIR
      CON:
      K  :    -7.790000

    4:     -27067.00000     1591.000000        AIR
    5:         INFINITY      400.000000
    6:         INFINITY        0.000000
      XDE:     0.000000   YDE:     0.000000   ZDE:     0.000000
      ADE:    11.000000   BDE:     0.000000   CDE:     0.000000

    7:         INFINITY      -35.000000
    8:        160.61582     -195.785851  REFL
      CON:
      K  :   -11.517956
      CUM:     0.000000   THM:    20.000000

    9:        366.13072        0.000000  REFL
      CON:
      K  :    -3.277802
      CUM:     0.000000   THM:    20.000000
```

```
 10:         INFINITY          0.000000
    XDE:     0.000000   YDE:  -14.515198   ZDE:     0.000000
    ADE:    -1.678189   BDE:    0.000000   CDE:     0.000000

 11:         INFINITY        323.241880
    XDE:     0.000000   YDE:    0.000000   ZDE:     0.000000
    ADE:     0.000000   BDE:    0.000000   CDE:   -25.000000

 12:         INFINITY          0.000000  REFL
    XDE:     0.000000   YDE:    0.000000   ZDE:     0.000000   BEN
    ADE:    30.000000   BDE:    0.000000   CDE:     0.000000
    CUM:     0.000000   THM:   23.100000

 13:         INFINITY       -220.472354
 14:         INFINITY          0.000000  REFL
    XDE:     0.000000   YDE:    0.000000   ZDE:     0.000000   BEN
    ADE:   -30.000000   BDE:    0.000000   CDE:     0.000000
    CUM:     0.000000   THM:   23.100000

 15:         INFINITY        305.000000
 16:         INFINITY          0.000000  REFL
    XDE:     0.000000   YDE:    0.000000   ZDE:     0.000000   BEN
    ADE:    30.000000   BDE:    0.000000   CDE:     0.000000
    CUM:     0.000000   THM:   23.100000

 17:         INFINITY        -82.000000
    XDE:     0.000000   YDE:    0.000000   ZDE:     0.000000
    ADE:     0.000000   BDE:    0.000000   CDE:    25.000000

 18:      1375.15232          0.000000  REFL
    XTO:
    RDX:  1272.89670   CCX:         0
    K  :     0.000000
    XDE:     0.000000   YDE:    0.000000   ZDE:     0.000000   BEN
    ADE:    15.891946   BDE:    0.000000   CDE:     0.000000

 19:         INFINITY       1234.353471
IMG:         INFINITY          0.000000

SPECIFICATION DATA
  EPD      3592.00000
  DIM              MM
```

```
   WL          550.00
   REF              1
   WTW              1
   INI            JSP
   XAN      0.00000       0.00000       0.00000       0.00306      -0.00306
            0.00153       0.00153      -0.00153      -0.00153
   YAN      0.00000       0.00306      -0.00306       0.00000       0.00000
            0.00153      -0.00153      -0.00153       0.00153
   VUX      0.00000       0.00000       0.00000       0.00000       0.00000
            0.00000       0.00000       0.00000       0.00000
   VLX      0.00000       0.00000       0.00000       0.00000       0.00000
            0.00000       0.00000       0.00000       0.00000
   VUY      0.00000       0.00000       0.00000       0.00000       0.00000
            0.00000       0.00000       0.00000       0.00000
   VLY      0.00000       0.00000       0.00000       0.00000       0.00000
            0.00000       0.00000       0.00000       0.00000

APERTURE DATA/EDGE DEFINITIONS
   CA
   CIR S1   OBS L'sec'    790.000000
   CIR S12  EDG            23.100000
   CIR S14  EDG            23.100000
   CIR S16  EDG            32.500000

No refractive materials defined in system

No solves defined in system

No pickups defined in system


        This is a decentered system.  If elements with power are
        decentered or tilted, the first order properties are probably
        inadequate in describing the system characteristics.

INFINITE CONJUGATES
   EFL     -0.1753E+06
   BFL       1327.0765
   FFL     -0.1392E+08
   FNO        -48.7921
   IMG DIS   1234.3535
   OAL      10638.9837
```

```
   PARAXIAL IMAGE
    HT          4.6733
   ANG          0.0015
   ENTRANCE PUPIL
    DIA      3592.0000
    THI      8553.0000
   EXIT PUPIL
    DIA        45.2079
    THI      -878.7106
CODE V>
```

Appendix E

Glossary of Technical Terms and Acronyms

Airy Disk : The diameter of the central disk of the diffraction pattern created by a perfect lens. For a circular aperture the Airy disk contains 84% of the total light from a point source. The full diameter of the Airy disk is $2.44\lambda F$ where λ is the wavelength of the light being observed, and F is the focal ratio of the lens.

ADC — Atmospheric Dispersion Corrector : a system of prisms designed to correct for the optical dispersion of the atmosphere above the telescope (see section 5.3).

AOB — Adaptive Optics Bonnette : An adaptive optics system designed to be mounted at the Cassegrain focus of the CFHT (see section 5.1.1).

C_n^2 distribution : The vertical profile of the refractive index structure constant, C_n^2, in the atmosphere. The refractive index structure constant, C_n^2, is a quantitative measure of how much the refractive index changes from point to point in the atmosphere (see page 9).

CCD — Charge Coupled Device : A semiconductor chip which has an array of light sensitive pixels. The light sensitive pixels accumulate a charge of elections when they are exposed to light. The device is designed to allow the charge accumulated in a particular pixel to be moved to the next pixel with very little loss of charge (thus the term charge coupled device). The charges are moved from pixel to pixel to allow the charges accumulated in the array of pixels to be read out into an analog to digital converter to digitize the image.

CFHT — Canada-France-Hawaii Telescope : A $3.58m$ diameter telescope located at Mauna Kea, Hawaii. The telescope is jointly operated by Canada, France, and the University of Hawaii.

DM — Deformable Mirror : A mirror with a surface that can be changed in shape using electrical signals (see section 2.4).

Focal Anisoplanatism : The effects caused by the light from the laser guide star propagating as a cone of light from the upper atmosphere to the telescope (see page 40).

Isoplanatic Angle : This is the angular area in the sky which the adaptive optics system can correct the image to a high degree of accuracy (see page 6).

ISS — Instrument Support Structure : The structure which the Gemini adaptive optics module will be installed in (see page 57).

MTF — Modulation Transfer Function : A graph of the contrast (or modulation) of the image for objects of varying spacial frequencies (see Smith[53] for a complete description).

Petzval sum : The sum of the curvatures of all the mirrors in a reflective system. The Petzval sum, to a first order approximation, is equal to the curvature of the image surface.

Pupil : The aperture, or the image of the aperture, whose size is independent of the field of view of the optical system. For a telescope, the pupil is usually the primary mirror.

RMS — Root Mean Square

SCIDAR camera — Scintillation Detection And Ranging camera : A camera which takes high speed images of the pupil when a telescope is pointed at a double star. The images are statistically analysed to determine the C_n^2 distribution.

SNR — Signal to Noise Ratio

Strehl ratio : The ratio of the peak intensity obtained to theoretical peak intensity for the image profile of an un-aberrated diffraction image of a point light source (see page 21).

VITA

Surname: Pazder — Given Names: John Stanley

Place of Birth: Edmonton, Alberta, Canada — Date of Birth: November 7, 1967

Educational Institutions Attended:

University of Victoria	1986–1996
Camosun Collage	1986–1987

Degrees Awarded:

B.Sc. Physics. (Honours Co-op)	University of Victoria	1991

Honours and Awards:

NSERC Undergrad Research Award	1990
John L. Climenhaga Scholarship	1988
Don Ingham Memorial Scholarship	1988
Grade Twelve Provincial Scholarship	1986

Publications:

G.S.Burley, G.A.H.Walker, J.S.Pazder. The CHRISP adaptive optics system. *BAAS 27:1394*, 1995

J.S.Pazder, E.H.Richardson, G.Barrick. Optical Designs of the Adaptive Optics Systems for the CFHT and Gemini Telescopes. *Proceedings of the ICO-16 Conference* , Garching, August 1993

S. van den Bergh, J. Pazder. The Luminosity of Supernovae of Type Ia: I. Apparent Magnitudes at Maximum Light. *ApJ 390:34-38*, 1992 May 1

S. van den Bergh, C. Morbey, J. Pazder. Diameters of Galactic Globular Clusters. *ApJ 375:594-599*, 1991 July 10

J.B. Hutchings, I.B. Thompson, S. Cartedge, J. Pazder. A Study of The Young Massive Cluster N90 in the SMC. *AJ 101:933-936*, 1991 March

J.B. Hutchings, D.Durand, J. Pazder. Quasars in Radio Source Catalogues. *PASP 103:21-25*, 1991 January

PARTIAL COPYRIGHT LICENSE

I hereby grant the right to lend my thesis to users of the University of Victoria Library, and to make single copies only for such users or in response to a request from the Library of any other university, or similar institution, on its behalf or for one of its users. I further agree that permission for extensive copying of this thesis for scholarly purposes may be granted by me or a member of the University designated by me. It is understood that copying or publication of this thesis for financial gain shall not be allowed without my written permission.

Title of Thesis:

The Optical Design of an Adaptive Optics System Imaging Two Selectable Atmospheric Layers

Author: [redacted]
John Stanley Pazder

Oct. 31, 1996
Date